THE UNIVERSITY *of* EDINBURGH

Channel Modelling and Relay for Powerline Communications

Bo Tan

A thesis submitted for the degree of Doctor of Philosophy.
The University of Edinburgh.
June 2013

Abstract

The thesis discusses the channel modelling and relay techniques in powerline communications (PLC) which is considered as a promising technology for the Smart Grid communications, Internet access and home area network (HAN). In this thesis, the statistical PLC channel characteristics are investigated, a new statistical channel modelling method is proposed for the in-door PLC. Then a series of the relay protocols are suggested for the broadband communications over power grid.

The statistical channel modelling method is proposed to surmount the limits of the traditional deterministic PLC channel models such as multipath model and transmission line model. To develop the channel model, the properties of the multipath magnitudes, interval between the paths, cable loss and the channel classification are investigated in detail. Then, each property is described by statistical distribution or formula. The simulation results show that the statistical model can describe the PLC channels as accurate as deterministic models without the topology information which is a time-consuming work for collecting.

The relay transmission is proposed to help PLC adapting the diverse application scenarios. The protocols covers the main relay aspects which include decode/amplify forwarding, single/multiple relay nodes, full/half duplex relay working mode. The capacity performance of each protocol is given and compared. A series of the facts which improve the performance of the PLC networks are figured out according to simulation results. The facts include that the decode-and-forward is more suitable for the PLC environment, deviation or transforming station is better location for placing relay node and full duplex relay working mode help exploiting the capacity potential of the PLC networks.

Some future works are pointed out based on the work of statistical channel model and relay. In the last part of this thesis, an unit based statistical channel model is initialled for adapting various PLC channel conditions, a more practical relay scenario which contains multiple data terminals is proposed for approaching the realistic transmission scenario. At last, the relay for the narrowband PLC Smart Grid is also mentioned as future research topic.

Declaration of originality

I hereby declare that the research recorded in this thesis and the thesis itself was composed and originated entirely by myself in the School of Engineering at The University of Edinburgh.

Bo Tan

Acknowledgements

First and foremost, I would like to thank my supervisor Professor John S. Thompson for his insightful, patient advising during my Ph.D. study, especial the during period when I was in London. His immense knowledge and kindly help are the indispensable parts of my research experience in The University of Edinburgh. His serious attitude on scientific research, intelligence and diligence on work set me a superb example in my future work.

I sincerely thank my family. The support from my mother Aiyun Guo and sister Weiwei Tan warm up the dark and endless winter in northern land. Thanks to my father Bingli Tan who always gazes at me from sky. Now, I think I am standing on the right spot as his expecting. A special thanks to Dr. Juan Han for her continuous encourage and support.

A lot of thanks to my colleagues whose give nice and relaxing chatting and discussion in Institute for Digital Communications (IDCOM) which make the research experience not that harsh. Many thanks to my friends in Edinburgh. They bring me the sunshine in gloomy weather.

Thanks guys in Inch Park Basketball Club for the weekly game. Thanks Blackford Hill for providing me peaceful walking place after work.

At last, I would acknowledge the support from UK/China Scholarship for Excellence for the financial support of my Ph.D. research.

Contents

List of figures

List of tables

Acronyms and abbreviations

2PN	Two-port network
ACG	Average channel gain
AF	Amplify-and-forward
AMR	Automatic meter reading
AWGN	Additive white Gaussian noise
CCo	Centre coordinator
CDF	Cumulative distribution function
CDMA	Cumulative distribution function
CPDF	Complementary probability distribution function
CSI	Channel state information
CR	Chain rule
CSMA	Carrier sense multiple access
DB	Derivation box
DF	Decode-and-forward
DMT	Discrete multi-tone
DR	Demand response
DSTBC	Distributed space time block coding
DSP	Digital signal processing
GEV	Generalised extreme value
HAN	Home area network
HDTV	High definition television
IAT	Interarrival times
LAN	Local area network
LDPC	Low-density parity-check
LMMSE	Linear minimum mean square error
LS	Least-square
LTE	Long term evolution
MAC	Medium access control
MC	Markov chain

MIMO	Multiple-input and multiple-output
OFDM	Orthogonal frequency-division multiplexing
PDF	Probability density function
PLC	Powerline communications
PSD	Power spectrum density
PSK	Phase-shift keying
QoS	Quality of service
RX	Receiver
RMS-DS	Root-mean-square delay spread
SNR	Signal noise ratio
STC	Space time coding
TDMA	Time division multiple access
TLT	Transmission line theory
TWAC	Two-way automation communications
TX	Transmitter
VoIP	Voice over Internet protocol
WGN	White Gaussian noise
WiMAX	Worldwide interoperability for microwave access
xDSL	X digital subscribe line

Nomenclature

$\mathbf{A}$	Transmission/reflection coefficient matrix
a_{ij}	Transmission/reflection coefficient between the directional segment j and the directional segment i
$\overline{A_k}$	Amplitude of the kth narrowband interference
$A_i(t)$	Impulse shape of the ith reflection
$A(f, d_i)$	Impulse shape of the path with d_i propagation distance
$\overline{B_k}$	Parameter of the exponential function of the ith narrowband interference
C	Channel capacity
$C^{'}$	Capacitance
d_{ratio}	Disturbance ratio of impulse noise
$\mathbf{D}(f_x)$	Transfer diagonal matrix on frequency point f_x
e	Natural logarithm
E_m	Channel estimation error vector
$\overline{f_{(0,k)}}$	Parameter of the exponential function of the ith narrowband interference
$\overline{f_1}$	Parameter of the exponential function of the background noise
$f_{IAT}(k)$	The CPDF of the IAT width
$f_w(k)$	The CPDF of the impulse width
g_k	Amplify factor on the kth subcarrier for single relay node unidirectional protocol
$g^k_{bi_{2step}}$	Amplify factor for the 2-step bidirectional AF protocol on the kth subcarrier
$G^{'}$	Conductivity
$\mathbf{G}$	Transition probabilities matrix of impulse states
$g_{i,j}$	Transition probability from ith impulse state to impulse jth state
H^{ls}_m	Least-square (LS) estimation of channel vector
$\widehat{h}^k_m$	LS estimated channel gain on kth sub-carrier
$\widehat{H}_m$	The estimated channel based on LMMSE estimation criterion
h^k_m	Real-world channel gain on the kth subcarrier in the channel estimation process
$\mathbf{h}(t)$	Time domain channel impulse response

h_{xy}^{k}	Channel gain of kth subcarrier of x to y link
H	Average channel gain on frequency domain
$\widehat{H}_k(f_x)$	Estimated channel gain on on frequency point f_x in kth iteration
$\overline{I}$	The current on the two port network
I_i	Magnitude of ith path
I_{input}	Input current of the two-port network
I_{output}	Output current of the two-port network
l	Length of the two-port network segment
$\mathbf{L_{TC}}$	Length matrix of the terminal nodes and internal nodes
$\mathbf{L_{CC}}$	Length matrix of the internal nodes
$\mathbf{L_{TOT}}$	Complete length matrix
$L^{'}$	Inductance
L	Segment length vector
$\mathbf{L_L}$	Connectivity matrix
$\overline{N}$	Number of the narrowband interferences
$\overline{N_0}$	Power density of background noise floor
$\overline{N_1}$	Parameter of the exponential function of the background noise
N_{imp}	number of impulses noise
N	Power of noise on the node
N_o	Power spectrum density of noise
N_{on}	Noise power spectrum density on nth subcarrier
$\mathcal{N}(\mu_{i,k}, \sigma_{i,k})$	Gaussian distribution of the $i$the class and kth cluster
$p_{i,j}$	The transition probability from state i to state j
$p_{i,j}^{'}$	Transition probability after rate conversion
P	Transmission power
P_n	Power spectrum density on the nth subcarrier
$\mathbf{P}$	Transition probability matrix of Markov Chain
$\mathbf{P}(f_x)$	Reection/transmission matrix on f_x frequency point
$\mathbf{P}_U$	Probabilities matrix of the staying in idle states
$\mathbf{P}_G$	Probabilities matrix of the staying in impulse states
$\mathbf{P}_{UG}$	Probabilities matrix of transit from idle to impulse
$\mathbf{P}_{GU}$	Probabilities matrix of transit from impulse to idle
r_{imp}	Impulse rate of impulse noise

$R^{'}$	Resistance
R_{xy}	Bit rate of x to y link
R_{xyz}	Bit rate of x to z link via node y
$\overline{R}_{xy}$	Bit rate of x to y link with channel estimation error
$\overline{R}_{xyz}$	Bit rate of x to z link via node y with channel estimation error
$R_{uni\_DF}^{single\_invalid}$	Data rate of the signal relay decode-and-forward protocol with invalid direct link
R_{2nd}^{valid}	Data rate of the second phase signal relay decode-and-forward protocol with valid direct link
$R_{uni\_DF}^{single\_valid}$	Data rate of the signal relay decode-and-forward protocol with valid direct link
R_{1st}^{multi}	Data rate of the first phase of the multiple relay DF protocol
R_{2nd}^{multi}	Data rate of the second phase of the multiple relay DF protocol
$R_{uni\_DF}^{multi}$	Data rate of the multiple relay DF protocol
$R_{uni\_AF}^{single}$	Data rate of the amplify-and-forward protocol
$R_{bi\_DF}^{3step}$	Data of the 3-step bidirectional DF protocol
$R_{bi\_DF}^{2step^{'}}$	Data of the 2-step bidirectional DF protocol when decode the arbitrary terminal first
$R_{bi\_DF}^{2step^{''}}$	Data of the 2-step bidirectional DF protocol when decode the the other terminal first
$R_{bi\_DF}^{2step}$	Data of the 2-step bidirectional DF protocol
$R_{bi\_AF}^{t_1rt_{2_{3step}}}$	Data rate of one of the data stream in 3-step bidirectional AF protocol
$R_{bi\_AF}^{t_2rt_{1_{3step}}}$	Data rate of the the of the data stream in 3-step bidirectional AF protocol
$R_{bi\_AF}^{bb3step}$	Data rate of the 3-step bidirectional AF protocol
$R_{bi\_AF}^{t_1rt_{2_{2step}}}$	Data rate of one of the data stream in 2-step bidirectional AF protocol
$R_{bi\_AF}^{t_2rt_{1_{2step}}}$	Data rate of the of the data stream in 2-step bidirectional AF protocol
$R_{bi\_AF}^{2step}$	Data rate of the 2-step bidirectional AF protocol
R_{HH}	Covariance matrix of channel vector
$\overline{R}_{uni\_DF}^{invalid}$	Data rate for the single relay DF protocol with invalid direct link and channel estimation error
$\overline{R}_{uni\_DF}^{valid}$	Data rate for the single relay DF protocol with valid direct link and channel estimation error

$\overline{R}_{DF}^{3step}$	Data rate for the 3-step bidirectional DF protocol with channel estimation error
$\overline{R}_{2S}^{t_2rt_1}$	Data rate for t_2 to t_1 data stream of the 2-step bidirectional DF protocol with channel estimation error
$\overline{R}_{2S}^{t_1rt_2}$	Data rate for t_1 to t_2 data stream of the 2-step bidirectional DF protocol with channel estimation error
$\overline{R}_{bi\_DF}^{2step'}$	Data rate for the 2-step bidirectional DF protocol when decode arbitrary terminal first with channel estimation error
$\overline{R}_{bi\_DF}^{2step''}$	Data rate for the 2-step bidirectional DF protocol when decode the other terminal first with channel estimation error
$\overline{R}_{bi\_DF}^{2step}$	Data rate for the 2-step bidirectional DF protocol with channel estimation error
ΔR	The data rate gap between imperfect channel estimation and perfect channel estimation
$R_{imp\_channel}$	Data rate with imperfect channel estimation
$R_{p\_channel}$	Data rate with perfect channel estimation
S	Power of signal
$S_{nn}^{M}(f)$	Power spectrum density of the background noise
SNR_{xy}^{k}	Signal to noise ratio of x to y link on kth subcarrier
$SNR_{AF_{invalid}}^{k}$	SNR of the single relay AF protocol with invalid direct link
$SNR_{AF_{valid}}^{k}$	SNR of the single relay AF protocol with valid direct link
$SNR_{AF\_multi}^{k}$	SNR of multiple relay node AF protocol on kth subcarrier
$\{SNR_{AF}\}_i$	SNR of the achieved from the ith achieved from relay node in multiple relay AF protocol
$\overline{SNR}_{xy}^{k}$	Signal to noise ratio of x to y link on kth subcarrier with channel estimation error
$t_{w,i}$	The time duration of the ith impulse noise
$t_a^{'}$	Target sampling interval
t_a	Original sampling interval
T_{win}	Observing window
$\mathbf{T}(f)$	The transmission function of the cascaded 2PNs
$\overline{\mathbf{T}}$	Transmission coefficient matrix of cascaded 2PNs
$\mathbf{T_s}$	Transmission matrix of the shunt segment

$\mathbf{T_f^i}(f)$	Transmission matrix of the ith segment in the cascaded 2PNs
$\overline{U}$	The voltage on the 2 port network
$\mathbf{U_U}$	Index matrix
$\mathbf{U}$	Transition probabilities matrix in idle state
$\mathbf{V_k}(f_x)$	The n_0th column of $\mathbf{P}(f_x)$
v_p	The propagation of the velocity of the electromagnetic waves in the cable
V_1	Input voltage of the two-port network
V_2	Output voltage of the two-port network
W	Channel bandwidth
Z_L	Load impedance of on terminal
Z_o	Characteristic impedance of the current directional segment
Z_{in}	Input impedance
$\mathbf{Z_{TC}}$	Characteristics impedance matrix
$\alpha(f)$	Real part of the complex propagation constant
β	Image part of the complex propagation constant
γ	Complex propagation constant
Γ	SNR gap
$\delta(t)$	Impulse function
ϵ_m^k	Channel estimation error for the mth pilot in the kth sub-carrier
ϵ_{xy}^k	Channel estimation error of link x to y
ρ	Reflection coefficients
Θ_m	Variance matrix of the noise for the mth pilot on the receive terminal
τ_{m_0}	The transmission coefficient at the junction of the end directional segment m_0
τ_i	The propagation delay of the ith path
τ_{xy}	Transmission coefficient
φ_i	Weight factor of the ith path
σ_k^2	Noise power on kth sub-carrier
ω	Angular velocity
$diag[\cdots]$	To form a diagonal matrix
$(\cdot)^{\mathbf{T}}$	Transpose operator for matrix
$\lceil\cdot\rceil$	rounds the elements of X to the nearest integers towards infinity
$[\cdot]$	Round towards nearest integer

$\lvert \cdot \rvert$	Absolute value operator
$\hat{\cdot}$	Means the estimated value

Chapter 1
Introduction

1.1 Powerline Communications and Its Applications

Powerline Communications (PLC) is a concept that uses the electrical power delivery network as the information transmission medium. The technology was first developed in the early 20th century for simple remote control purposes and telephony [1]. But for a long period, PLC was not considered as a mainstream communications technology due to the fact that the power delivery grid is not a proper transmission medium for high frequency signals. The transmission capacity is limited by the signal power attenuation and deep fading induced by the multipath propagation.

Benefiting from the highly developed signal processing technologies in the communications field and more powerful processing components, research on PLC has been revived in recent decades. The demand for home area networks (HAN) and information infrastructure for the power delivery system are strong driving forces for research on PLC. As an underutilised communications medium with strong potential, PLC has recently drawn attention from both academia and industry. The research covers channel and noise characteristics investigation and modelling along with modulation and coding schemes for combating the hostile transmission environment. Besides physical layer technologies, Medium Access Control (MAC) schemes [2] are also being assessed for adapting the power grid topology and applications. According to the current work on PLC, the frequency signal over power cables suffers from multipath propagation which will cause deep frequency selective fading if broadband transmission is used. In order to model the PLC channel, two widely accepted deterministic methods are proposed according to multipath propagation properties and transmission line theory respectively. Then multi-tone modulation, for example Orthogonal Frequency Division Multiplexing (OFDM) and the related pulse OFDM [3] and wavelet OFDM [4] are proposed for data transmission over the power grid. Plus with channel coding, channel estimation and synchronisation specially designed for the PLC, high speed data communications over both broadband and narrowband PLC channels become feasible and a series of standards are proposed for different application scenarios, for instance, Homeplug AV series, IEEE 1901 and ITU-T G.hn.

According to differences in the utilised frequency bandwidth, communications over power grid can be categorised into narrowband and broadband PLC that can be found in [5] and [6]. The narrowband PLC has been available for a long period. Though only limited bandwidth is utilised, narrowband PLC still can cover a large range of applications. For example, electric equipment monitoring, home automation and telemetry within the a bandwidth of less then 200 kHz. In recent years, with the increasing management demands on energy distribution networks, the narrowband PLC start to carry higher date rate applications such as: automatic meter reading (AMR), load management, even customer billing and contract management. Though the bandwidth is limited, narrowband PLC can be also used the Internet access. Beyond narrowband applications, broadband internet communications is also an important applications field. The first proposed broadband application of the PLC is Internet Access which benefits from the universal accessibility of the power grid in house and building. Besides Internet Access, the Home Area Network (HAN) is a major application area of broadband PLC. A very mature application of HAN which employs the power grid in the house to extend WiFi signals for improving WiFi coverage quality has been on market for years. With the increasing demand for home entertainment and applications, a series of the broadband applications such as high definition television (HDTV), home audio distribution and video gaming are proposed as PLC applications. Also, the data for smart metering, energy saving and load management can also be carried by broadband PLC. Though there are variety of potential applications, PLC is still not a widely deployed technology in practice. Thus, research on communications technology over power grid is needed for pushing the PLC technology from laboratory to application.

1.2 Motivation and Contributions

1.2.1 Motivation of Work

As an access network or a local area network technology, the evolution pace of PLC is much slower then wireless communications or other xDSL technology. The reason for this phenomenon is the lack of research and standards for communications over power grid. Comparing the traditional communications media such as the wireless channel, fiber or communications cables, the power grid has harsh transmission conditions for wide bandwidth signals, for example, a highly frequency selective fading channel, signal attenuation, coloured background noise and random occurred impulse noise. Due to these adverse facts, both academia and industry did not consider power grid as a medium for a long period. Thus, lots of topics in PLC is need to

be exploited. The topics includes the channel and noise modelling methods, modulation and coding schemes for frequency selective channels, synchronisation for the PLC network, as well as the medium access control technologies.

Among the topics, channel modelling for broadband PLC and relay enhanced PLC network are selected as in this work. The reason for choosing channel modelling is that a proper channel model is foundation of the communications research. Thus, a reliable and simple channel model is necessary for PLC. Two deterministic channel modelling methods have been developed late in the 1990s: the multipath model and the transmission line theory (TLT) model. However, the usage of these two models is limited by the fact that they require the network topology information and electrical properties of the cable as the precondition which obstructs wide application of the models. Thus in this work, a statistical channel is proposed to avoid these problem. They present the PLC channel characteristics as accurately as the deterministic models with a faster computation process.

Besides the channel model, another challenge of PLC is how to adapt it to variety of application scenarios. As mentioned before, PLC has to fulfill different data rate, coverage and robustness in different applications. The adverse transmission environment of the power grid limits the bit rate and coverage range of PLC. Thus, the relay which has been applied in wireless communications for gaining spatial diversity, increasing the overall system capcity and expanding the network coverage is introduced to enhanced in PLC. Considering the fact that there are transformer stations, deviation boxes and unoccupied sockets that can be potential locations to place relay nodes, relay enhanced PLC networks are proposed in this work for the purpose of exploiting communications capability over power grid.

1.2.2 Contribution

A series of the contributions were made in the process of accomplishing the proposed works:

First, the consistency of the multipath and TLT channel modelling methods was first verified. In previous research papers on PLC channel modelling, the authors only focused on the multipath or the TLT channel model, then the general properties such as frequency selective fading, and attenuation are presented. But there is no work to check the exact consistency of the these two methods. The reason for this is that most of the previous works were done separately by different researchers using different topologies and cable electrical parameters. In this thesis, the two

model are first verified for consistency. Also, some other important factors that will impact the channel characteristics, for example, length and density of the branches, are identified in this work.

Secondly, a statistical channel modelling method is proposed for the indoor PLC network. In this work, the random distributions of the multipath parameters such as the magnitude of the path, the path interval, and the number of paths are investigated. By doing so, the randomness caused by the topology and load are converted into a series of probability distributions which can be represented by a set of parameters. With the statistical model, prior knowledge of network topology and physical cable parameters are not necessary. Also, the method used for extracting the distributions parameters can be applied to for different scenarios. The work has been summarised as a journal paper submitted to IET Communications.

Thirdly, a set of the relay protocols are proposed for broadband PLC networks. The protocols cover major aspects in relays, including the forwarding mode (decode-and-forward or amplify-and-forward), the number of the relay nodes and the directions of the data streams. The performances of the protocols are simulated and analysed under the PLC transmission environment. The facts which will help to increase the transmission capacity of the PLC network are pointed out. The capacity performance of the protocols with imperfect channel information are also investigated. This work has already summarised and published in the ICC 2011 and EUSIPCO 2011 conferences respectively. Based on the relay enhanced PLC, the research work on relay enhanced communications for power grid has been extended to wireless aided smart grid communication which has been published on IEEE Communications Magazine 2012.

1.3 Thesis Organisation

This thesis is organised as follows:

Chapter 2 gives the general history of the technology evolution of powerline communications and the current standards. In the last part of this chapter, the performance evaluation method used for evaluating replay protocol performance is introduced.

In Chapter 3, the multipath and TLT channel modelling methods are implemented and compared. The consistency of the methods are verified. In addition, noise modelling is also reviewed and implemented in this chapter. The channel and noise models in this chapter are the

foundation of the research work of Chapters 4 and 5.

Chapter 4 describes the statistical channel modelling method in detail. The characteristics of the first arrival path is emphasised, and a channel classification method is proposed according to the magnitude distribution of the first arrival path. Then, the path interval and magnitude of each channel class derived. Finally comparisons of the statistical model and the deterministic model shows that the proposed model can present consistent channel characteristics as accurate as the previous models.

In Chapter 5, relay protocols for PLC are described and compared. The existing researches of relays for PLC is reviewed. Then, relay protocols are described and the corresponding capacity performance is simulated based on the channel and noise implemented in the previous chapters. The relay approaches that will benefit to PLC capacity performance are discussed based on the simulations results. Also, channel estimation error impact on the relay enhanced PLC is investigated and the optimised channel estimation pilot length is discussed.

Chapter 6 summaries this thesis. Furthermore, three following up works: a new statistical channel modelling methods, multi-user PLC relays, and relays for the narrowband PLC are proposed for the future research.

Chapter 2
Background

The power grid is the most widely deployed network on earth. Except for electrical power transmission, the power grid can be also treated as the information exchange medium. The concept of transmitting information over power cables is known as powerline communications. With the development of the communications technology, powerline communications now covers a large range of communications scenarios which includes Internet Access, home area network (HAN) and Smart Grid communications. In order to exploit the potential of powerline communications, recent research into PLC has considered channel modelling, modulation, channel coding, synchronisation, and relay for PLC. Among the research topics in PLC network, we pay close attention on channel modelling and relay in this thesis. A proper and effective channel model will be the foundation of the research, such as the modulation and channel coding schemes are determined by the frequency selective fading channel characteristics in the power grid. To enhance the coverage and capacity of the PLC network, relays can be used to enhance the current PLC network. This chapter provides the general history and current standards of PLC, channel characteristics, relays for PLC and performance evaluation methods.

This chapter is organised as following: Section 2.1 introduces the general development and standards of PLC. Channel characterstics and modelling method is introduced in Section 2.2. Demand of relay in PLC and the performance evaluation method are analysed in Section 2.3. Section 2.4 summarises the chapter.

2.1 Communications Over Powerline

2.1.1 General History of Powerline Communications

In 1920s, voice over powerline was developed [7]. During the 1940s, the powerline has been used for the first time as the medium for digital communications [8]. The main purpose of the powerline communications during this period is sending control signals in automation products at a very low data rate. In the 1970's [9], an experimental bi-directional information facility

was built for connecting hundreds of devices. Also, a commercial distribution line communications system over 5-10 kHz was developed by General Electric Company at a similar time [10] when the channel and noise characteristics of powerline was first studied in detail. Later on, a local area network (LAN) over power grid solution was proposed for personal computer communications with basic phase-shift keying (PSK) in physical layer and carrier sense multiple access (CSMA) in MAC layer. In [11] a study in 1990 in the UK proved that a 1 bits/s/Hz average information rate can be approached for remote meter reading. Furthermore, low data rate two-way automation communications (TWAC) schemes are proposed using time division multiple access (TDMA) and code division multiple access (CDMA) modes in [12] and [13] for the AMR/AMI, distribution automation and demand response (DR) applications.

Driven by the growing demand for Internet access, digital signal processing (DSP) and very-large-scale integration (VLSI) technology, the research and application of PLC was expanded to broadband communications during late 1990s and early 2000s, The first PLC Internet access trial was developed by Nortel and Norweb Communications [14] in UK in 1997 with a 1 Mb/s data rate. The trial was ended in 1999 because of the electromagnetic compatibility issues. Recently, efforts on powerline Internet Access have been developed by the Open PLC European Research Alliance (OPERA). Beyond Internet Access, the interest of broadband PLC applications are starting to shift to in-home applications such as home area network (HAN), HDTV and other in-home entertainment. As a precondition for the analysis of any communication system, channel models for broadband PLC has been studied intensively in the last decade. The broadband PLC channel is considered as a frequency selective fading, multipath channel, which is described in [15], [16] and [17]. A well known multipath channel modelling scheme is proposed by Dostert in [18] in 2002. Some researchers have proposed deterministic channel modelling methods according to the transmission line theory in [19] and [20]. In order to exploit the potential of PLC, Zeddem proposed a frequency domain statistical channel model which extends the frequency band from 30 MHz to 100 MHz. Then, in [21] and [22], authors start to pay attention to the time domain statistical properties PLC channels. Based on a results from the broadband channel model, a series of broadband applications are proposed and communications products have been launched in the last decade years. So far, powerline extenders for in-door wireless communications have been popular products on the market. Broadband PLC communication trials have been carried out in several countries and districts [11], [23] for Internet access. The broadband PLC channel provides the possibility for a variety of other applications such as HAN, HDTV, in-home audio system and energy management which are

included in the Homeplug AV series standard [24].

Besides market demand, another important driving force for broadband communications over powerline is the development of the digital signal processing technology for the communications. In early products, spread frequency shift keying was used for narrowband, low data rate PLC [25]. For the broadband PLC channel, single tone modulation which is called wideband impulse modulation in [26] can be also applied with the CDMA and bit-interleaved coding. Considering the frequency selective fading effects in the broadband PLC channel, the single tone modulation may not have the ability to adapt to the effect of deep fading at particular frequencies. Thus the multi-tone modulation is proposed in [27] and [28] for the broadband PLC. In order to combat the colored background noise, pulse shaped OFDM is proposed in [3] and [29]. Filtering multi-tone modulation and wavelet OFDM are also applied in [30] and [31] for similar purposes. Along with modulation techniques, the coding schemes are also proposed for combating another significant impairing in PLC channels - impulse noise. Since impulse noise often causes bursts of errors for the communications system, the first coding scheme for PLC is interleaving which has been introduced in [32]. Also, Turbo code and low-density parity-check (LDPC) code have been proved superior in the PLC impulse noise environment [33] and [34]. In [35], the oversampled filter banks (OSFB) is applied as channel coding to combat the correlated noise in PLC. With the advantages of the above modulation and coding technologies, high data rate broadband communications over powerline has been a well accepted solution for many scenarios.

In recent years, driven by the increasing energy saving and information managing requirements, communications over and for the power grid which is also called Smart Grid communications (SGC) has emerged as an important technology. Among all the possible communications solutions such as Long Term Evolution (LTE), Worldwide Interoperability for Microwave Access (WiMAX) and ZigBee, PLC is one competitive candidate because of its natural combination with the power grid. As introduced in [36], PLC can play lots of different roles in the Smart Grid, for example, automatic meter reading (AMR) and advanced metering infrastructure (AMI), Vehicle-to-Grid Communications, Demand Side Management, in-home entertainment and in-vehicle communications [37] and [38] or communications inside of space shuttle [39]. The narrowband PLC performance for long distance Smart Grid communication is evaluated in [40] with assistant of filter bank based transceivers. The potential range of the PLC applications is described by the following Figure 2.1:

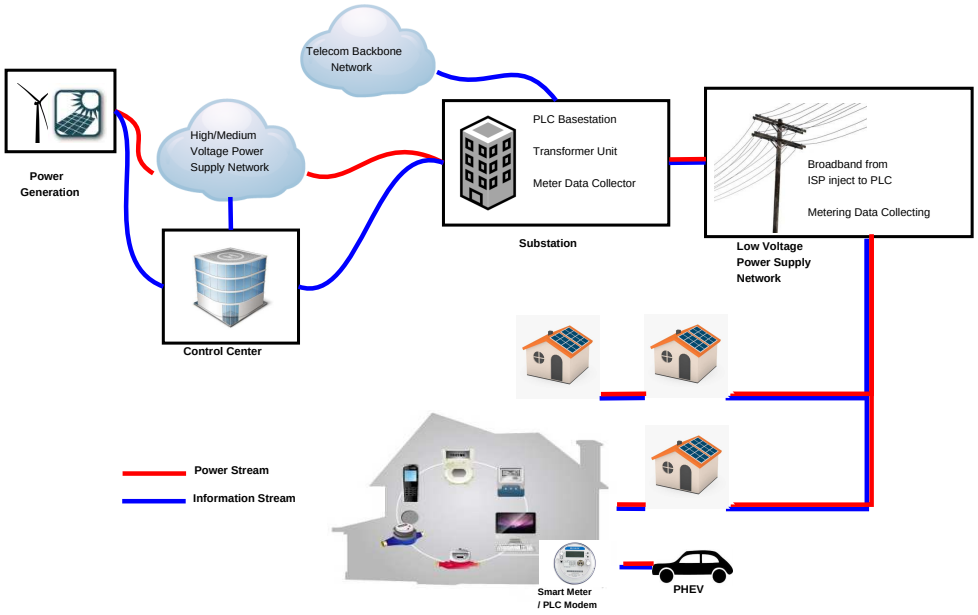

Figure 2.1: *A panoramic view of current PLC applications nowadays. PHEV: plug-in hybrid electric vehicle, ISP: Internet service provider*

2.1.2 Powerline Communications Standardisation

Generally, PLC is classified into the narrowband and broadband communications that supported by series of the standards which are promoted by different organisations for different purposes.

Narrowband Standards

Although there are some other technologies which operate at very low frequencies, usually 0.3-3 khz, this band range is not considered by current standards. At present, typical operational bandwith includes European Committee for Electromechanical Standardisation (CENELEC) bands (3-148.5kHz) which divided in to A, B, C and D sub-bands, US Federal Communications Commission (FCC) bands (10-490 kHz), Japan Association of Radio Industries and Businesses (ARIB) (10-450 kHz) band and Chinese bands (3-500 kHz). The standards for narrowband communications includes ISO/IEC 14908-3 (LonWorks) which supports data rate to 5.4 and 3.6 Kbit/s, ISO/IEC 14908-3-5 (KNX) which supports 1.2 and 2.4 Kbit/s data transmission and CEA-600.31(CEBus) which operates at 10 Kbit/s mentioned in [41] and [42] for low data rate narrowband communication. ITU-T G.hnem which nominal raw bit rates may exceed 1 Mbit/s [43] and IEEE 1901.2 which reaches up to 500 Kbit/s are proposed recently to provide higher data rates for energy management in HAN, plug-in/hybrid electric vehicles (PHEV) and advanced metering infrastructure (AMI) applications. Also, another OFDM based

standard which is called G3-PLC which reaches 300 kbit/s and supports the IPv6 protocol is recently released for FCC, CENELEC and ARIB bands. Another standard which is designed for intelligent metering applications called PoweRline Intelligent Metering Evolution (PRIME) is reported performing ranging from 21.4 Kbit/s to 128.6 Kbit/s on CENELEC A band. The standardisation of the narrowban PLC communications is still in evolution due to the fact that the new applications are continuously proposed for PLC.

Broadband Standards

Communications over HF/VHF bands (1.8-250 MHz) are usually defined as broadband Powerline Communications. Nowadays, most work on broadband communications performance over the bandwidth up to 30 MHz has been investigated comprehensively for channel modelling, transmission schemes and network structure aspects. More recently, channel modelling for up to 100 MHz bandwidth has been studied in [44] and [45]. Following evaluation with broadband channel models, a series of industrial standards have been released in the last few years..

1. **TIA-1113/HomePlug**

   The first standard for broadband powerline communications is TIA-1113 [46] which is approved by ANSI. The standard defines a 14 Mbps OFDM based physical layer according to the HomePlug 1.0 [47] and [48]. In the standard, the two modulation scheme, BPSK and QPSK, are proposed to adapt the data rate according to the channel conditions. These two standards have proved successful by in widely used products in the home and industry. Following HomePlug 1.0, HomePlug AV is released in August 2005 which reaches 200 Mbps that sufficient for HDTV and VoIP applications. And a 500 Mbps transmission is achieved with HomePlug AV by using a wider spectrum (2 to 68 MHz). Most recently, HomePlug AV2 is released in 2012 which is target for Gbps transmission and supports MIMO channel. HomePlug AV2 is a standard that is interoperable with HomePlug AV and compatible with IEEE 1901.

2. **IEEE 1901**

   The IEEE 1901 standard was approved in 2010 for high speed HAN and Internet access applications with data rates in exception of 100 Mbps operating over a 30 MHz bandwidth. The main features of the IEEE 1901 standard is described in [49], [50] and [51] and it includes two different physical layers. The first option is called the FFT PHY which combines FFT-OFDM modulation and a convolution turbo code (CTC) as forward error correction (FEC). This option provides backward compatibility with HomePlug AV

based devices. The second option is the Wavelet PHY which employs Wavelet-OFDM concatenated with Reed-Solomon (RS) or Convolution codes, with the option to replace by LDPC code. This option provides backward compatibility for devices based on the High Data Rate PLC Alliance. The new physical layer techniques push the PLC physical layer data rate up to 200 Mbits/s. In addition, IEEE 1901 also provides mandatory coexistence mechanism with other devices with different in the physical layer in the network. Thus, it is big step towards a wider home networking market for PLC.

3. **ITU-T G.hn** approved in 2009 [52], provides unified HAN transceiver capability over all the home cables: phone line, coax and Cat 5 cables can operate to 1 Gbps with this physical layer standard. The effort of the ITU-T G.hn is to design a single transceiver that adapts to all wiring data transmission media. In the physical layer, G.hn is based on FFT-OFDM modulation scheme concatenated with LDPC FEC code.

2.1.3 Challenge of PLC

The first practical challenge encountered in PLC is signal coupling which means it is difficult to extract the high frequency signals from the mains current. The coupling circuit designed for broadband PLC can be found from [53], [54], [55] and [56]. However this topic is out of the scope of our work. In this thesis, we assume the perfect signal coupling is made over the expected frequency band. Another obvious challenge in PLC is coexistence. As can be seen from the previous sections, a variety of standards are proposed for different kinds of applications. Currently, most of the standards are non-interoperable due to differences in the physical layer technologies applied. For example, Wavelet-OFDM, FFT-OFDM and spread spectrum are used for different standards. The details of proposed mechanisms can be found in [57], but coexistence mechanisms are out of the scope of this thesis. Another limitations in PLC is noise. According to [58], [59], [60] [61] and [62], the noise in power grid is a combination of coloured background noise, strong narrowband interference and random impulse noise. In [63] and [64], the influence of impulsive noise in PLC is shown through numerical results. Iterative impulse suppression algorithms, joint dipping-blanking and interleaved coding are proposed in [64], [65] and [66] to combat the impact of impulsive noise in PLC. Except for the challenges mentioned above, we focus on the channel modelling and relay extension of PLC for the following reasons: first, any research for PLC, especially, the reseach on deployment and communications theory approaches deeply depend on the channel model. But, there is still not

a widely accepted convenient channel model for PLC. Second, it is necessary to find new technologies to make PLC appliable in diverse scenarios, thus, making it a competitive candidate among the other communications solutions.

As can be seen from the above description, the proposed PLC standards are quite diverse. The reason for this situation is that the current reseach on PLC is mostly lead by industry who often wish to exploit their own technologies. For a long time, there has been insufficient work from academies to develop a common methodological approach for PLC. Among the problems facing PLC, accurate channel models are one of the most essential issues. So far, there is no commonly agreed channel model [67]. Based on the current research on the PLC channel, some obvious characteristics, for example, frequency selective fading, increasing attenuation with frequency and transmission distance of PLC channel have been pointed out. Some channel modelling methods proposed in [18], [68] and [69] have been widely used for PLC research. The proposed methods can model the attenuation and frequency selective fading of PLC channels very well. However, most of the current proposed methods are deterministic models, which means the channel model can be applied only with a given PLC network topology. While in practice, the network topology and some other properties such as terminal load and appliance switching will vary or are unknown from scene to scene. In order to capture the effects of different locations, the PLC channel should also have statistical property which is not present in the deterministic model. The topology of a typical in-door PLC can be seen in Figure 2.2. In

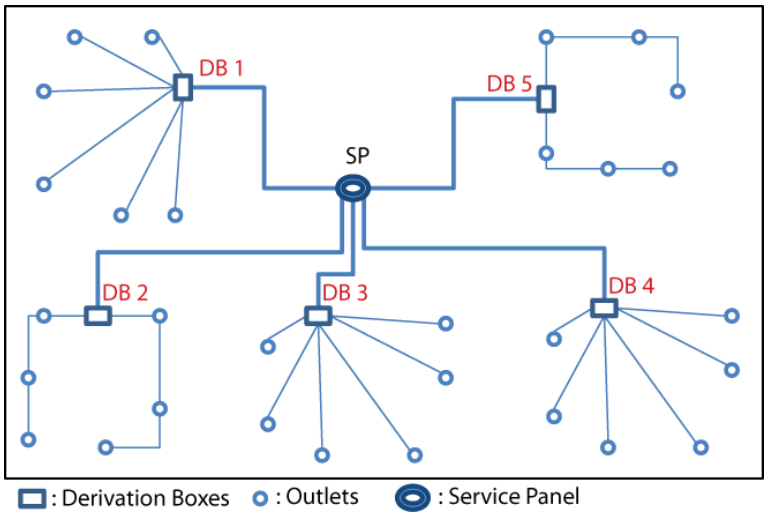

Figure 2.2: *A in-door PLC topology example*

practice, the length of the cables, the values of loads on outlets, also the number of derivation

boxes shown in Figure 2.2 are random which leads to the statistical properties of PLC channels. In [22], [70] and [71], some statistical properties are extracted. However, the research on channel models that include the statistical characteristics of the PLC channel is quite limited.

Besides the difficulties with the channel model, another challenge of the PLC technology is that PLC need to be adapted to variety of application scenarios. Based on the statement above, we can see that PLC can be used for both narrowband and broadband communications. Figure 2.3 shows a general relation between the bandwidth and coverage of different applications scenarios. The transmission capacity and network coverage of PLC are limited by a series

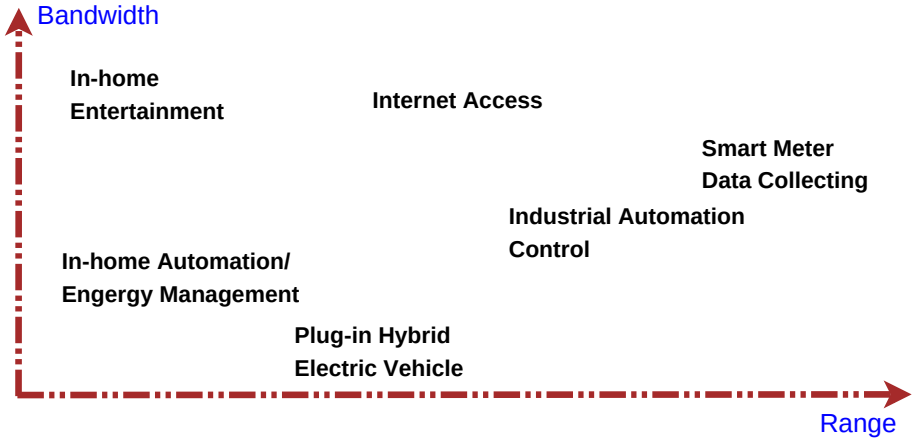

Figure 2.3: *Potential applications of PLC plotted VS bandwidth and range*

of facts. First, the transmitter power in restricted by regulation for the purpose of avoiding disturbance to other devices or communication systems. Meanwhile, the signals in power grid suffer from frequency selective fading, high attenuation, coloured background noise and impulse noises. To combat the above adverse effects, the technologies which have been used in wireless or other wire communications are also exploited improve the performance of PLC. The technologies that have been applied includes channel coding, multiple carrier modulation and channel estimation [72]. Even the MIMO concept is applied to improve the transmission capacity for PLC networks in [73] and [74]. But considering the correlation between different coupling modes [75] and spatial correlation discussed in [76], the performance gain brought by MIMO is limited. Another concept which is worth studies for PLC networks is Relay. Relays have been used in wireless communications to help increasing the capacity, link stability and network coverage by enhancing the receiving SNR and exploiting diversity gain. Thus the PLC network is proposed in this work. Though the diversity gain in relay enhanced PLC network

is difficult to achieve due to the correlation of the channel. It is still worthwhile to investigate the gain that can be potentially achieved through the SNR enhancement, and full duplex relay working mode.

In order to meet the challenges described above: effective channel model and diverse application scenario, two main issues - channel modelling methods and relay mechanism are studied in this work.

2.2 PLC Channel Characteristics and Modelling

Knowledge of the channel is a prerequisite of all communications technology research. In this section, the multipath characteristics of the PLC channel is introduced. Then, the challenges during channel modelling are stated as well.

2.2.1 Channel Characteristics

There has been a wide variety of research on individual PLC channels. The two most significant characteristics that can be summarised from the previous research are: frequency selective fading (multipath propagation) and attenuation.

In communication systems, the frequency selective fading is generally caused by the partial cancellation effect which is generated by delayed copies of the signal, which is also called multipath propagation. This concept has been used in radio communications for long time. In wireless communication, the receiver detects the direct signal and reflected signals from the other objects. The reflections can be regarded as the delayed and attenuated copies of the direct signal. These duplicates will cause deep null at some frequencies points due to the destructive interference between paths, which is also called fading. In the PLC environment, the signal power may be split among different paths at the junction boxes. These signals then will be reflected at the circuit terminal due to impedance mismatches. The reflected signal will then arrive at the receiver with a certain delay and attenuation. According to Fourier Transform properties, a delay in the time domain will cause a periodic phase shift in the frequency domain. When summing the direct signal and the phase shift reflection, notches may be generated at particular frequencies which is called frequency selective fading. For signals transmitted over networks, they will contains a series of reflected signals from the terminals, which will cause

notches in frequency domain. Figure 2.4 shows an example of multipath propagation for the PLC channel. Thus, the channel response can be written as the sum of the reflections:

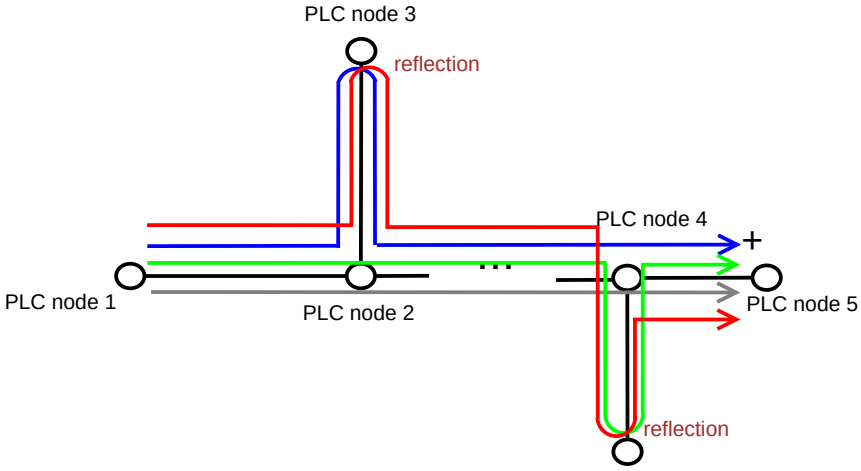

Figure 2.4: *A example of multipath propagation in PLC*

$$h(t) = \sum_{i=1}^{\infty} I_i A_i(t - T_i) \tag{2.1}$$

where, I_i is the magnitude of the ith path, and $A_i(t - T_i)$ is impulse of the ith reflection, T_i is the propagation delay of the ith path.

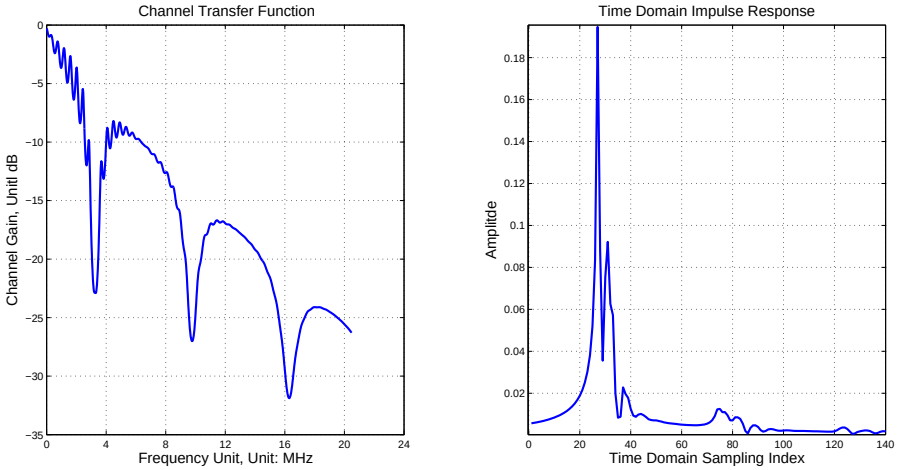

Figure 2.5: *a) Frequency domain transfer function and b) corresponding time domain impulse response of the example channel*

From the frequency domain channel transfer function in Figure 2.5, besides the frequency selective fading, another important characteristic of PLC channel is attenuation. As can be seen from previous work as [18], the attenuation will increase with the transmission distance and frequency. Unlike the fading characteristic, the attenuation of the PLC channel is mainly related to the electrical characteristics of the power cable. According to transmission line theory, the electrical characteristics of a cable segment can be described by four parameters: resistance, capacitance, conductivity and inductance, depend on the cable geometry, the electrical parameters of cable conductor and insulator, and the signal frequency. According to equation (A.3) in Appendix A, the resistance of the cable with a unit length inceases proportionality with the square root of the frequency. This property explains why the PLC channel causes larger attenuation for higher frequency signals. For the long distance transmission, the channel can be approximately considered as cascaded cable units, which also can be approximately as resistors if only signal attenuation issue is taken into account. Thus, the attenuation will increase with longer distance transmission.

The selective frequency fading and attenuation facts for a single PLC channel have just been described. However, in practice the channels do not always remain fixed. The channel response will be impacted by a series of random effects, for example switching on/off of appliances. Thus, the channel response contains some random properties, for example, deep fading frequencies and the depth of the fading may vary with time. On the other hand, PLC network topologies in different locations or buildings will be very different which will cause random fluctuation of the channel response. When we observe the PLC channels as group, they represent a random set rather than totally deterministic.

In wireless multipath channels, the delay and power of the multipath are usually very difficult to predict due to the complex scattering of the wireless signal propagation. Different fading types such as Rayleigh, Rician and Nakagami fading has been proposed for describing wireless communications. Contrasting with the highly random distributed and fast fading in wireless channels, the delay and power of the multipaths in PLC channel are more deterministic due to fact that the topology of PLC networks vary quite slow comparing with the wireless environment. Thus, A series of challenges is encountered when modelling PLC channel.

2.2.2 Channel Modelling and Challenges

Though PLC channel and wireless channel have similarities, the PLC channel has it own features for example, frequency selective fading with certain extent deterministic fact, quasi-static channel but with slow time variation and two dimension attenuation characteristics. Thus, to model a realistic PLC channel become a challenging topic. To obtain the transfer function of the PLC channel, different approaches have been developed the last few years. The method can be generally divide into two categories: the multipath approach and the transmission line approach.

For the multipath approach, the main focus is on figuring out the number of paths and corresponding path magnitude and delay. Currently, the multipath approaches are based on the field measurement results on a fixed network. That means we can only generate the channel responses for limited scenarios by the multipath model. For the transmission line approaches, more flexibility can be obtained. By applying the transmission line theory, the channel topology can be decomposed into small units. The transfer function for each unit can be calculated separately, then the channel response for the whole link can be obtained by using the Chain Rule (CR) in transmission line theory [68]. Theoretically, the transmission line approach can be applied to calculate the PLC channel response with an arbitrary given topology. However, the problem is that it is difficult to design an unified calculation process for different topologies. Thus if the transmission line approach is applied, the calculation process should be designed for each topology manually, which obviously a time-consuming task.

As can be seen from above description, the multipath model and the transmission line approach are both deterministic channel models. Only when the network topology is determined can these methods be applied to derive the PLC channel response. However, the deterministic channel models are not suitable for presenting the statistical properties of the channel. Thus, statistical PLC channel modelling method has recently draw attention. The statistical channel model, in theory, is necessary for evaluating the coverage, deployment and transmission capacity of PLC networks. It is obvious that the works on network coverage, channel coding and modulation techniques can not be evaluated according to one or two specific network situations. Thus, with the increasing demand for powerline communications, the statistical channel modelling is required to evaluate PLC performance across networks.

Though the work on PLC channel modelling is in demand, the challenges are also existing. The

first challenge is from the electrical parameters of the cable. In transmission line theory, the cable is often evaluated using the lumped parameters resistance (R), capacitance (C), conductivity (G) and inductance (L) which should be reconsidered in the high frequency scenario. Usually, the R, C, G and L parameters are determined by the geometric structure of the cable, conductor and insulator materials. The cable types used in different papers, such as [68], [77] and [69], are from different countries, which means that it is difficult to compare the modelling results from different papers. Also it is an obstacle to verifying the consistency of modelling results of different methods. Thus, finding a common set of cable parameters to prove the consistency of different modelling results become a challenging work. The second challenge is the topology. As stated above, the statistical channel property is arises from random variation of the topology across different homes and offices. The topology of the PLC network varies in different scenarios. For example, the topologies in residential and office areas, or the topologies in Europe, Asia and America. Thus, to find out the a proper topology for channel modelling is another key issue in PLC. Generally, the PLC network topology can be described by a tree structure [6]. Thus, the statistical property of the PLC channel results from the random branch lengths, terminal loads and switching on/off of appliances. It is difficult to collect this information of the PLC in practice. The third challenge for PLC channel modelling comes from the inconsistency of the previous research. For research in wireless communications, there have been already some channel fading types and models with common agreement, such as Nakagami, Rayleigh, Rician fading and Hata model for different terrains. Thus for the research results based on these channels can be directly compared with for each other. By contrast, the channel modelling work done for PLC networks is in quite diverse scenarios. Thus, it is time-consuming work to collect the detailed modelling information for different scenarios and to verify the correctness of the result in each paper.

2.3 Relays for PLC

With the development of channel modelling and data transmission technologies, communications applications over power cable are no longer limited to low data rate voice and control signalling. High bit rate over broadband applications such as audio, video, internet access and more complex compound control data are now in demand recently. For each application, PLC should provide a proper communication solution to adapt to the requirements. For example, Internet Access often covers video on demand and VoIP which require broadband connections

and high data rate. The in-home entertainment which includes home office networking, IPTV and video game streams also requires broadband connections and high data rates over power cables. Smart Grid is a comparable new and attractive concept in recent years which tries to inter-connect the electrical power network to control generation, transmission, distribution and consumption. It requires a large communications networks on top of the traditional power grid. The powerline which is naturally embedded in the power grid is the one of the candidate communication media for Smart Grid data. The applications over the smart grid include Smart meters, and home/industrial automation some more applications. These applications generally need robust, large coverage and two-way communications over power networks. For the in-vehicle communications network scenario, the PLC provides the communications channels for device command, control signals and multimedia service distribution between the central control module and the target parts in vehicle without extra communications facilities.

According to the above the statement of PLC application scenarios and the characteristics of the PLC channel, to implement those applications is a challenging task. The main challenges come from the aspects of capacity and coverage. The capacity requirement is pushed by high data rate applications such as Internet Access, IPTV and in-home entertainment. Nowadays, with the growth of video on demand, VoIP and online gaming services, Internet Access becomes even higher data rate scenario. For the in-home entertainment scenario, for instance HDTV can be up to 24 Mbps for a single stream. Thus, in order to guarantee the Quality of Service (QoS) of the these applications, PLC must provide enough data transmission capacity. As we know that the PLC channel suffers from both selective fading and inherently colored noise which limit the transmission distance. But in some scenario as shown in [78] the PLC devices may be located far from the data source or Centre Coordinator (CCo), especially in the Smart Grid scenario. Thus, to cover all the PLC devices in the power grid becomes another major challenge in PLC networks.

With the development of the new communications technologies such as channel coding, multi-carrier modulation, and radio resource allocations, the high speed data transmission over powerline has became possible, But the considering the diverse communications requirement in future, still some effort need to be done on PLC. In order to make PLC adapting to more applications, we study the concept of relays which has been extensively studied and proved helpful in increasing the network coverage and system capacity in the wireless channel environment in the power grid environment. In fact there are some physical locations, for example the deviation

box, transfer station, or even an unoccupied power socket on the wall, have potential to place a relay nodes in the power grid. In the wireless environment, the relay is often used for achieving the diversity gain in the radio channels. Unlike the wireless transmission environment, relays may not help in obtaining diversity gain due to the fact that the channels in PLC networks are not fully independent. But considering the frequency selective fading of PLC channel, the relay node has the potential to made up the data rate loss which is caused by the deep fading on the source to destination node link by exploiting the good channel conditions of the source to relay link and the relay to destination link. Thus, with the relay node and a proper bit allocation mechanism, the relay aided PLC network can support higher data transmission rate compared with direct data transmission. Another potential benefit brought by relays in PLC is that they can enhance the attenuated signal which has experienced long distance propagation. As stated above, the signal in PLC channel suffers high attenuation with transmission distance. In order to reach every possible PLC devices which may located far from the data source, placing some relay nodes to repeat attenuated signal is a possible solution to meet the challenge. A relay aided PLC scenario can be demonstrated by the following Figure 2.6 In Figure 2.6, if there is

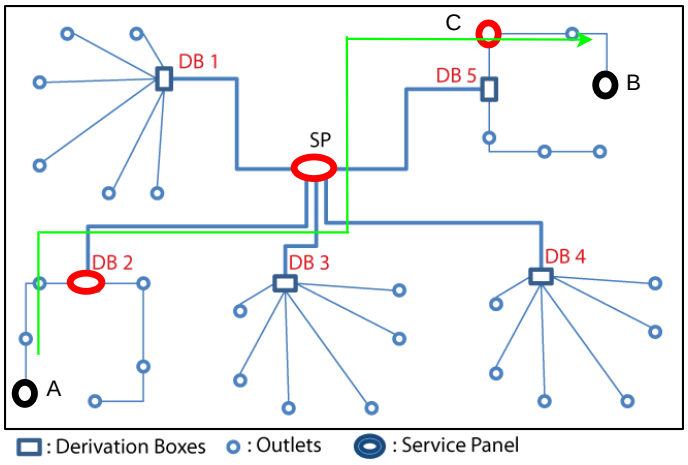

Figure 2.6: *Relay nodes location in PLC network*

a PLC device A which can not successfully transmit data to device B in a certain data rate due to the distance or fading problems, the nodes between these two devices, for example, outlet C, SP, DB2 or DB5, are all potential relay node to help A forward the data to B. With the help from the relay node, the transmission capability is extended.

2.3.1 Performance Evaluation Methodology

In this section, the methodology used for evaluating the performance in the relay protocols is explained. The methodologies introduced below are based on the frequency selective channel of PLC.

2.3.1.1 Discrete Multitone Method

The nature of discrete multi-tone (DMT) is to use a discrete value to demonstrate the continuous channel gain on each expected sub-carrier. By doing so, the whole bandwidth is divided into a group of subchannels, and the data can be allocated to the each subchannel according to the signal to noise ratio of this subchannel. Thus, a subchannel with a better channel gain can be fully utilised and a subchannel with worse conditions can have a lower data rate or be avoided totally if the error rate is too high. The following Figure 2.7 is an example of how DMT is applied: From the Figure 2.7, we can see that the modulation pattern on each

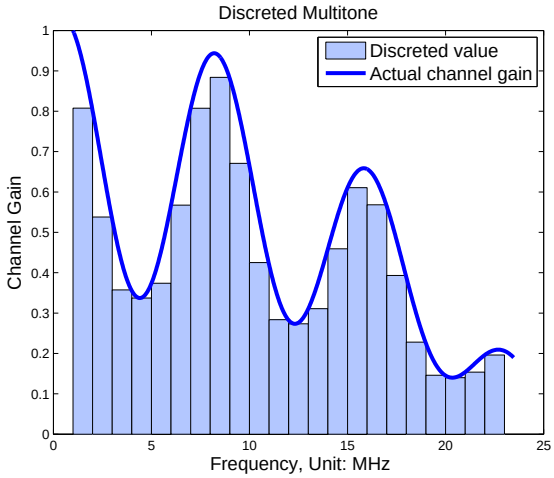

Figure 2.7: *Example of DMT in frequency selective fading channel*

subchannel can be adjusted according to the channel condition. This mechanism provides high flexibility for the channel with varying frequency characteristics, for example the frequency selective powerline communications channel. Combining with the multi-carrier modulation technology, for example, OFDM or DMT, different data rates can be easily allocated onto specific subchannels

2.3.1.2 Shannon Capacity for DMT System

As defined in [79] and used universally, the Shannon-Hartley theorem is used for evaluating the upper bound of capacity of communications system:

$$C = W \log_2 \left(1 + \frac{S}{N}\right) \tag{2.2}$$

where, W is the bandwidth of the channel measured in Hz, S and N are the signal and noise power measured in watts, while C denotes the upper bound on the data transmission capacity of the channel which is measured in bits/s. Also, the theorem is deduced based on the assumption that additive white Gaussian noise (AWGN) is present at the receiver. In some cases, the noise power is replaced by the spectrum power density N_o. Thus, equation (2.2) can be rewritten as:

$$C = W \log_2 \left(1 + \frac{P \cdot \mid H \mid^2}{N_o \cdot W}\right) \tag{2.3}$$

where, P is transmitting power, $\mid H \mid$ is the channel gain, N_o is the noise power spectrum density (PSD) and W is the bandwidth of expecting system.

But the above equations are not accurate enough to describe the channels with significant frequency varying characteristics and coloured noise which are two significant condition in PLC channels. As a frequency selective fading channel, it is hard to use a single $\mid H \mid$ to indicate the channel characteristics over the whole frequency range. Also, a single parameter N_o is not enough to describe the coloured background noise in PLC network. Thus, for the frequency selective channel, we can divide the the bandwidth into N subcarriers. Then, the achievable spectrum efficiency can be written as:

$$C = \frac{1}{N} \sum_{n=1}^{N} \log_2 \left(1 + \frac{P_n \cdot \mid h^n \mid^2}{N_{on}}\right) \tag{2.4}$$

where, P_n, h^n and N_{on} are the PSD of the transmitter, channel gain and PSD of the noise on the nth subcarrier.

2.3.1.3 The Achievable Data in Practice

In the last section, the Shannon capacity of the DMT system is given. But the in practice, the achievable data rate can not reach the upper boundary due to a series of the facts which will

cause information rate loss. The facts includes redundant bit introduced by channel coding, the noise induced by the channel estimation, the synchronisation overhead which is used for improving the link robustness and the bit error rate performance. Due to these facts, the factor Γ is induced here to evaluate the achievable spectrum efficiency in practice.

$$R = \frac{1}{N}\sum_{n=1}^{N}\log_2\left(1+\frac{P_n\cdot \mid h^n \mid^2}{N_{on}\cdot\Gamma}\right) \tag{2.5}$$

From the statement in [80], for the uncoded modulation system, the achievable spectrum efficiency is often 10dB less than the Shannon capacity. If convolution code is applied, the performance will be improved by 7 to 8dB. Thus, here we make the assumption that a loss $\Gamma = 3$dB is reasonable for practice.

2.4 Summary

In this chapter, the general history, current standardisation and the challenges of the powerline communications are described. An obvious conclusion from the above discussion is that the PLC will be an important candidate for the Smart Grid, in-home communication and Internet access. But, for the purpose of deploying a satisfactory PLC network for these scenarios, some challenges need to be resolved. The first issue is the channel modelling method which can express the statistical characteristics of PLC channels in some particular scenario. This kind of channel model will be helpful for the performance evaluation of the communications technologies in a universal channel environment rather than for one or two specific networks. Since the application scenarios of PLC are diverse, it is necessary to find a solution the to make PLC more adaptive for diversity of networks. Among the current data transmission methods, relays represent as one promising data forwarding scheme that can help increasing data rate and enlarge network coverage. In the following chapters, the traditional channel modelling methods are reviewed and compared, and a new statistical channel model is developed for PLC networks. Also, a series of the relay protocols are proposed and investigated in the PLC environment.

Chapter 3
Channel and Noise Modelling

Generally, two fundamental points are often investigated in research on a certain digital communications system: characteristics of the data transmission media and features of data transmission environment which can be identified as channel and noise respectively. As mentioned in the previous chapter, the PLC channel presents significant frequency selective fading characteristics. The reason for this phenomenon is multipath signal propagation. Multipath propagation directly lead to a PLC channel modelling method. In this type of channel modelling, the focus is describing the signal propagation behaviour in a tree type PLC network, and considering the overall channel as sum of multiple delayed paths. Another important approach investigates the channel features by dividing the whole network into the basic segments and computes the frequency domain transfer function of each segment based on transmission line theory. Thus, the transfer characteristics of the overall network can be considered as a series of cascaded segments. Besides the channel characteristics, the noise environment in power grid is different form the other communications medias. Unlike the additive White Gaussian Noise (AWGN) used in much communications research, the noise in the PLC network, often appears as a combination of slow varying colour background noise and fast changing impulse noise.

The transmission environment which includes the channel and noise characteristics is the foundation of the communications technology research over powerline networks. Some work has been done to model the power cable as communication channel in diverse network situations with various types of cables and different topology. Though these modelling results from different methods indicate the similarities on frequency selective fading and attenuation, there is no sign that these models lead to consistent channel modelling results. Thus, in this chapter, two main modelling methods are investigated and implemented to demonstrate consistency in the modelling results. The modelled channel model and the implemented noise model forms the foundation for other research on powerline communications in the later chapters.

The structure of this chapter is as follows: first, the literature review of the PLC channel modelling research is given in Section 3.1. Then, the multipath model method and transmission

line theory model are introduced in Section 3.2 and Section 3.3 respectively. In Section 3.4 the implementation result of the channel models are given and compared. In Section 3.5 the noise categories and approaching method for each category are demonstrated. At last, the conclusions of this chapter are given in Section 3.6.

3.1 Channel Characteristics and Model Review

In the beginning of this chapter the channel characteristics of the powerline communications and a literature review of the current channel modelling methods for PLC networks are described. The advantages and the limitations of each modelling method are also discussed. The scope of the communications channels over power cable investigated in this work is from 1.6 Hz up to 30 MHz which is the broadband channel in many research and standards.

For the PLC channels within frequency range, the multipath propagation characteristics and the signal attenuation are two obvious characteristics and described in many papers. In some other communications systems, especially wireless systems, the channel characteristics that vary over time are also an important topic. In PLC networks, the channel may stay stationary for comparably long time. Thus variability of the channel with time is not a significant topic in the literature as well as in this work.

Multipath Propagation Multipath propagation, known as the frequency selective fading in the frequency domain, in PLC networks is caused by reflected signals which result from impedance mismatch in the complex PLC networks. In [18], a simple PLC network is described to demonstrate the multipath propagation. Due to the existence of splitting during the signal propagation and the impedance mismatch on the end of the branch, some reflected signal from the branch end will arrive at the receiver with a time delay. Thus, a multipath propagation is formed. In [18], a mathematical channel model is also developed for a simple PLC network. In [81], the influence of the branch load impedance, length are discussed in detail, which will impact the strength and delay time of the paths.

Attenuation Besides multipath propagation, the other important property of the PLC channel is the attenuation. As described out in [18], the signal magnitude with attenuate with the propagating distance and frequency increasing. As described in [18], the signal attenuation is caused by the real part of the propagation constant which is controlled by the primary cable parameters such as resistance, conductance, capacitance and inductance.

All off these parameters are determined by the conductor, outer insulating materials and the geometry of the cable. Of course, the signal attenuation presents different characteristics at different frequencies since the resistance, conductance, capacitance and inductance are functions of frequency.

Time Variation The effect of time variation is not a significant objective of this work. Since the channel amplitude deeply depends on the network topology which will not change as frequently as the wireless channel, the channel state is likely to remain stationary for long time duration - seconds even minutes. But there are some papers investigating PLC channel time variation. The time variation of the PLC channel is mainly caused by the connected appliances which have synchronously load with the mains voltage and periodic change of the mains voltage, which is described in [82], [83] and [84] and called linear periodically time-varying (LPTV). The time variation is out of the scope of this thesis since it is not the major fact that impacts performance.

To model the powerline cable as the a broadband communications channel that presents the above characteristics, some modelling methods have been proposed in the years. The proposed channel modelling methods can be classified into three main categories: the multipath model, the transmission line theory (TLT) model and the statistical model. For the broadband communications scenario, the multipath model is first proposed to modelling the PLC channel. The most widely referred multipath modelling methods is proposed by Zimmerman and Dostert in [18] and [77]. In the proposed multipath model, the channel transfer function is considered as the summation of the selected paths with corresponding weight factors and propagation delays for each path. The path weight factors and propagation delays are determined by the network properties facts such as cable type, network topology and impedance load. In [18] and [77], the weight factor and delay for the selected paths are obtained through the analysing a large set of measurements. If the any of the network properties change, for example the network topology, the parameters for the multipath model would need to be recalculated. Then, Ding proposed a matrix based calculation method for the multipath model in [85]. In Ding's model, a universal calculation process is built by introducing a matrix which is used to demonstrated the topology of the PLC network, and changes on topology can be easily represented in the topology matrix. This mathod is introduced and implemented in the later section of this chapter.

In order to build a flexible channel model for powerline communications, another the modelling method is developed according to the transmission line theory. Meng and Galli proposed their

own TLT models in [68], [69], [86], [87] and [88] respectively. The key point of the TLT model are is to evaluate the channel transfer function in frequency domain. To calculate the transfer function of the whole network, the transfer function of the basic network unit, the cable segment, should be known first. Based on the knowledge of the cable geometry properties, namely the electrical characteristics of the conductor and dielectric, the transfer function of the cable segment can be calculated by considering the cable segment as a 2-Port Network (2PN). In Meng's model [69], the impact of realistic appliance impedance is considered during the transfer function calculation of every single cable segment. In Galli's model [68], the impact of grounding in transformer which usually appears in PLC networks is taken into account. To extend the application of the TLT model, the Chain Rule is introduced to connect all the cable segments to form the whole network. In theory, the transfer function of any PLC network with arbitrary topologies can be computed if the cable electrical characteristics are known, but the precise calculation process for different topologies varies a lot from case to case. Thus to calculate the transfer functions for networks with a complex topology or a time varying topology becomes a time-consuming process.

The multipath model and TLT model perform well to evaluate the frequency selective fading and the attenuation properties of the PLC channel. However, the literature considers many different PLC network environments with a variety of cable types and network topologies. For example, Dostert's multipath model is built for low power distribution networks with NAYY cable in Germany. In Galli's TLT model, the NM-B 14/2 and AWG series cables are involved. In Meng's work, a typical house wiring cable from Singapore is used, but the cable type is not clearly indicated. Besides the different cable types, the electrical parameters for a given cable are difficult to determine in the high frequency band since the cables are designed for the low frequency high voltage usage. Due to the above differences, it is very difficult to verify the consistency of the proposed models. When considering the use of these channel models in future research, both the multipath and TLT models have drawbacks. For example, it is impossible to model the networks with complex topology without measurements, even the example given in [18] and [77] may not be applicable if the the topology changes or the cable type is switched. The TLT model also deeply depends on the network topology, thus, the flexibility of the model is reduced.

To build a reference for the later research reported in this thesis, the multipath model and TLT are implemented and verified first. Then a set of parameters are found to maintain the

consistency of two models. Some detailed discussions of the TLT model are also provided. To avoid the drawbacks of the multipath and TLT model, another category of modelling methods which are based on the statistical properties of the channel have been proposed recently. A new statistical channel model will be discussed in detail in the next chapter.

3.2 Multipath Modelling Method

To model the PLC channel, Dostert first proposed a widely used method based on the multipath propagation characteristics in [18] and [77]. However, when the network topology becomes complex, it will be difficult to extract the correct weight factors and simulate all the paths in Dostert's model. In [85] Ding developed a systematic multipath modelling method to adapt the complex topology by integrating the signal reflection and propagation effects in one matrix. The infinite signal reflection feature is also captured in [85] by using an iterative algorithm.

3.2.1 Basic Multi Path Modelling

Here a simple T-Type PLC network is used to demonstrate the basic multipath modelling method. The topology is shown as follows, As can be seen in Figure 3.1, the receive signal at terminal *C* is a combination of the direct signal from *A* and the reflected signals from **B**. The signals arrive at *C* with different time delays, thus, the transmission feature of PLC network presents a multipath channel which is often also seen in wireless communications. The signal

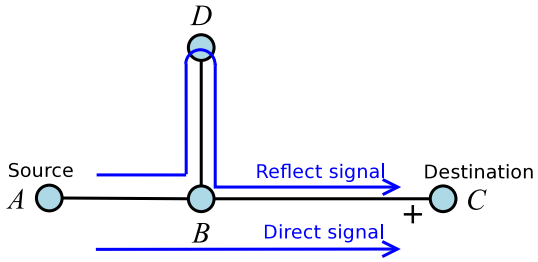

Figure 3.1: *A Typical T-Type PLC network Topology*

propagation paths for the T-Type network thus can be written as:

$$\begin{aligned}
&\text{Path0}: \quad A \rightarrow B \rightarrow C \\
&\text{Path1}: \quad A \rightarrow B \rightarrow D \rightarrow B \rightarrow C \\
&\text{Path2}: \quad A \rightarrow B \rightarrow D \rightarrow B \rightarrow D \rightarrow B \rightarrow C \\
&\text{Path3}: \quad A \rightarrow B \rightarrow D \rightarrow \ldots B \rightarrow C \\
&\text{PathN}: \quad etc.
\end{aligned}$$

Theoretically, the number of reflection paths should be infinite. Thus, as introduced in [18] the frequency response for the $A \rightarrow C$ link can be expressed as:

$$H\left(f\right) = \sum_{i=1}^{\infty} \varphi_i \cdot A(f, d_i) \cdot e^{-j2\pi f t_i} \tag{3.1}$$

where, φ_i, d_i and t_i are the weight factor, the propagation distance and the propagation delay of the i_{th} path respectively. The function $A(f, d_i)$ indicates the attenuation caused by the losses of the cable. $t_i = \frac{d_i}{v_p}$, where v_p is the electromagnetic wave velocity in the cable.

As stated in [77], the attenuation $A(f, d_i)$ of the PLC channel is affected by the propagation distance and the frequency. Intuitively, the attenuation will increase with the both distance and frequency. The relation is analysed in the following description, the transfer function $H(f)$ can be written as:

$$H(f) = \frac{\overline{U}(d = l)}{\overline{U}(d = 0)} = e^{-\gamma \cdot l} \tag{3.2}$$

where, $\overline{U}(d = l)$ and $\overline{U}(d = 0)$ denote the voltage at distance l and 0. The scalar γ is the complex propagation constant:

$$\gamma = \sqrt{(R' + j\omega L')(G' + j\omega C')} = \alpha + j\beta \tag{3.3}$$

where, $R^{'}$, $L^{'}$, $G^{'}$ and $C^{'}$ are the resistance, inductance, conductance and capacitance of the cable. The result of $C^{'}$ and $L^{'}$ are determined by the cable's geometrical characteristics and some material properties. As a digital communications medium, we mainly consider the frequency band in the megahertz range, from 1.6 to 30 MHz, thus, $R^{'}$ is determined by the skin effect and proportional to is $\sqrt{f}$. The conductance $G^{'}$ is an indicator of the dissipation factor of the cable dielectric material, in most cases PVC, which proportional to f. In the frequency

range of interest, we usually have $R^{'} \ll \omega L^{'}$ and $G^{'} \ll \omega C^{'}$. Thus, the complex propagation constant γ can be determined using the simplified expression:

$$\gamma = k_1\sqrt{f} + k_2 f + jk_3 f \tag{3.4}$$

the constants k_1, k_2 and k_3 summarise the material and geometry properties, are determined by the material of the cable. Here, we use the attenuation factor $\alpha(f)$ to express the first two terms in (3.4) which increase with frequency. The relation between $\alpha(f)$ and f can be proportional to $\sqrt{f}$ or f, and this depends on whether k_1 or k_2 is dominant according to:

$$\alpha(f) = a_0 + a_1 \cdot f^k \tag{3.5}$$

where, the value of k is between 0.5 and 1. Therefore, the attenuation $A(f, d_i)$ in (3.1) can be written as:

$$A(f, d_i) = e^{-\alpha(f)\cdot d} = e^{-(a_0 + a_1 \cdot f^k)\cdot d} \tag{3.6}$$

According to [18], the parameters a_0, a_1 and k cannot easily be extracted from the cable parameters because it is difficult to summarise all the necessary cable and geometry data for a real network. However, their value can be derived from measured transfer functions. In chapter 4, the calculation method and result of these two parameters is introduced..

Based on the above description, the transfer function can be written as:

$$H\,(f) = \sum_{i=1}^{N} \varphi_i \cdot e^{-(a_0 + a_1 \cdot f^k) d_i} \cdot e^{-j2\pi f(t_i)} \tag{3.7}$$

In (3.7) the path number is N instead of infinity in (3.1) because only a paths with significant amplitudes are retained in this model. The path number N, weight factor φ_i, attenuation factor a_0 and a_1, exponential k and t_i can be derived based on measurement data.

3.2.2 Extended Multipath Modelling

Basic multipath modelling can accurately construct the transfer function if the parameters for (3.7) can be precisely extracted from the measurement data. Otherwise the propagation paths need to be found and evaluated individually, which becomes very computationally demanding in a large scale network or network with a complex topology. Ding then proposed an approach

in [85] by performing recursive matrix operations rather than systematic management of multipath branches of a PLC network. The channel response between arbitrary terminal pairs in the network can be obtained by Ding's approach. The channel transfer calculation method introduced in section 3.2.2 is based upon [85]. A typical complex PLC topology is given in Figure 3.2 and [89]. Considering the bidirectional signal propagation characteristics of a cable, each cable segment in Figure 3.2 is labelled by 2 directional segments. Thus the paths for the $T_x \rightarrow R_x$ link can be represented by the directional segments:

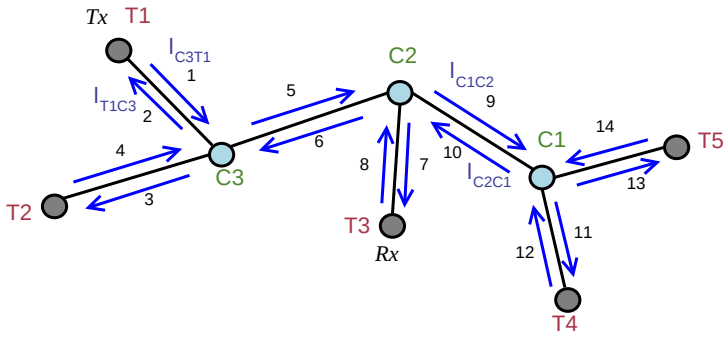

Figure 3.2: *A example of complex PLC network topology*

$$
\begin{aligned}
\text{path0}: &\quad 1 \rightarrow 5 \rightarrow 7 \\
\text{path1}: &\quad 1 \rightarrow 2 \rightarrow 1 \rightarrow 5 \rightarrow 7 \\
\text{path2}: &\quad 1 \rightarrow 5 \rightarrow 7 \rightarrow 8 \rightarrow 7 \\
\text{path3}: &\quad 1 \rightarrow 2 \rightarrow 4 \rightarrow 5 \rightarrow 7 \\
\text{pathN}: &\quad etc.
\end{aligned}
$$

The transmission function for a given directional segment can be written as (3.2). Thus, the transmission characteristics can be demonstrated as the following Figure 3.3: a_{ji} and a_{kj} in Figure 3.3 represent either a reflection or a transmission coefficient for the $i \rightarrow j$ and $j \rightarrow k$ links respectively. In this scenario, we consider the transfer function between 2 terminals in network based on the directional segments that connect with the terminals or the directional segment passed by the signal propagation path. Except for the special case of direct transmission without any junction present, the transmission path will at least cover at least 2 directional segments. Thus, the transfer function for the propagation path which covers 2 segments is

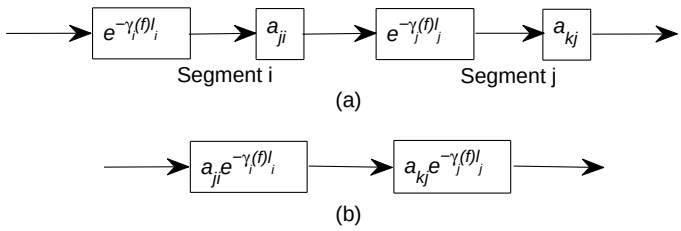

Figure 3.3: *(a) Block diagram of a signal propagation path. (b) Simplified diagram as described in [78]*

written as:

$$H_0(f) = \tau_{m_0} e^{-\gamma_{m_0}(f) l_{m_0}} \cdot a_{m_0 n_0} e^{-\gamma_{n_0}(f) l_{n_0}} \approx \tau_{m_0} a_{m_0 n_0} e^{-\gamma(f)(l_{m_0}+l_{n_0})} \tag{3.8}$$

where, τ_{m_0} denotes the transmission coefficient at the junction of the second directional segment m_0. and $a_{m_0 n_0}$ denotes the transmission coefficient between the first directional segment n_0 and the second directional segment m_0. Considering the transmission paths that cover 3 directional segments:

$$\begin{aligned} H_1(f) &= \sum_i \tau_{m_0} e^{-\gamma_{m_0}(f) l_{m_0}} \cdot a_{m_0 i} e^{-\gamma_i(f) l_i} \cdot a_{i n_0} e^{-\gamma_{n_0}(f) l_{n_0}} \\ &\approx \sum_i \tau_{m_0} a_{m_0 i} a_{i n_0} e^{-\gamma(f)(l_{m_0}+l_i+l_{n_0})} \end{aligned} \tag{3.9}$$

The reason for using a summation form in (3.9) is that there may not be only one path from segment n_0 to segment m_0 they may pass another segment. All the possible directional segments are represented by the variable i in (3.9). Also the condition for the validity of the approximation in (3.8) and (3.9) is that the cables in the network have the same insulating material, which is applicable in this work. Thus, the we can consider that $\gamma_{n0}(f) = \gamma_{m0}(f) = \gamma_{l_i}(f)$. Based on the above description, the transfer function for the paths that cover the $(k+2)$ directional segments can be written as:

$$\begin{aligned} H_K(f) \approx & \sum_{i_K=1} \sum_{i_{K-1}=1} \cdots \sum_{i_1=1} \\ & \tau_{m_0} a_{m_0 i_K} a_{i_K i_{K-1}} \cdots a_{i_2 i_1} a_{i_1 n_0} e^{-\gamma(f)(l_{m_0}+l_{i_K}+l_{i_{K-1}}+\cdots+l_{i_1}+l_{n_0})} \end{aligned} \tag{3.10}$$

In a summary, the transfer function for 2 terminals in a given network is:

$$H(f) \approx \sum_{i=0}^{K} H_i(f) \tag{3.11}$$

where $H_i(f)$ is the transfer function of the path which traverses $i+2$ directional segments. In order to implement the above process systematically, a numerical method is proposed in [85]. The method can be divided into 2 stages in general: **Initialisation** and **Recursion**.

Initialisation The main task for the initialisation stage is to obtain the transmission/reflection coefficient matrix $\mathbf{A}$. Assume there are $\frac{N}{2}$ segments with N corresponding directional segments. The matrix $\mathbf{A}$ can be formulated as:

$$\mathbf{A} = \begin{bmatrix} a_{11} & a_{12} & \cdots & a_{1N} \\ a_{21} & a_{22} & \cdots & a_{2N} \\ \vdots & \vdots & \ddots & \vdots \\ a_{N1} & a_{N2} & \cdots & a_{NN} \end{bmatrix} \tag{3.12}$$

each row and column in (3.12) correspond to a directional segment. If a reflection occurs at a particular transition point from directional segment i to j, the corresponding a_{ji} in $\mathbf{A}$ will be filled with a reflection coefficient, while if a transmission takes place, the entry will be filled with a transmission coefficient. In the case that two directional segments are not connected directly, or connected but with opposite directions, the entry will be set to 0. Further, all the diagonal entries of $\mathbf{A}$ are set to 0. In order to compute $\mathbf{A}$, two length metrics $\mathbf{L_{TC}}$ and $\mathbf{L_{CC}}$ are defined first:

$$\mathbf{L_{TC}} = \begin{bmatrix} l_{T_1C_1} & l_{T_1C_2} & \cdots & l_{T_1C_Q} \\ l_{T_2C_1} & l_{T_2C_2} & \cdots & l_{T_2C_Q} \\ \vdots & \vdots & \ddots & \vdots \\ l_{T_PC_1} & l_{T_PC_2} & \cdots & l_{T_PC_Q} \end{bmatrix} \tag{3.13}$$

where T_i and C_i indicate the terminal nodes and internal nodes respectively as shown in the Figure 3.2. The entry $l_{T_iC_j}$ is the length of the directional segment T_iC_j, if T_i and C_j

are not connected directly, set $l_{T_iC_j}$ 0. Similarly, $\mathbf{L_{CC}}$ is defined as:

$$\mathbf{L_{CC}} = \begin{bmatrix} 0 & l_{C_1C_2} & \cdots & l_{C_1C_Q} \\ l_{C_2C_1} & 0 & \cdots & l_{C_2C_Q} \\ \vdots & \vdots & \ddots & \vdots \\ l_{C_QC_1} & l_{C_QC_2} & \cdots & 0 \end{bmatrix} \tag{3.14}$$

then the matrix $\mathbf{L_{TOT}}$ is constructed:

$$\mathbf{L_{TOT}} = \begin{bmatrix} \mathbf{L_{CC}} & \mathbf{L_{CT}} \\ \mathbf{L_{TC}} & 0 \end{bmatrix} \tag{3.15}$$

where, $\mathbf{L_{CT}} = \mathbf{L_{TC}^T}$. Similar to the definition for $\mathbf{L_{TC}}$, we can define $\mathbf{Z_{TC}}$ as:

$$\mathbf{Z_{TC}} = \begin{bmatrix} \mathbf{Z_{CC}} & \mathbf{Z_{CT}} \\ \mathbf{Z_{TC}} & 0 \end{bmatrix} \tag{3.16}$$

where $\mathbf{Z_{CT}} = \mathbf{Z_{TC}^T}$. The entry $Z_{T_iC_j}$ in $\mathbf{Z_{TC}}$ denotes the characteristic impedance of the cable T_iC_j if segment i and j are connected and have consistent direction. The entry $Z_{C_iC_j}$ in $\mathbf{Z_{CC}}$ denotes the characteristic impedance of the cable C_iC_j if segment i and j are connected and have consistent direction. For the non-connected directional segments, the entries are set to zero. Based on the constructed $\mathbf{L_{TC}}$, two other vectors can be derived:

$$L = \left[l_1^{'}, l_1^{'}, l_2^{'}, l_2^{'} \cdots l_{\frac{N}{2}}^{'}, l_{\frac{N}{2}}^{'}\right]^T \tag{3.17}$$

$$\mathbf{U_U} = \left[U_1, U_2, \cdots, U_{N/2}\right]^T \tag{3.18}$$

$$U_i = \begin{bmatrix} x_i & y_i \\ y_i & x_i \end{bmatrix} \tag{3.19}$$

where, x_i and y_i are the row and column indices of the nonzero element in $\mathbf{L_{TC}}$. The reason to repeat $l_i^{'}$ is that each cable segment corresponds to two directional segments.

The entries in the first column of $\mathbf{U_U}$ can be assumed to be the end point index of the directional segment, while the entries in the second column indicate the starting point index. Thus, each row presents a directional segment. If the end point index of a directional segment equals the starting index of another directional segment, we can consider that these 2 directional segments are directly connected. By comparing all the end points with all the starting points, a connectivity matrix $\mathbf{L_L}$ is defined as:

$$\mathbf{L_L} = \begin{bmatrix} 0 & ll_{12} & \cdots & ll_{1N} \\ ll_{21} & 0 & \cdots & ll_{2N} \\ \vdots & \vdots & \ddots & \vdots \\ ll_{N1} & ll_{N2} & \cdots & 0 \end{bmatrix} \tag{3.20}$$

The value of ll_{ji} is 1 if there is a direct connection from directional segment i to directional segment j, 0 otherwise. When observing the i_{th} row of the $\mathbf{U_U}$, if there is only 1 nonzero entry in x_ith row of $\mathbf{L_{TC}}$, it means that the x_ith directional segment heads to a terminal, and the transmission coefficient $\tau_{x_i y_i}$ can be calculated by using:

$$\tau = 1 + \rho = \frac{2Z_L}{Z_L + Z_o} \tag{3.21}$$

where, Z_L is the terminal load and Z_o is the characteristic impedance of this directional segment. If there are more then 1 nonzero entries in x_ith row of $\mathbf{L_{TC}}$, it means that the x_ith directional segment heads to a internal node. The transmission coefficient of this directional segment can also be calculated by (3.21). However, Z_L is the total impedance resulting from the shunt connection of all nonzero impedance that appear in the x_ith row of $\mathbf{L_{TC}}$. By repeating the above process from the x_1th to x_Nth row of $\mathbf{U_U}$, the transmission coefficients $\tau_{y_1 x_1}$, $\tau_{x_2 y_2}$, $\tau_{y_2 x_2}$, $\cdots$ and $\tau_{y_{\frac{N}{2}} x_{\frac{N}{2}}}$ can be evaluated and the diagonal matrix $\overline{\mathbf{T}}$ is obtained:

$$\overline{\mathbf{T}} = \begin{bmatrix} \tau_{x_1 y_1} & 0 & \cdots & 0 \\ 0 & \tau_{y_1 x_1} & \cdots & 0 \\ \vdots & \vdots & \ddots & \vdots \\ 0 & 0 & \cdots & \tau_{y_{\frac{N}{2}} x_{\frac{N}{2}}} \end{bmatrix} \tag{3.22}$$

The transmission coefficient matrix $\mathbf{A}^{'}$ is witten as:

$$\mathbf{A}^{'} = \mathbf{L_L} \cdot \overline{\mathbf{T}} \tag{3.23}$$

By observing Figure 3.2 and equation (3.18), directional segments with adjacent indices only involve signal reflection rather than transmission. Thus the entries with indices as $(i, i+1)$ and $(i+1, i)$ in $\mathbf{A}^{'}$, should be replaced by reflection coefficients by using the following relation:

$$\rho = \tau - 1 \tag{3.24}$$

After the replacement operation for $\mathbf{A}^{'}$, the transmission/reflection-coefficient (TRC) matrix $\mathbf{A}$ is obtained.

Recursion In order to implement the process from (3.8) to (3.11), the matrix $\mathbf{D}(f_x)$ is constructed as:

$$\mathbf{D}(f_x) = \begin{bmatrix} e^{-\gamma(f_x)l_1} & 0 & \cdots & 0 \\ 0 & e^{-\gamma(f_x)l_2} & \cdots & 0 \\ \vdots & \vdots & \ddots & \vdots \\ 0 & 0 & \cdots & e^{-\gamma(f_x)l_N} \end{bmatrix} \tag{3.25}$$

The propagation constant γ will in general vary with increasing frequency. Thus, for different frequency points f_{x_i}, a different matrix $\mathbf{D}(f_{x_i})$ is obtained for demonstrating the transfer function of a given segment. Joint considering the TRC matrix $\mathbf{A}$, the $\mathbf{P}$ matrix on frequency sampling point f_x is written as:

$$\mathbf{P}(f_x) = \mathbf{A} \cdot \mathbf{D}(f_x) \tag{3.26}$$

Assume that the starting directional segment is n_0 and the end directional segment is m_0, then define the n_0th column of the matrix $\mathbf{P}(f_x)$ as $\mathbf{V_0}(f_x)$. Thus the matrix $\mathbf{H_0}(f_x)$ in (3.11) can be obtained by multiplying $\tau_{m_0} e^{-\gamma(f_x)l_{m_0}}$ with m_0th entry of $\mathbf{V_0}(f_x)$. Then, the recursive process begins as (3.27) to (3.29):

$$\mathbf{V_k}(f_x) = \mathbf{P}(f_x) \cdot \mathbf{V_{k-1}}(f_x) \tag{3.27}$$

$$H_k(f_x) = \tau_{m_0} e^{-\gamma(f_x)l_{m_0}} \cdot \mathbf{V_k}(f_x)(m_0, n_0) \tag{3.28}$$

$$\widehat{H}_k(f_x) = \widehat{H}_{k-1}(f_x) + H_k(f_x) \tag{3.29}$$

It can be found that, the magnitude of $H_k(f_x)$ will decrease as the recursion processes. Thus, the convergence condition for the recursive process is given by:

$$0 <\mid H_k(f_x) \mid < \varepsilon \mid \widehat{H}_{k-1}(f_x) \mid \tag{3.30}$$

where, ε is a small positive fraction. Following the above **Initialisation** and **Recursion** process, the transfer function at a certain frequency sampling point can be computed. By changing the frequency used in the above process, the transfer function for the whole frequency band can be obtained.

3.3 Transmission line theory Modelling Method

Another important PLC channel modelling category which is based on transmission line theory is introduced in [68] and [69]. For the TLT modelling method, the network in disassembled into basic segments. The frequency transfer function for each segment can be achieved by TLT. The transfer function for the whole network can then be obtained by using the Chain Rule (CR).

Considering the simple T-Type topology PLC network shown in Figure 3.1, the whole network is composed of three cable segments: AB, BD and BC. Each cable segment can be modelled as a 2-port-network (2PN) as shown in Figure 3.4: the relations between the inputs and outputs

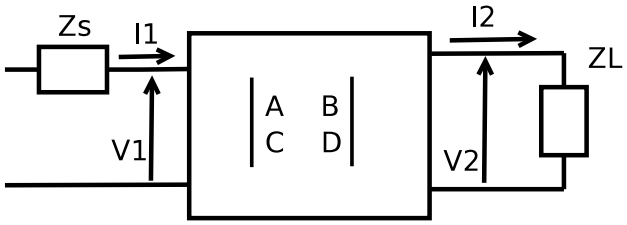

Figure 3.4: *An example of 2PN of a segment*

of the 2PN can be formulated as:

$$\begin{vmatrix} V_{input} \\ I_{input} \end{vmatrix} = \begin{vmatrix} A & B \\ C & D \end{vmatrix} \begin{vmatrix} V_{output} \\ I_{output} \end{vmatrix} = T_f \begin{vmatrix} V_{output} \\ I_{output} \end{vmatrix} \tag{3.31}$$

where, T_f is called the transmission matrix. The discussion of A, B, C and D is out of the scale

of this paper, the calculation method is given in this chapter later. A, B, C and D are functions of frequency. Then, the transfer function of this segment can be written as:

$$H(f) = \frac{Z_L}{AZ_L + B + CZ_SZ_L + DZ_S} \tag{3.32}$$

According to the transmission line theory, the A, B, C and D coefficients in (3.31) and (3.32) are expressed as:

$$\begin{aligned} A &= D = \cosh \gamma l \\ B &= Z_o \sinh \gamma l \\ C &= \tfrac{1}{Z_o} \sinh \gamma l \end{aligned} \tag{3.33}$$

where, γ and Z_o are the propagation constant and the characteristic impedance of the cable and l is the length of the cable. the value of Z_o is computed as:

$$Z_o = \sqrt{\frac{R' + j\omega L'}{G' + j\omega C'}} \tag{3.34}$$

Considering the 1.6-30 MHz frequency range for operation, Z_o is approximately equal to $\sqrt{\frac{L'}{C'}}$. The calculation of γ and Z_o depend on the parameters such as $R^{'}$, $G^{'}$, $L^{'}$ and $C^{'}$ that determined by the the cable geometry and material properties. The calculation of these parameters is shown in Appendix A.

As can be seen from Figure 3.1, segment BD is shunted rather than cascaded on the network. For this segment, the transmission matrix should have this form:

$$\mathbf{T}_s = \begin{vmatrix} 1 & 0 \\ \frac{1}{Z_{in}} & 1 \end{vmatrix} \tag{3.35}$$

where, $Z_{in} = \frac{A}{C}$. After the transformation, the network above can be considered as a series of cascaded segments. After applying Chain Rule (CR), the transmission matrix for the complete network is given by:

$$\mathbf{T}(f) = \prod_{i=1}^{N} \mathbf{T}_f^i(f) \tag{3.36}$$

where, $\mathbf{T}_f^i(f)$ is the transmission function of the i_{th} segment. Note that all the shunted segments here have been transformed by (3.35). Based on the transfer matrix $\mathbf{T}(f)$ achieved in

i	1	2	3	4
φ_i	0.64	0.38	-0.15	0.05
d_i/m	200	224	248	272

Table 3.1: *Weight factors and propagation distances for a 4-path model*

i	1	2	3	4	5	6
φ_i	0.54	0.275	-0.15	0.08	-0.03	-0.02
d_i/m	200	224	248	272	296	540

Table 3.2: *Weight factors and propagation distances for a 6-path model*

(3.36), the overall transfer function for the whole network can be obtained according to (3.32).

3.4 Modelling Results and Discussion

In this section, modelling results are obtained according to the multipath model and TLT model introduced above. As mentioned before, the modelling methods in the references are developed with a variety of PLC networks environment and cables as shown in [77], [68], [85] and [90]. To prove the consistency of PLC channel modelling, the same network topology and cable type are used for both methods. The calculation results based on two different methods should then be consistent.

3.4.1 Modeling Results and Consistency

The network topology used in this work based on the described in [18] and [77]. The AB segment has a length of 30 m, the BC segment has length of 170 m and the BD segment is 12 m long with an open load. The AB and BC segments are NAYY 150 cable and the BD segment is NAYY35 cable. Also, the load on socket D is infinity which means it is open load. The cable properties can be found in Appendix A. There are 2 parameter sets given for this topology in [18] and [77] for the 4-path model and 6-path model respectively, that can be applied in equation (3.7).

For the 4-path model $k = 1$, $a_0 = 0$, $a_1 = 7.8 \cdot 10^{(-10)} s/m$ while $k = 1$, $a_0 = -2.1 \cdot 10^{(-3)}$, $a_1 = 8.1 \cdot 10^{(-10)} s/m$ for the 6-path model.

Figure 3.5 shows the results together with the transmission line theory model result for the test

topology: .

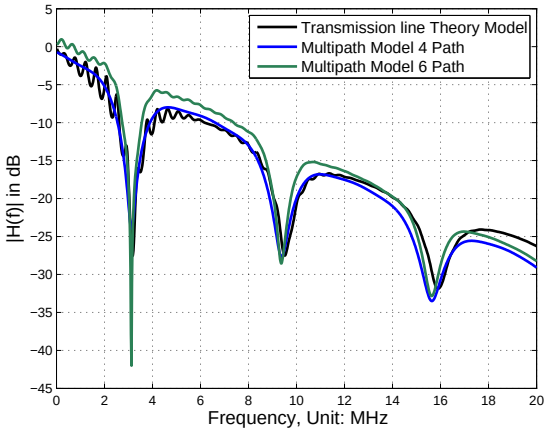

Figure 3.5: *Modelling results according to multipath model and transmission line theory model*

Then, according to TLT method the segments AB, BC and BD can be considered as 2PNs, where segment AB and BC are cascaded 2PNs and segment BD is the shunted 2PN which should be calculated according to equation (3.35), using the cable electrical parameters in Appendix A. Assume the transmission matrix for segments AB, BC and BD are $\mathbf{T}_f^1(f)$, $\mathbf{T}_f^2(f)$ and $\mathbf{T}_f^3(f)$ respectively. Thus the transmission matrix for the whole network is:

$$\mathbf{T}(f) = \mathbf{T}_f^1(f) \cdot \mathbf{T}_f^2(f) \cdot \mathbf{T}_f^3(f) \tag{3.37}$$

The transfer function then can be calculated by (3.32).

From Figure 3.5, we can see that the simulation results based on the two different models show similar attenuation features with similar frequency fading positions. An obvious difference of the results that the TLT based result presents deeper fading then the multipath modelling result. The reason for this phenomenon is that only a finite number of paths is considered in the multipath model while all the possible multipath impacts are represented in the TLT model. Since there is only 1 fixed length branch, all the reflections will appear on the same frequency points. Thus the severity of the fading on these frequency points will be increased. Though some differences exist, both models demonstrate the consistent attenuation and frequency selective fading features in the PLC network and are thus valuable for PLC research.

3.4.2 Impacts Facts and Discussion

After verifying the consistency of the two different models, the impact of changing the branch structure are investigate. First, the impact of the branch length is observed. Different branch lengths are investigated for showing the the impacts of the branch. The modelling results are shown in Figure 3.6. These results are obtained by using the TLT model because the parameters needed in the multipath model cannot be extracted without measurement data. This is a significant limitation of the multipath model. From Figure 3.6, we can see that a longer branch will result is more rapid fading notches which can be clearly seen in the frequency domain transfer functions. The explanation of this phenomenon is that for the longer branches, the reflected signal requires more time to arrive the destination. In consequence, the longer interval in the time domain appears in the frequency domain as a more frequent fading notch.

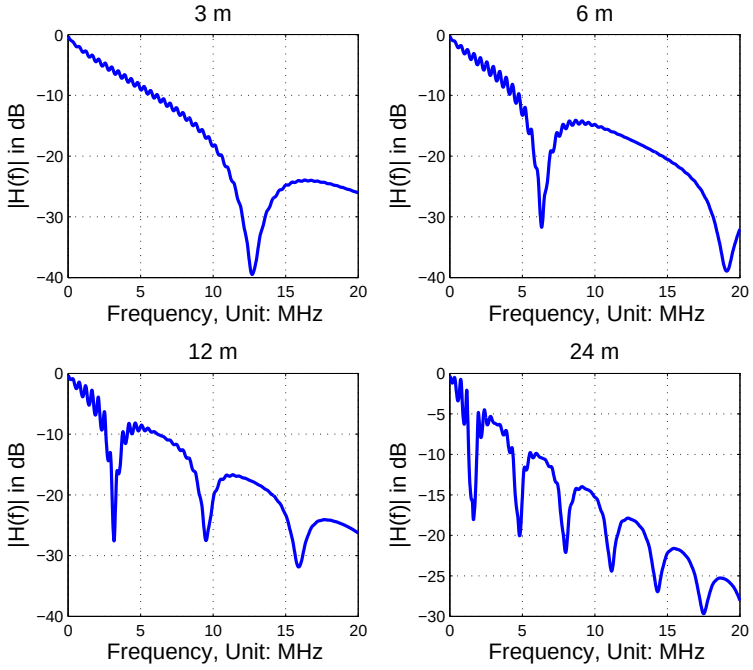

Figure 3.6: *transfer functions for different branch lengths for fixed 100 m P2P distance. (a) with 3 meters branch, (b) with 6 meters branch, (c) with 12 meters branch and (d) with 24 meters branch*

.

Besides the length of the branch, the number of branches along with the propagation will vary in practice. Thus, transfer functions for 1, 2, 4 and 8 branches PLC topologies are investigated.

Here, we fix the location and length of the first branch, and the other branches are randomly distributed between the first branch and destination with random lengths. From Figure 3.7, when the number of branches between the two data transmission terminals is small, the transfer function feature is dominated by the properties of the first branch such as location, length and load. When the number of branches becomes large, the impact from other branches will alter significantly the features caused by the first branch. As the number of the branches increases, the frequency selective fading becomes deeper. We can see from Figure 3.7, that the deepest fading positions are around -30 dB when there are one or two branches between that data source and the destination. The fading level reduces to to -45 dB if there are four branches and goes below -80 dB when the number of branches equals eight.

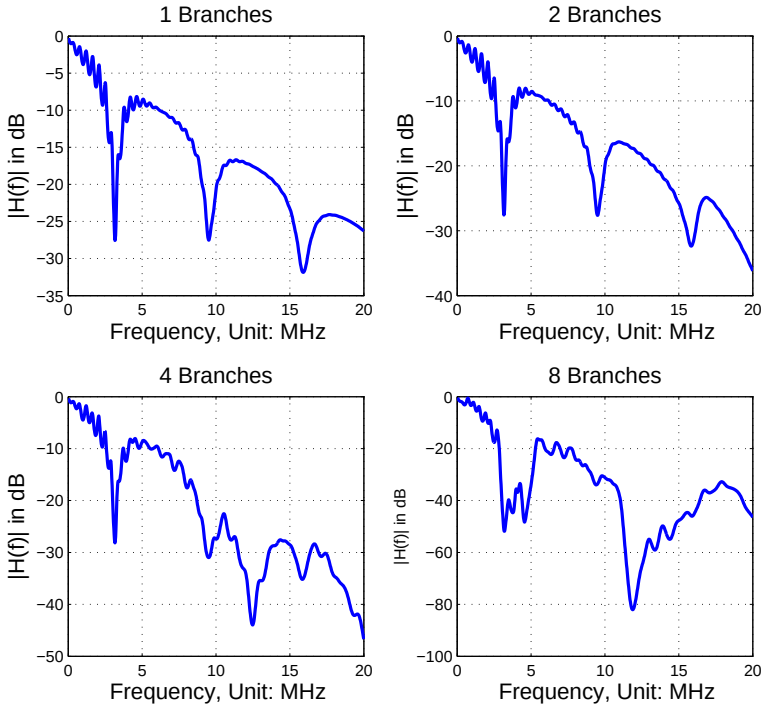

Figure 3.7: *transfer functions for the PLC networks with different number of branches, (a) with 1 branch, (b) with 2 branches, (c) with 4 branches and (d) with 8 branches.*

.

3.5 Noise Modelling

Besides the path loss and multipath propagation, another challenge for implementing low power and high data rate digital communications over power grid is the harsh transmission environment. Unlike the additional white Gaussian noise (AWGN) model used in many other communications environments, the noise situation in powerline is more complex. in [58] , five general classes of noise are introduced:

1. *Colored Background Noise:* Summation of numerous low power spectral density (PSD) noise whose parameters are slow varying. Generally the noise has a higher PSD at lower frequencies.

2. *Narrowband Interference:* This arises from medium or short wave broadcasts with large PSD value and narrow bandwidths. The PSD of the narrowband interference will vary slowly over the duration of one day.

3. *Periodic Impulsive Noise Asynchronous to the Mains Frequency:* Caused by switched power supplies, this source of interference falls in the frequency range 50 to 200 kHz, with a discrete line spectrum.

4. *Periodic Impulsive Noise Synchronous to the Mains Frequency:* This source leads to a decreasing PSD with frequency where the shot duration (often microseconds) is caused by switching rectifier diodes

5. *Asynchronous Impulsive Noise:* Caused by switching transients in the network. The impulses have durations of some microseconds up to a few milliseconds with a random occurrence. The power level of this type of noise can instantaneously reach values of more than 50 dB above the background noise.

Among the above noise types, Class 1 and Class 2 vary slowly over time. Thus in this thesis, they are recognised as background noise. The other three noise sources change rapidly are regarded as impulse noise. The noise Class 3 and Class 4 types have a comparably constant impact on the network performance. Thus, this work only investigates Class 5 which is the major source of impulse noise and causes the varable impact on the performance.

3.5.1 Background Noise Modelling

In [91] and [92], the background noise power spectrum density (PSD) without narrowband interference for residential and industrial environments are given. The narrowband noise density and amplitude for 2 environments in the spectrum of the interest is also given in [91]. Meng in [93] points out that the amplitude of the background noise in PLC can be described by the Nakagami distribution. Rather than separately considering the low power background noise and narrowband interference, the two noise source are jointly investigated in Meng's model. Dirk proposed a synthesis method to simulate the background noise in [94] which is used inn our work. The synthesis method is to make a white Gaussian noise(WGN) sequence pass through a coloured filter. The transfer function of the filter is determined by the PSD of the background noise. The PSD of the background noise which integrates the low power noise and narrowband noise is given in the following formula:

$$S_{nn}^{M}(f) = \underbrace{\overline{N_0} + \overline{N_1} \cdot e^{-\frac{f}{\overline{f_1}}}}_{\text{Background noise}} + \underbrace{\sum_{k=1}^{N} \overline{A_k} \cdot e^{-\frac{(f - \overline{f_{(0,k)}})^2}{2 \cdot \overline{B_k}^2}}}_{\text{Narrowband interference}} \tag{3.38}$$

As can be seen from (3.38) three parameters $(\overline{N_0}, \overline{N_1}, \overline{f_1})$ specify the background noise and four parameters $(\overline{A_k}, \overline{f_{(0,k)}}, \overline{B_k}, \overline{N})$ control the narrow band interference in this model. The *probability distribution functions* (PDFs) of these seven parameters and the parameters distribution for PDFs under different scenarios are given in [94].

3.5.2 Impulse Noise Modelling

Comparing with the frequency domain background noise modelling method, the impulse noise modelling is typically in time domain. In [95], the Middleton's Class A noise model which is often used in wireless communications is used to simulate impulse noise behaviour in PLC. References [96] and [97] proposed models based on impulse duration and bandwidth. Zeddam in [98] described the impulses caused from different appliances such as laptops, coffee makers, TVs, and microwaves and classified the impulses based appliances type that generates the impulses. According to [98], the impulses in the network can be derived based on the impulse source and transfer function between the source and expected destination. The Middleton model in [95] is used for wireless and mobile research. Zeddam's impulse noise model deeply

depends on the measurement, and it is not a mature mathematical model which can be represented by a series of parameters. The impulse modelling method used in this thesis is based upon [99].

In [99], the impulse rate r_{imp} and disturbance ratio d_{ratio} are defined to indicate the severity of the impulse noise in a network:

$$r_{imp} = \frac{N_{imp}}{T_{win}} \tag{3.39}$$

$$d_{ratio} = \frac{\sum_{i=1}^{N_{imp}} t_{\omega,i}}{T_{win}} \tag{3.40}$$

where N_{imp} is the number of impulses, and T_{win} is the observing window. To use the predefined values of r_{imp} and d_{ratio} plus other features such as impulse width $t_{w,i}$, impulse amplitude and interarrival times (IAT), a method based on the Markov Chain (MC) is developed to simulate the impulse behaviour in the PLC network. Usually, the Gilbert-Elliot approach model is used to simulate the IAT and width of impulse events with two states exhibiting exponentially distributed durations. The basic idea of the modelling method is to judge whether the next state is the impulse state or the idle state based on the current state. Based on the assumption that the modelling is in the time domain, each state transition indicates one time domain sample. A simple 2 state transfer model can be shown in Figure 3.8. As stated in

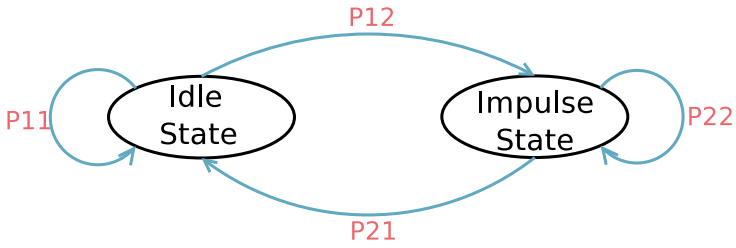

Figure 3.8: *Representation of a Markov chain with two states by a state graph*

[99], the IATs and impulse width in the PLC network, often present a superposed exponential distribution. To model such a scenario, a partitioned $n(n \geqslant 2)$ MC approach is developed in [99]. The transition probability matrix is defined in (3.41). The entry $p_{i,j}$ in $\mathbf{P}$ is the transition

probability from ith state to jth state.

$$\mathbf{P} = \begin{bmatrix} p_{1,1} & p_{1,2} & \cdots & p_{1,n} \\ p_{2,1} & p_{2,2} & \ddots & \vdots \\ \vdots & \ddots & \ddots & p_{n-1,n} \\ p_{n,1} & \cdots & p_{n,n-1} & p_{n,n} \end{bmatrix} \tag{3.41}$$

There are a total of n states in (3.41), where $p_{i,j}$ denotes the probability of transferring from state i to state j. In this work, there are two main states, the Idle State and the Impulse State. In each main state there are number of sub-states to present the probability of staying in the current main state or transiting to the other main state. The reason for use the multiple sub-states is that the transition probability in this situation depend on how long it has been in impulse/idle state, for example, when it is just jump to the impulse state, it is more like to stay in impulse states then jump to idle state, vise verse. In order to demonstrate this characteristics, the sub-state is used. Usually, the partitioned MC is used to demonstrate this transfer. In a partitioned MC system, the n states are divided into 2 groups: the idle group ($i = 1, 2, \cdots, v$) and the event group ($i = v+1, v+2, \cdots, n+w$), where $w = n-v$. The sub-states in the idle group includes the probabilities of staying in the idle state or transferring to the impulse state. The substates in impulse group include the probabilities of staying in the impulse state or transferring to idle state. The states transition for the partitioned MC can be demonstrated as shown in Figure 3.9.

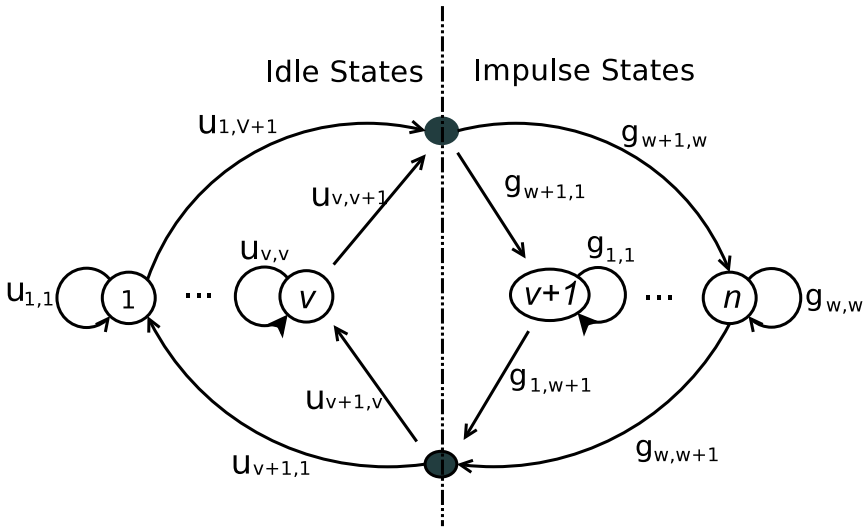

Figure 3.9: *Partitioned Markov chain for the representation of asynchronous impulsive noise events*

Both the idle states and impulse states can be described by transition probability matrices **U** and **G** respectively:

$$\mathbf{U} = \begin{bmatrix} u_{1,1} & 0 & \cdots & 0 & u_{1,v+1} \\ 0 & u_{2,2} & \ddots & \vdots & u_{2,v+1} \\ \vdots & \ddots & \ddots & 0 & \vdots \\ 0 & \cdots & 0 & u_{v,v} & u_{v,v+1} \\ u_{v+1,1} & u_{v+1,2} & \cdots & u_{v+1,v} & 0 \end{bmatrix} \tag{3.42}$$

and

$$\mathbf{G} = \begin{bmatrix} g_{1,1} & 0 & \cdots & 0 & g_{1,w+1} \\ 0 & g_{2,2} & \ddots & \vdots & g_{2,w+1} \\ \vdots & \ddots & \ddots & 0 & \vdots \\ 0 & \cdots & 0 & g_{w,w} & g_{w,w+1} \\ g_{w+1,1} & g_{w+1,2} & \cdots & g_{w+1,w} & 0 \end{bmatrix} \tag{3.43}$$

The diagonal entries of **U** denote the probabilities of staying in the idle state and the entries in the last column denote the probabilities of transferring from the idle state to the impulse state. The entries in the last row denote which sub-state will be in the idle state when there a state jump from the impulse states. The meaning of the entries in **G** can be explained by the same way.

In order to construct the overall transition matrix **P**, the following metrices are formed based on **U** and **G**:

$$\mathbf{P}_U = \begin{bmatrix} u_{1,1} & & 0 \\ & \ddots & \\ 0 & & u_{v,v} \end{bmatrix} \tag{3.44}$$

$$\mathbf{P}_G = \begin{bmatrix} g_{1,1} & & 0 \\ & \ddots & \\ 0 & & g_{w,w} \end{bmatrix} \tag{3.45}$$

and

$$\mathbf{P}_{UG} = \begin{bmatrix} u_{1,v+1} \cdot g_{w+1,1} & \cdots & u_{1,v+1} \cdot g_{w+1,w} \\ \vdots & \ddots & \vdots \\ u_{v,v+1} \cdot g_{w+1,1} & \cdots & u_{v,v+1} \cdot g_{w+1,w} \end{bmatrix} \tag{3.46}$$

$$\mathbf{P}_{GU} = \begin{bmatrix} g_{1,w+1} \cdot u_{v+1,1} & \cdots & g_{1,w+1} \cdot u_{v+1,w} \\ \vdots & \ddots & \vdots \\ g_{w,w+1} \cdot u_{v+1,1} & \cdots & g_{w,w+1} \cdot u_{v+1,v} \end{bmatrix} \tag{3.47}$$

Finally, the transition probability matrix $\mathbf{P}$ is obtained:

$$\mathbf{P} = \begin{bmatrix} \mathbf{P}_U & \mathbf{P}_{UG} \\ \mathbf{P}_{GU} & \mathbf{P}_G \end{bmatrix} \tag{3.48}$$

where the diagonal matrices $\mathbf{P}_U$ and $\mathbf{P}_G$ denote the probabilities of the staying the current state. Matrix $\mathbf{P}_{UG}$ denotes the probabilities of which sub-state will be in the impulse state when a state jump from the idle state to the impulse state occurs. The matrix $\mathbf{P}_{GU}$ denotes the probabilities of which sub-state will be the idle state when a state jump from the impulse state to the idle state occurs. This is because each transition in the above MC process denotes a time domain sampling action. Thus, when the sampling rate is changed, the probability entries in $\mathbf{P}$ should be changed as well. Thus, following paragraph describes the process of how to modify the entries if the sampling rate is changed. The reason to discuss varying the sampling rate is that a different sampling rate may be applied in different research activities. Thus the method for transferring the fixed sampling matrix to any other possible sampling rate is necessary. Assume that the original sampling interval is t_a, and target sampling interval is $t_a^{'}$, the diagonal entries of $\mathbf{P}$ should be changed follows:

$$p_{i,i}^{'} = (p_{i,i})^{\frac{t_a^{'}}{t_a}} \tag{3.49}$$

The other entries should be changed follows:

$$p_{i,j}^{'} = p_{i,j} \cdot \frac{1 - p_{i,i}^{'}}{1 - p_{i,i}} \tag{3.50}$$

The above transforms are suitable for the situation that the duration $t_{50\%}$ of the signal states may not be changed. If the duration $t_{50\%}$ is altered, the new diagonal entries should be the following:

$$p_{i,i}^{'} = 1 - \frac{t_a^{'}}{t_a}(1 - p_{i,i}) \tag{3.51}$$

The other entries still follow (3.50). According to the above steps the transition probability matrix for any sampling rate $\mathbf{P}$ can be computed.

3.5.3 Modelling Results and Discussion

3.5.3.1 Modelling Result for Background Noise

According to the model shown in (3.38) and the given parameters in [94], the sample background noise on PSDs for a residential and an office building can be simulated. As can be seen from the simulation results, the background noise in PLC network decreases exponentially up to 5 MHz. Above this frequency the noise floor is approximately flat. Narrowband interference appears, all over the whole frequency band, but with a higher density in the low frequency band, for example the frequency band which is lower then 10 MHz.

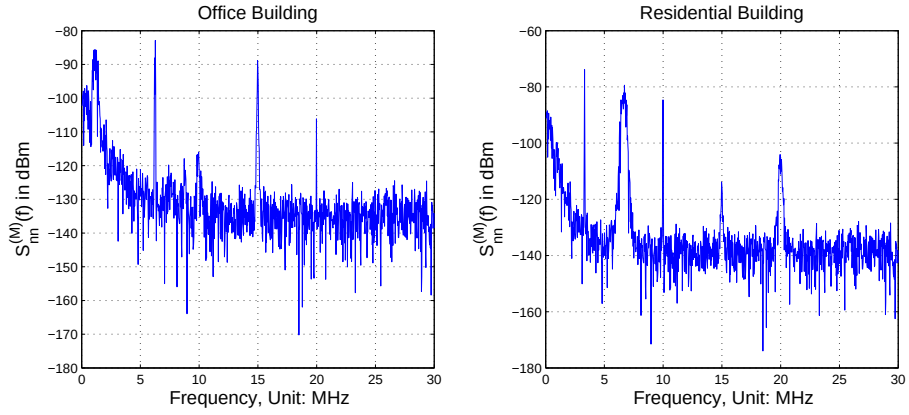

Figure 3.10: *The sample PSDs of PLC background noise in residential and office building*

3.5.3.2 Modelling Result for Impulse Noise

The situation for impulse noise is more complex than the background noise. It is difficult to extract the entries for the transition probability matrix. Thus, a seven state partitioned MC chain model with an 80 μs sampling interval which is used in [99] is applied here to simulate impulse

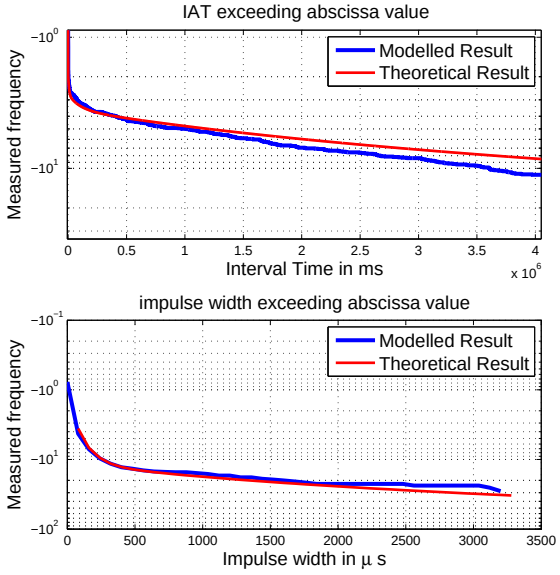

Figure 3.11: *CPDFs of the the IAT and impulse width for PLC network*

noise in a PLC network. The complementary probability distribution function (CPDF) of the IAT and impulse width are given. The CPDF denotes the probability P of a random variable X exceeding a value x: $cpf(x) = P(X > x)$. The theoretical CPDFs for IAT and impulse width are:

$$f_{IAT}(k) = 1 \qquad for \;\; k = 0 \tag{3.52}$$

$$f_{IAT}(k) = \sum_{j=1}^{v} u_{v+1,j} \cdot u_{j,j}^{k} \quad for \;\; k = 1, 2, ... \tag{3.53}$$

and

$$f_{w}(k) = 1 \qquad for \;\; k = 0 \tag{3.54}$$

$$f_{w}(k) = \sum_{j=1}^{w} g_{w+1,j} \cdot g_{j,j}^{k} \quad for \;\; k = 1, 2, ... \tag{3.55}$$

From the result, we can see that the simulated IAT and impulse width of the impulse noise fit the theory analysis, especially when the duration is short. The difference between the simulation result and theory become larger because of the limitation of the simulation time. Another important character of the impulse noise in PLC is the amplitude. The amplitude of the impulse noise is described as exponential distribution in [95]. Also, according to the measurement in [99], more than 90% of the amplitudes of the detected impulses were less than 200 mV, less than

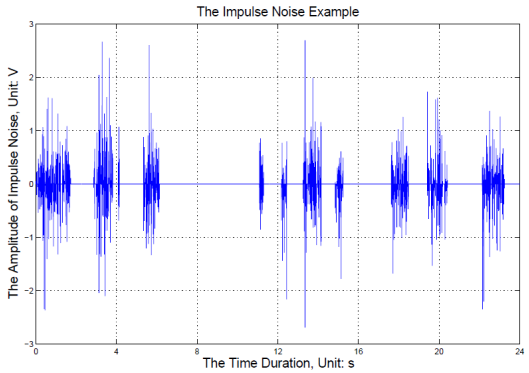

Figure 3.12: *An example of the impulse noise in the time domain*

1% amplitudes of the detected larger than 2 V. Based on the above description, an exponential distribution with parameter $\lambda = 1.164$ is used to compute the amplitude of each impulse. A time series for the impulse noise is given in Figure 3.12.

3.6 Conclusion

In this chapter, the basic environment and channel characteristics for digital data transmission over powerlines are introduced. Modelling methods for the PLC channel and noise are fully reviewed. The consistency of the simulation results of this work shows that both multipath model and transmission line can present the expected attenuation and frequency selective fading behaviour of the PLC channel. However, both channel models have their limitations. The multipath model describes the signal propagation behaviour but it is difficult to select the path weight and delay without a significant field measurement campaign. Also it is difficult to fit precisely the large number of paths required for the networks with complex topologies. The transmission line theory model is more flexible for different network topologies, but it still needs to know the precise network topology information before calculating the transfer function.

Chapter 4
Statistics Channel Modelling and Applications

As described in the last chapter, both transmission line channel model and multipath channel model have limitations. Thus, the statistical channel model for PLC network draws attention of many researchers recent years. Generally, dependence on topology is exempted in statistical channel models, since the statistics characteristics are extracted from tremendous channels based on variety of topologies. In [100] Zeddam reconstructs the channel transfer function by using extracted statistical features of peak/notch distribution, phased model and attenuation pattern in frequency domain, proposed a frequency domain statistics model for PLC network up to 100 MHz. Tonnelo in [90] submitted a random topology model to fit the EU in-home PLC environment. Based on the topology, statistical channel parameters such as average channel gain (ACG), root-mean-square (RMS-DS), path loss on time domain are found. In [71], Galli points out that the channel attenuation and RMS-DS of in-door PLC channels are correlated lognormal random variable. Also, two-tap statistical model by setting the amplitude and spread delay for two channel tap following the ACG and RMS-DS distribution is proposed in [71] for US PLC links. Also, the relation between geometrical distance and channel statistical characteristics is studied in [101]. In [102], a statistical channel model is proposed binary tree network topology and a clear statistical load modelling is also proposed in this paper. But the statistics models above still cannot precisely describe the path properties, such as magnitude, delay, phase, and path interval. Thus, the multipath properties are investigated and channel can be modelled according to the extracted properties in this work.

This chapter is organised as following: Section 4.2 described the PLC channel feature on time domain and the proposed methodology. The applications on communications theory approach for PLC and correlative impulse noise modelling based on proposed statistical model are introduced in 4.3 and 4.4 respectively.

4.1 Network Topology and Transfer Function

In order to capture the signal propagation behaviour characteristics of a large number of PLC network, a randomly generated networks topology is used. In some paper such as [6], [85] and [90], the tree type topology of the PLC network for both in-door and wide area network have been described. The PLC network can be considered as a series of branches connected by backbone cables. There may be sub-branches spreading out. Notice that all the sub-branches can be merged into the corresponding connected branch according to the impedance carry-back method in [90]. Thus the PLC network can be considered equivalent to the topology shown in Fig. 4.1 which consists of backbone cables and branches. The components and configuration of the network topology are described as follows:

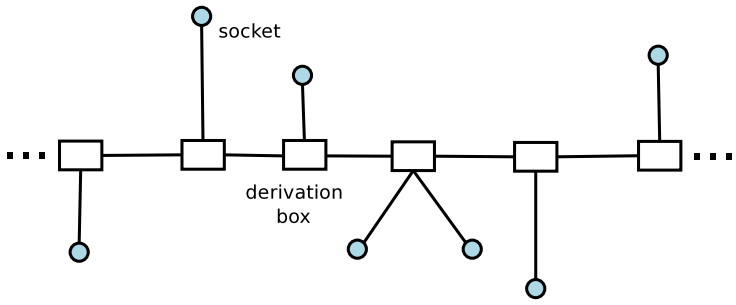

Figure 4.1: *An example of complex network topology*

- **Components:** From Fig. 4.1 three components, namely cables, outlet (circles) and junctions (squares) are used to form a PLC network. Cables are used to connect the outlets and junctions. In this paper, the cable types NAYY35 and NAYY150, which are widely used for indoor power distribution are used for outlet-junction and inter-junction connections respectively. The junctions can be a derivation box in practice. The outlets can be an open circuit power socket or a socket plugged with an appliance. Reflection signals occur at terminals with open sockets or mismatched appliances.

- **Branch density:** In powerline networks, the branch density may vary in different scenarios. A random branch density which yields a $\rho = 5$ Poisson distribution is applied for indicating the amount of the branches during a given transmission distance, 100 meters in this discussion. This is comparable low branch density for the purpose of extracting the precise statistical path properties from recognisable paths in the time domain.

- **Branch location:** For a given transmission distance and number of branches, branches

being uniformly distributed along the transmission path is a reasonable assumption which is also used in [90].

- **Branch length:** In [90] three connection types are described. For each connection type, the Probability Density Function (PDF) of branch length is given as function of the side length of the cell in building. In this paper, the branch length is generated according the PDFs in [90] with a maximum side length of up to 20m.

- **Terminal load:** To approach a realistic scenario, half of the terminals are randomly set to open circuit. For the remaining sockets, the impedance are randomly allocated a discrete value between 5 Ohms to 200 Ohms with a 5 Ohm interval. Similar assumptions can be also found in [85] and [90].

As described in Chapter 3, the PLC channel is typical multipath propagation channel. The number of reflection paths can be infinite in theory. Thus the channel impulse response for the $A \rightarrow C$ link can be expressed as:

$$h\left(t\right) = \sum_{i=1}^{\infty} I_i \cdot A_i(t, T_i) \tag{4.1}$$

where, I_i, $A_i(t, T_i)$ are the magnitude and pulse shape of the ith path respectively.

For the parameters in (4.1), I_i is impacted by the propagation constant and reflection coefficients of the junctions and branch terminations. When the network topology becomes complex, and the load impedance are random, it becomes very difficult to evaluate these parameters for each path. Thus, the statistical features of the channel are evaluated in the later parts of this paper. The delay T_i is a direct representation of the propagation distance of the ith path, $T_i = \frac{d_i}{v_p}$, where, d_i is the propagation distance of ith path and v_p is the signal propagation velocity in the power cable which is determined by the dielectric constant of the insulating material. In order to model channel according to (4.1), the following parameter - path magnitude, path interval and cable loss should be figured out.

In order to obtain these targets, a criterion is used to select the path. Theoretically speaking, there should be infinitely paths in a single multipath channel impulse response. In order to extract the path features, herein only paths with a magnitude which is larger than a certain threshold (20dB below the maximum peak magnitude, shown as Fig. 4.2 b.) are retained for analysis. This criterion is also used in [91]. In the investigation, the channel categorising

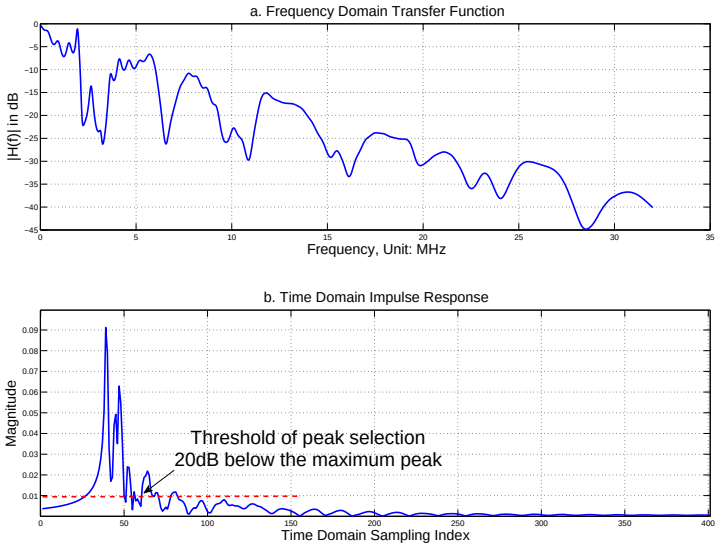

Figure 4.2: *An example of channel transfer function against the frequency and impulse response against the time domain sampling index, with 100 m transmission distance*

methods is proposed according to the magnitude of the first arrival path. Then, the other features are considered in each category. Base on the extracted channel features, the synthesis and verifying results are given in this section. In the following sections, the channel feature for the fixed distance transmission channel is investigated, then extends to the varying distance transmission.

4.2 Statistical Channel Modelling

4.2.1 Channel Statistical Feature for Fixed Distance Channel

In this section, the channel characteristics are analysed for the fix distance (set to 100 meters here) transmission. Some important multipath channel parameters are investigated, such as number of paths, path magnitude and path interval. The conclusion of fix distance will be the basis for the arbitrary distance PLC channel modelling. In the following parts, the time domain sampling index is used to indicate the time changing. The sampling interval is $\tau = \frac{1}{30\times10^6}$s.

4.2.1.1 Channel Classification

By observing a group of 100 meter fixed distance transmission PLC channels, a step change can be found in the magnitudes of the first arrival paths. As an important reference parameter in the multipath channel, the number of the path in a given channel is also investigated in term of the corresponding first arrival path magnitude. The result in Figure 4.3 is extracted from the

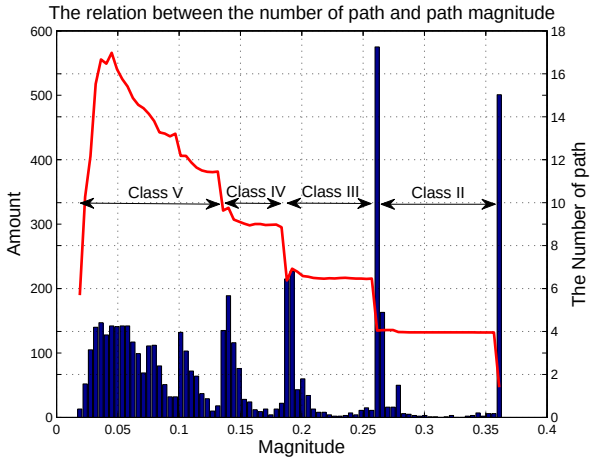

Figure 4.3: *The relation between the magnitude of the first arrival path and the number of path*

a group of 5000 100 meter transmission PLC channels. From the result we can see the channels whose magnitude of the first arrival path falls in a certain range, the number of multipaths will also keep in a similar level. For example, when the first arrival path magnitude falls between 0.35 and 0.26, the average path numbers of corresponding channels are about 4. Thus, the channels can be classified into different **Class** according the magnitude of first arrival path. The boundaries for the each class should be the jumping point shown in Figure 4.3

4.2.1.2 Number of Path

Though the number of paths for the channels in a class presents a certain level, the exact path numbers do not always stick to the average path number. Except the channels in the Class I, the number of paths for the channels in the same class yields the normal distribution. The phenomenon can be described by Figure 4.4. Due to the fact that the signal in Class I will not be impact by the reflection in of Class I, thus the path number in Class I only have one path.

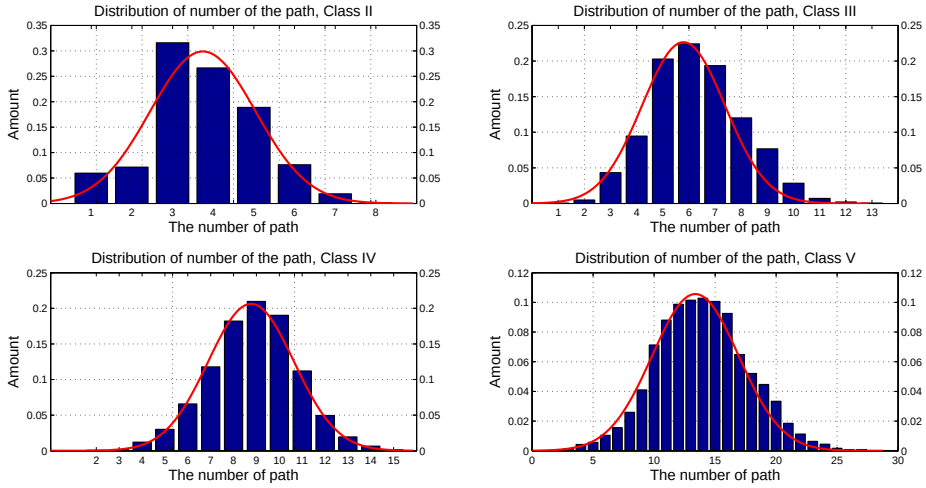

Figure 4.4: *The path number distribution of Class II, III, IV, V with 100 m fixed distance transmission PLC channels*

4.2.1.3 Magnitude Feature

As can be predicted, the magnitude of the path will reduce with the increasing the signal propagation distance due to the propagating attenuation. In Figure 4.5 the decay features of the paths in different classes are given in term of the time sampling index which can indicate the propagating distance. The magnitude changing trends can be describe by the exponential function with the time domain sampling index of the argument.

4.2.1.4 Path Interval

For the multipath channels, the arrival time of the paths determine the locations of deep fading in the transfer function in the frequency domain. Thus the arrival time is a very important parameter for the PLC channel. The path arrival time in the PLC channel is determined by a serial of factors such as the branch density, the length of branches. It is easy to identify the path arrival time if the topology is given. But considering an universal channel modelling method, the statistical feature of the path arrival time should be figured out for PLC channels. Here, the path interval distribution of the 100 meters transmission channels feature is shown in Figure 4.6. For the fix distance transmission channels, the arrival time of the first path is fixed and determined by shortest the propagation distance which is the direct path. Thus, based on the first arrival time and the interval distribution, the arrival time for each path can be determined.

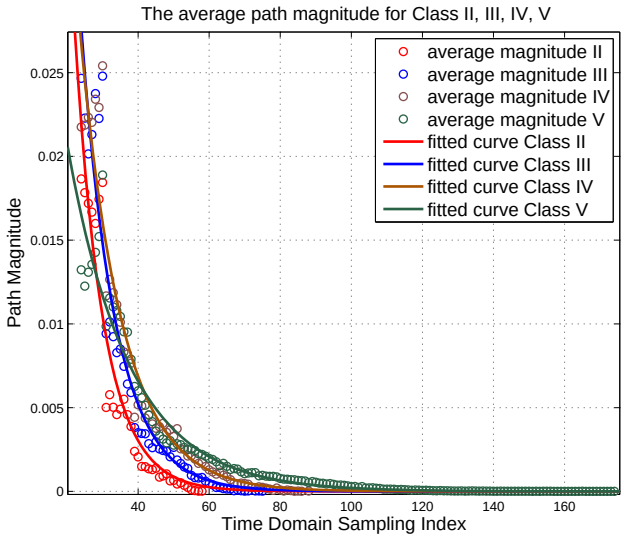

Figure 4.5: *The exponential decay feature of the path magnitude and corresponding fitted curves*

The number of the sampling points is used to demonstrate the time span of the interval. Also, the Generalised Extreme Value (GEV) distribution is used to fit the path interval distribution.

4.2.1.5 Phase

In many multipath channel researches, especially in wireless environment, the phase on each time domain sampling point often considered as the uniform random distributed between -2π to 2π, due to the full scattering during the signal propagation. In PLC network, the available reflection in PLC network is not as complex as the wireless environment. Thus the phase changing of PLC channel should be figured out, rather than using uniform distribution. Regardless the phase difference caused by the receiver, the phase of the PLC channel on time domain presents regular changing trends along with the time sampling index. Figure 4.7 shows the average phase over 10000 PLC channels with fixed 100 meter distance. .

But the average phase can not accurately describe the phase characteristics of PLC channel. Here the phase characteristics of a channel with single branch is given to demonstrate the relation between phase and network topology. In Figure 4.8, we can see that the branch will bring the disturbances on phase periodically, the parameter t_d, t_w and A are use describe the behaviour of disturbances. t_d is the interval of adjacent two disturbances, which is determined

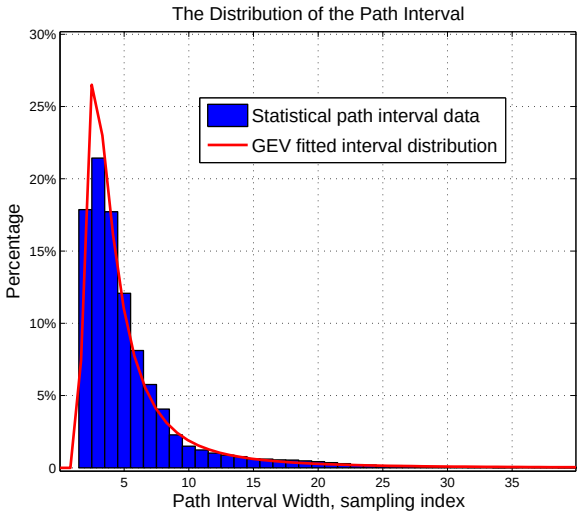

Figure 4.6: *The path interval distribution of the 100 meters fix distance transmission*

by transmission distance of the target channel. t_w is the width of disturbance is determined by the disturbance function. the amplitude of the disturbance can be obtained by measurement. Also the densities of disturbances are determined by the length of branch. For the channel with multi-branches, the phase of the channel can be considered as the superposing of a serial of disturbances caused by different independent branches. It is difficult to obtain the statistical feature of the phase changing trend for the a group of given channels. The modelling method of the phase will be described in the next section.

4.2.2 Channel Statistical Feature for Arbitrary Distance Channel

In the above sections, the general multipath characteristics such as classification, path magnitude, path interval and phase characters are investigated in detail for fixed 100 meters transmission PLC channels. But the above model can not be used as an universal model since the transmission distance should not be fixed in practical. In this section, we extend the above model into a more general scenario with vary transmission distance. Intuitively, with the varying of the transmission distance the arrival time and magnitude of first path, path interval, the path number of the channel will change as well. Interstingly, the step changing trend on the magnitude of the first arrival path, the additive of the phase still remain even though the transmission distance changes. In the following description, the statistical features along with the transmission distance varying are given.

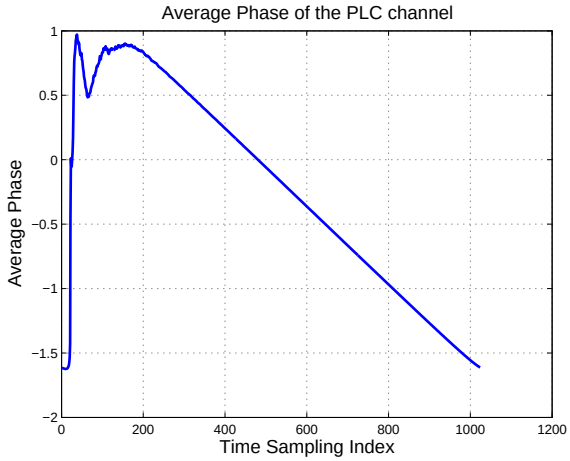

Figure 4.7: *Average phase along with the time sampling index*

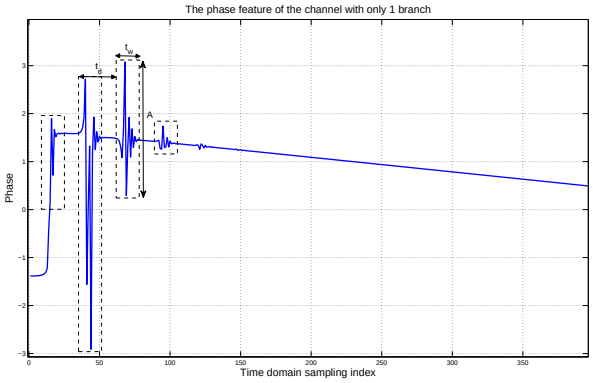

Figure 4.8: *The phase feature of the single branch PLC channel*

4.2.2.1 Channel Cluster

In order to identify the transmission distance, the conception **Cluster** is developed to demonstrate the distance property. Regardless of the practical frequency bands used in different PLC standards, a 30 MHz bandwidth which is used in most broadband PLC systems is investigated in this paper. Since the discrete time analysis is used in most systems, we use $\tau = \frac{1}{30\times10^6}$s as the sample period to describe the path behaviour in the time domain. In the following parts of this paper, the kth sampling point on time domain is termed as time sampling index k and the interval for two adjacent time sampling points is τ. Here, two indicators are investigated: the time sampling index of first arrival path and the impulse magnitude of non-impacted transmission which means there is no branches impact through the signal propagation. The features are

shown as Figure 4.9. From the Figure 4.9, we can see that the magnitude of the non-impacted

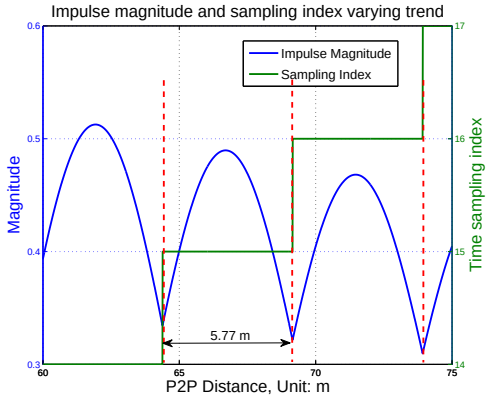

Figure 4.9: *The relation between the impulse magnitude and sampling index in term of the P2P distance*

path has an obvious periodic decay with increasing P2P distance. The first arrival path sampling index has a step jump with the P2P distance increasing. The changing or jump period is $J_p = 4.7695$ m. Based on this characteristic the conception **cluster** is induced herein to indicate the related channel features with transmission distance. The channel within the same cluster typical present similar features. Thus, the channel with the transmissions longer than 10 meters and less then 100 meters are assorted into 20 clusters, and the cluster index is defined as:

$$I_{interval} = \lceil \frac{(d - 11.923)}{4.77} \rceil \tag{4.2}$$

where, d is the P2P transmission distance, $\lceil \cdot \rceil$ denotes rounding the elements of X to the nearest integers towards infinity. The identifier **Cluster** here is used to indicate a channel falls in a transmission distance range rather than an exact distance. Then channels within a cluster can be classified into different Class use the similar feature shown in Section 4.2.1.1. In most situations the jump period is related to three parameters: permittivity, the permeability and the bandwidth of the expected channel. It also impacted by the cable cross-section geometry, but not significant. Considering the permittivity (PVC or other insulation) and permeability (cooper or aluminium) of the cables always in a certain level, the main fact that determines the jump period is the bandwidth of the expected channel. An empirical relation for the bandwidth and jump period can be written as $J_p = \frac{v_p}{2 \cdot B}$, where v_p is the signal propagation velocity in the given cable and B is the expected bandwidth.

4.2.2.2 Channel Class

When observing the magnitudes of the first arrival paths in a cluster, besides the fact that they arrive at the same time sampling index, the magnitudes present an obvious mutation changing phenomenon. In this work, the channels which have first arrival as the strongest path are considered. In some minority case, the channels that have the strongest path arriving as the second or third path are not included in the statistic. Furthermore, the mutation points in different clusters express similar relation with the maximum magnitude of that cluster. Thus channels in a cluster can be classified into 5 classes by using the mutation point as the boundaries. Further investigate the number of paths within a class, we find out the average number of paths for channels also appears mutation features. And the mutation boundaries are the same as the magnitude mutation boundary. Here, the classification method for the 10th cluster is shown in Figure 4.10. The boundaries for the other clusters appears in similar locations. Thus in the

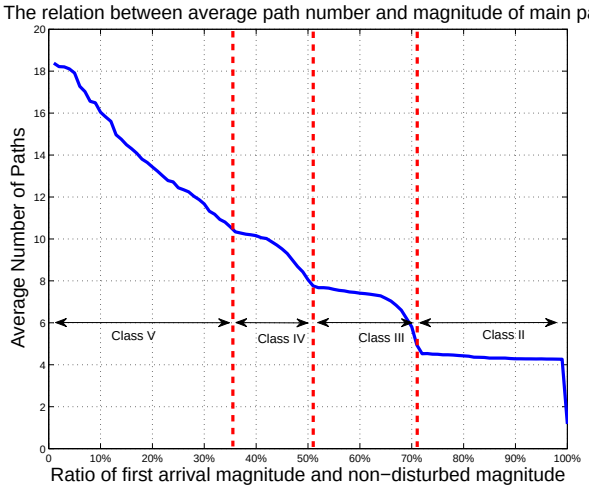

Figure 4.10: *Classification for* 10*th cluster*

later parts of this work, identifier **Cluster** and **Class** are used to mark a channel.

4.2.2.3 Distribution of Path Number

The average path number is roughly shown in Figure 4.10. But for an individual channel the path number is not fixed on the average level. By observing a group of channels of a certain class (except Class I) in a cluster, the path number for this group shows a Gaussian distribution which can be also seen in the other class of other cluster. Thus, 2 parameter sets, $\mu_{i,k}$ and $\sigma_{i,k}$

($i = 2, 3, 4, 5$), can be used to describe the path number feature for ith class of kth cluster. The changing trends of the parameters can be demonstrated by the Figure 4.11 and Figure 4.12.

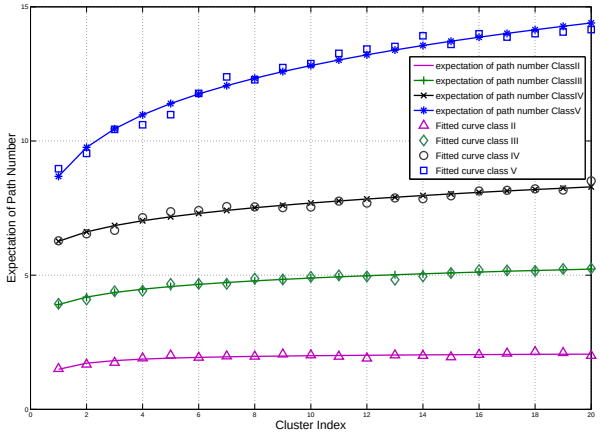

Figure 4.11: *The expectation of path number varying trend with cluster index*

Thus the path number for the ith class of kth cluster channels can be written:

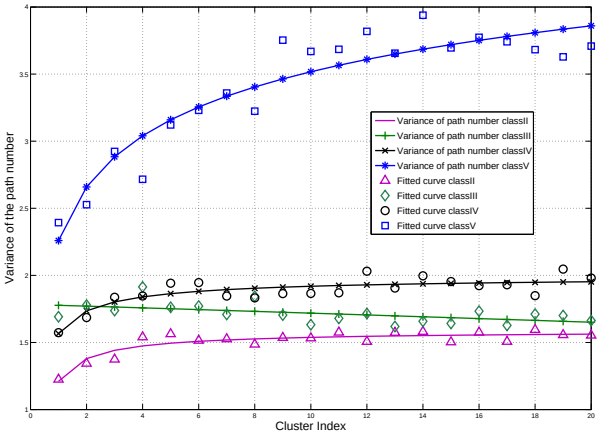

Figure 4.12: *The variance of the path number varying trend with cluster index*

$$N_{i,k} = [\mathcal{N}(\mu_{i,k}, \sigma_{i,k})] \tag{4.3}$$

where $[\cdot]$ means to round towards nearest integer. In some rare cases that negative numbers will be generated based on (4.3), the number should be dropped and a new positive path number regenerated. In order to obtain the path number for a particular channel by mathematical

method, power function is induced here to fit the changing trend of the expectation and variance of path number. the fitted curves can be seen in Figure 4.11 and 4.12. The expression $f(k) = p_1 k^{p_2} + p_3$ are use to describe the a power function, where k is the cluster index which act as argument in the expression, and p_1, p_2 and p_3 are scaling, power and offset parameters respectively. For each class, 2 sets of parameters are used to demonstrate the changing trends of expectation and variance respectively. The detail of the arguments set for $\mu_{i,k}$ and $\sigma_{i,k}$ and be found in Appendix B.

4.2.2.4 Magnitude Feature of Paths

- **First Arrival Path:** The magnitude of path depends on the how long the signal travels through the network. Thus, an anticipation that the magnitude of the main path will presents a decay feature with the increasing of cluster index. The decay feature shown in the Figure 4.13. In Figure 4.13, 5 double exponential functions are used to fit the

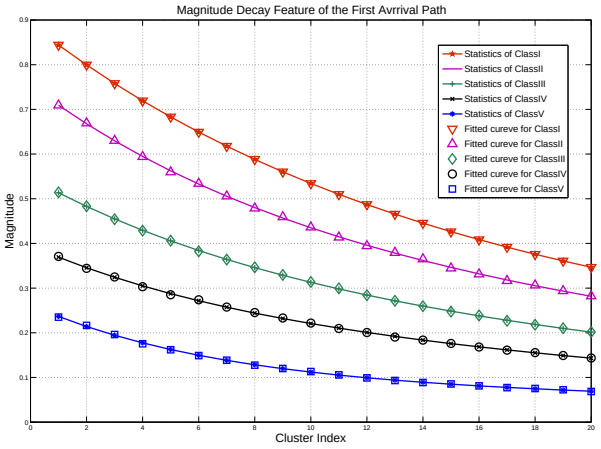

Figure 4.13: *Decay trend of first arrival path with cluster index increasing*

magnitude decay feature with the cluster index. Therefore, the average magnitude of the ith class of kth cluster can be expressed:

$$I_{i,k} = a_i^M e^{b_i^M k} + c_i^M e^{d_i^M k} \tag{4.4}$$

where. parameters a_i^M, b_i^M, c_i^M and d_i^M are given in Appendix B, k is the cluster index. The main path in Class I arrives at the destination without reflections. Thus the main path magnitude for Class I purely depends on the attenuation. For the main path

magnitudes of other classes, the power of the signal may be splitted by branches on the junctions, and absorbed on the terminal. Thus, the magnitude for these main paths show a random Rayleigh distribution according to [103], with the average magnitude in (4.4) as the parameter. In Appendix B, the detail of the parameters can be found.

- **Other Path:** Paths experience reflecting and decay in the other classes, thus the magnitudes for these paths do not present the obvious mutation feature. Thus, the for these paths, only the magnitude characteristics of the propagation distance (cluster) is investigated. The average magnitudes of different classes within a cluster present the very similar decay feature, thus, in this paper we do not figure out the magnitude differences between classes. To simplify the processing herein the time sampling index is used to indicate the propagation distance. The average magnitude decay trends of these paths also can be described by the double exponential functions, and Figure 4.14 shows the fitted double exponential curves for the Cluster 1, 10 and 20 as examples. The double exponential function for these paths is written as:

$$I_{k,j} = a_k^O e^{b_k^O j} + c_k^O e^{d_k^O j} \tag{4.5}$$

Where k is the cluster index and j is the time sampling index. a_k^O, b_k^O, c_k^O and d_k^O are given in Appendix B. As described in [103] the magnitudes on these paths present

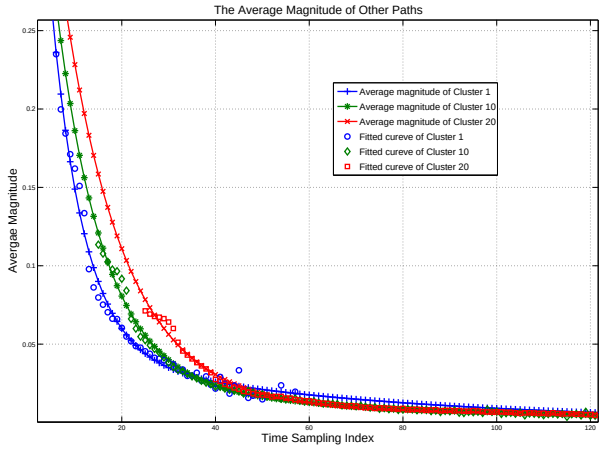

Figure 4.14: *Average Magnitude of Cluster 1, 10 and 20*

significant Rayleigh fading feature due to the random signal reflecting behaviour through the network,. Thus, the Rayleigh distribution is used to generate the path magnitude with

the average magnitude in (4.5) as the parameter.

4.2.2.5 Distribution of Path Interval

The main cause of the multipath delay interval is due to differences in multipath signal propagation distances. Different signals arrival at different time that can be indicated by the time sampling index. From the statistical results, a conclusion can be obtained that the path interval distribution follows a Generalised Extreme Value (GEV) distribution. Normally, 3 parameters are used to describe a GEV distribution. Thus the interval PDF of the ith class of kth cluster can be written as:

$$f_{gev}\left(x;\phi_{i,k},\eta_{i,k},\xi_{i,k}\right)=\frac{1}{\eta_{i,k}}\left(1+\xi_{i,k}\left(\frac{x-\epsilon_{i,k}}{\eta_{i,k}}\right)\right)^{-\frac{1}{\xi_{i,k}}-1}e^{-\left(1+\xi_{i,k}\left(\frac{x-\epsilon_{i,k}}{\eta_{i,k}}\right)\right)^{-\frac{1}{\xi_{i,k}}}} \tag{4.6}$$

The parameters $\phi_{i,k}$, $\eta_{i,k}$ and $\xi_{i,k}$ changing trend with cluster index can be seen in Figure 4.15: From Figure 4.15, besides the power function fitting for $\eta_{2,:}$ and $\xi_{2,:}$ of the Class II, the other

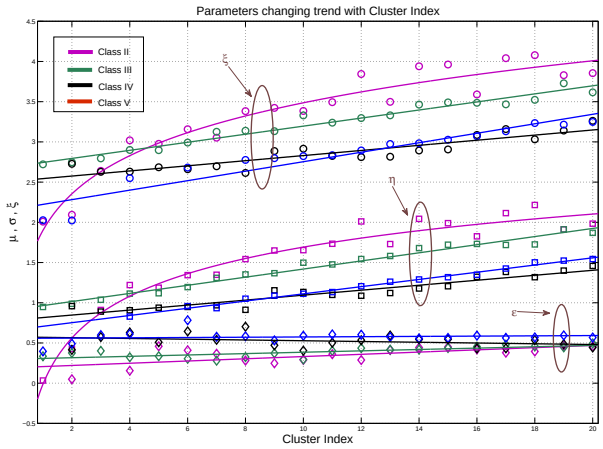

Figure 4.15: *The GEV Parameter Changing Trend in Term of Cluster Index*

parameters are fitted by linear functions. Also, all the fitted function parameters can be found in Appendix B. There is no path interval issue for channels of Class I since only 1 path exist in these channels.

4.2.3 Sampling Rate Conversion

According to the previous steps, a sampled sequence of paths for a fixed sample rate system can be obtained. As can be seen from the above description of path power delay profile and the path interval, we use the time domain sampling index as the metrics. But in practice, different sampling rates may be required e.g. for smart grid systematic operating over narrower bandwidth. Here a method based on the farrow structure filter is given for a user to apply this model to different sampling rates. Assume that the original sampling time is t_a and the required sampling time is $t_a^{'}$. Thus the conversion rate is $R = t_a/t_a^{'}$. The structure and designing of the Farrow filter can be found in [104]. To simplify the implementation of the sampling rate conversion, the coefficients of the Farrow filter can be obtained by using the function **mfilt.farrowsrc** in Matlab DSP system toolbox and the conversion rate R is the input argument for function. The channel path sequence under the expected sampling time $t_a^{'}$ can be obtained by passing the original sequence through the Farrow filter.

4.2.4 Cable Loss

Based on the mathematical models built in the above sections, the number of paths, the corresponding arrival time and magnitude for each path can be generated if the **Cluster** and **Class** are given. Thus, a discrete sampling sequence can be obtained. In Figure 4.16, the a serial of generated path magnitude and corresponding frequency transfer function is shown.

But in practice, the power dissipation effect of the cable will cause pulse shape distortion which is represented as a cable loss in the frequency domain. In [18], it has been stated that the average cable loss is determined by the real part of the propagation constant and signal propagation distance. Since the propagation constant of the cable is highly frequency dependent, the cable loss in the powerline channel will also be dependent on frequency and distance. According to [18], the cable losses in the frequency domain of a powerline can be approximated as:

$$A\left(f,d\right) = e^{-\left(a_0+a_1\cdot f^k\right)}e^{-jb_0 f} \tag{4.7}$$

where a_0, a_1 and k represent different types of attenuation factor. For a given cable, a_0 and a_1 are linear functions of path propagation d, and can be calculated by the cable parameters in Appendix B. The function $A(f,d)$ thus is the propagation attenuation of a certain signal at a given frequency. Unlike the cable loss formula in [18], in this paper the phase trend is also given

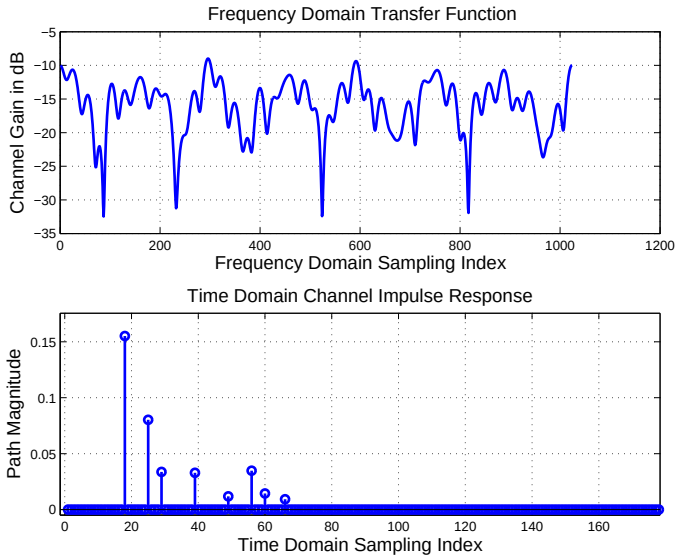

Figure 4.16: *The generated path magnitude and corresponding frequency domain transfer function without cable loss*

which is determined by cable properties and propagation distance. The phase can be described by the parameter b_0, which also follows a linear relationship with the path propagation d. The parameter b_0 can be found in Appendix B. Since a_0, a_1, k and b_0 are functions of propagation distance, the cable loss $A(f)$ will also be a function of the propagation distance. Based on the parameters in Appendix B, the cable loss will increase with the propagation distance. Since the arrival time τ_i of ith path can be obtained by first arrival path and the path interval, the propagation distance for each path in a certain channel can be calculated by $d_i = v\tau_i$ m. The scalar v_p is the Transverse Electromagnetic (TEM) wave propagation speed in the cable, which can be calculated according to the permittivity of the insulator of the cable. Since in this paper, the time domain properties are of interest, the cable loss effect in the time domain can evaluated as the inverse Fourier transform of (4.7), written as $A'_{ti}(t, v_p\tau_i)$ which is refereed as the pulse shape of the ith path. After assigning the corresponding path delay to the ith impulse, the impulse can be written as $A_t(t, T_i) = A'_{ti}(t, vT_i) \otimes \delta(t - T_i)$, where, T_i is the path delay of the ith path and $\otimes$ is the convolution operation. Finally, by referring A_t back to (4.1) the channel impulse response which fully presents multipath fading, cable losses, and phase features is obtained.

By using the cable loss both attenuation and phase characteristics of the channel can be precisely expressed in the proposed statistical model. After the interpolating, the channel impulse

response and transfer function is shown as Figure 4.17. .

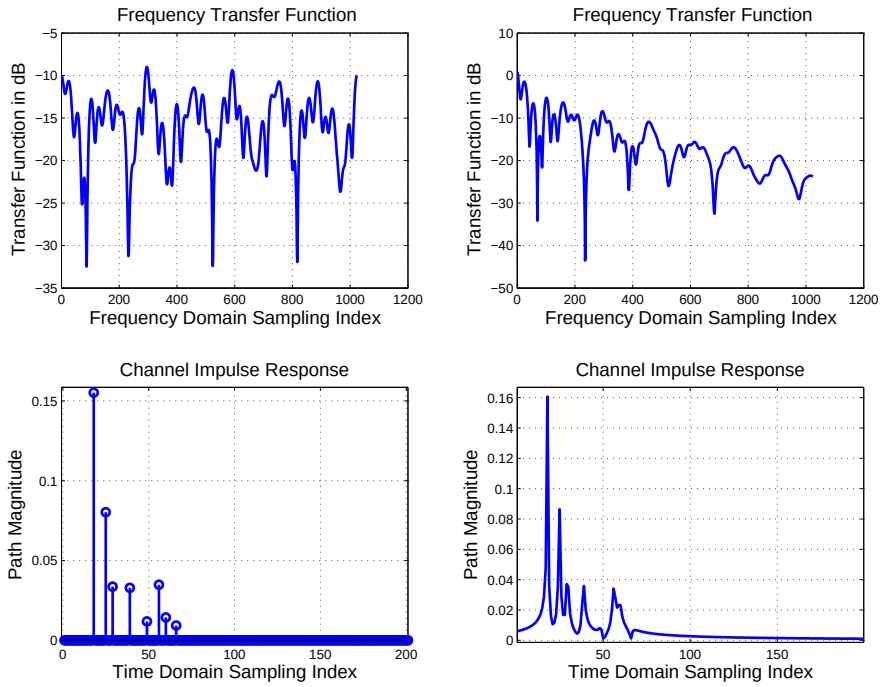

Figure 4.17: *The Comparison between the transfer functions before and after interpolating*

4.2.5 The Verifying of Proposed Method

To verify the proposed statistical model for PLC channel, a group of time domain channels is generated, and compared with the channel generated by using TLT theory on frequency domain. Figure 4.18 (a) shows the example of the generated channel impulse response.

Besides the average channel gain, the other two important indicators of a multipath channel are the delay spread and the effective length. The delay spread is the root mean square of the power delay profile and the effective length is the time interval which covers a certain percentage of the impulse energy. The delay spread and effective length distributions shown in Figure 4.19 are counted from the two groups of channels generated according to the statistical and the TLT model respectively. The generated channels contain transmission ranges from 20m to 100m which covers most indoor transmission distances. When considering delay spread, the statistical model shows high consistency with the TLT model. It means that our statistical model captured the characteristics of the selected paths. The criterion for selecting paths is introduced

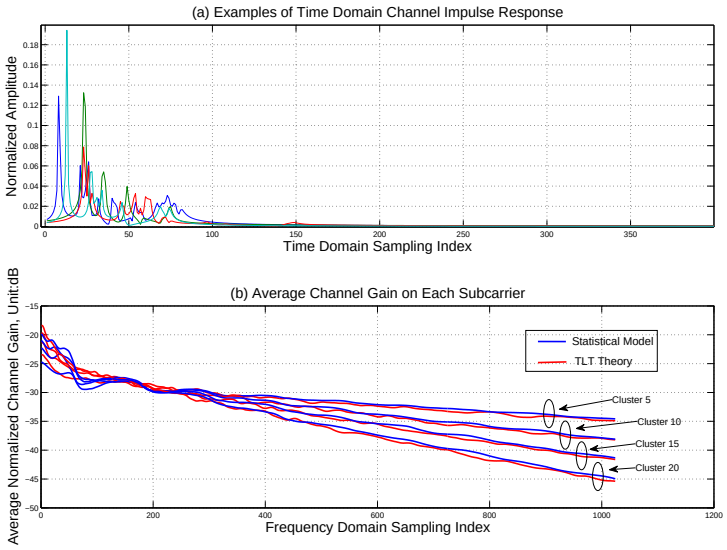

Figure 4.18: *The comparison of the statistical channel modelling result and TLT modelling result for Cluster5, 10, 15, 20*

in Section III Part A. Comparing with TLT channels, the effective length of statistical channels are more concentrated in a relatively short range (about 0.66 μs to 2.5 μs). This because that the paths which have very small power and thus have minimal impact on frequency selective fading are not considered in the statistical model. However, when considering the effective length of the channel, the power of these ignored paths will contribute additional power dispersion for the TLT model. Thus, the effective length distribution of the TLT model covers a relatively wider range (about 0.5 μs to 3.0 μs). However, consistency can still be seen from comparison of the two distributions. This means that the methodology used in this paper can accurately represent path interval behaviour.

4.3 Application I

The purpose of the statistical modelling is to spark the researches on general capacity evaluation, network deployment, and network coverage. In this section, the achievable information rate for each cluster is calculated and compared with the information rate based on the TLT channel model. The capacity changing trend over the cluster index is given in Figure 4.20 From Figure 4.20, the achievable information rate based on the channels shown in Figure 4.18 shows the consistent decrease trend as the information rate derived according to TLT theory. To

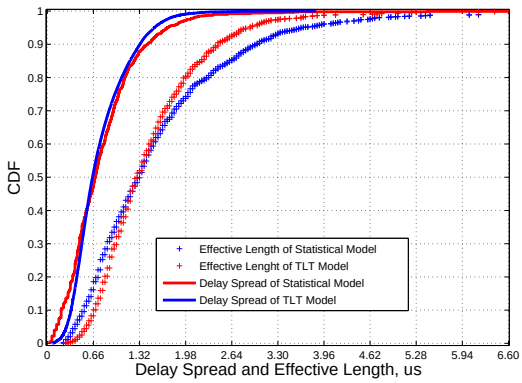

Figure 4.19: *The CDFs of effective lengths and delay spreads deduced from statistical model and TLT model*

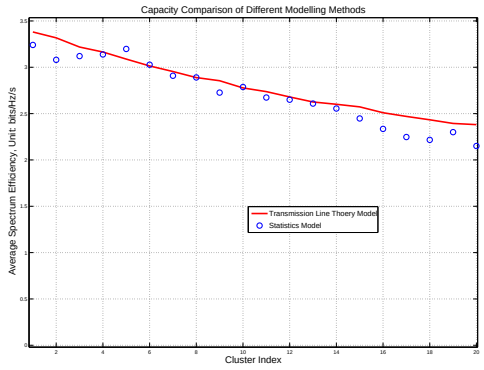

Figure 4.20: *The capacity changing trend with the P2P distance Increasing, here the normalised channel is used*

further speculate the information rate distribution over all the possible rates, the CDFs of the achievable information rates based on statistical model and TLT for Cluster 5, 10, 15 and 20 are shown in Figure 4.21. The information rates derived from both channel model present the similar rate distribution over all the possible information rate range. The similarity indicate that the statistical model can fully express PLC channel characteristics. The possibility of the bad or good channel conditions, attenuation property and frequency selective fading in statistical model can cover the research requirement of the PLC capacity evaluation.

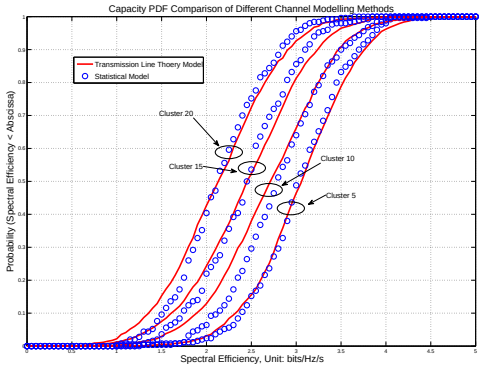

Figure 4.21: *CDFs of the capacities based on the statistics model and transmission line theory*

4.4 Application II

Impulse noise in PLC is composed of periodic and aperiodic impulsive noises. The periodic impulsive noise which is caused by power converters in power supplies and by rectifiers occurs in the alternating voltage current network. Sources for aperiodic impulsive noise are switched power supplies, the turning on/off of appliances, and so on. In [58] a Markov chain is used to simulate the impulse noise behaviour. Based on [58] the impulse noise will appear independently at each PLC node and socket in general. But considering the practical situation in PLC network, the impulse noise will propagate in a given PLC network through the power cables. Thus, the impulse noise on different sockets or nodes will be correlated. As shown in Fig. 4.22 impulse arises at Socket A due to the switch on/off of this socket. After spreading to Socket B and Socket C through Network_2 and Network_3, the impulse magnitude will be reduced, while the delay spread will increase. To build a more realistic signal propagation environment in PLC, a correlated impulse noise model is thus necessary. This is particularly important for concepts such as the relay enhanced PLC network as described in [105]. Assume Socket B and Socket C are the transceivers and Socket A is the relay node for the bi-directional protocols in [105]. In the bi-directional scenario, both data transmission will be disturbed when the impulse noise arises, since the impulse noise will propagate simultaneously with the signal. Thus, the model of impulse noise is particularly important for capacity evaluation of bi-directional relay protocols in PLC networks. Also, with a more realistic impulse noise, high performance noise cancellation schemes could be developed which exploit knowledge of the correlation of the impulse noise.

Considering a realistic scenario, if we intend to obtain the exact impulse noise on each socket

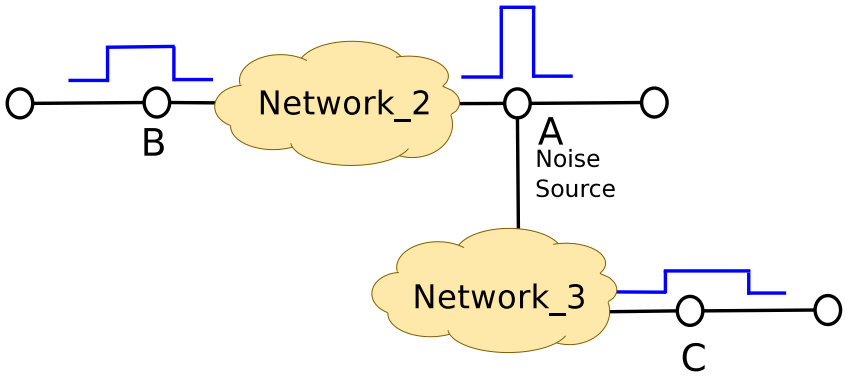

Figure 4.22: *The Impulse Noise Spread Model in PLC Network*

channel knowledge between every socket pair should be known, which is complex to evaluate in practice. If we apply the time domain statistical model of the PLC network into impulse noise modelling, the only knowledge required is the distance profile between each socket pair. The impact of the network topology and impedance on the terminals are integrated into the statistical data. Assume Network_2 and Network_3 in Fig. 4.22 are belong to Cluster 10 and Cluster 20 respectively. Here, we assume the rectangular impulse originates at node A. Two channels are generated according to the proposed statistical model for Cluster 10 and Cluster 20 respectively. After the convolution operation, the magnitudes and time spreads of an impulse on node B and C are shown as Fig. 4.23. Unlike current impulse noise modelling methods, the impulse noise at different PLC transmission nodes will be correlated. The simulation result in Fig. 4.23 shows that the amplitude of the impulse noise is attenuated when it passes through the channel, meanwhile the time span become wider.

The details of the attenuated amplitude M_i and spread time τ_{wi} can be calculated by using the proposed statistical channel model. Considering amplitude attenuation and time spread of the correlated impulse noise in PLC networks, related technologies such as performance evaluation calculations, channel coding and modulation can be reconsidered in PLC.

4.5 Conclusion

In this chapter, a statistical channel modelling method in the time domain is proposed for PLC networks. First, the channels are sorted into different categories based on the P2P distance and the magnitude of the first arrival path. Second, the multipath parameters such as path magnitude

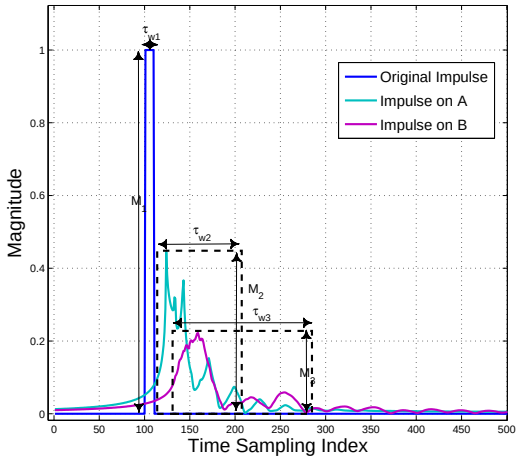

Figure 4.23: *The Impulse Noise Spread Model in PLC Network, the unit of the impulse noise is measured in voltage*

and path interval are extracted to build the time domain impulse response. Furthermore, a Farrow structure filter is proposed to make sampling rate conversion according to the practical scenario requirements. Finally, the proposed statistical model is used for capacity evaluations and correlative impulse noise modelling in PLC networks. The proposed statistics integrate the impact of topology and terminal loads. By comparing with the modelling results from the TLT method, the statistical model is proved to accurately capture the path delay and the average attenuation. Also, the Shanon capacity derived from statistical and transmission line models shows that the proposed model is a feasible tool for PLC research. Based on this statistical model, fast and efficient studies of deployment, coverage and capacity of the PLC network can be carried out. In order to extend the proposed methodology to a more general application scenarios, especially for the Smart Grid, more channel magnitude and time spread types for different power grids should be considered in future where the main issue is the impact of different branch densities on path magnitudes and path intervals.

Chapter 5
Relay for Powerline Communications

There has been a long history of using powerline as communications medium, but it was limited to narrowband low bit rate applications such as telephony and simple command and control for long time. With the development of communication techniques in higher frequency band up to 30 MHz or even 100 MHz, new applications such as Internet access, high definition (HDTV), in-home entertainment over powerline are proposed as broadband PLC. Also, with the development of the Smart Grid concept, the larger coverage and higher bit rate transmission over narrowband PLC is in demand. But the transmission capacity and network coverage of PLC network are limited due to the severity of the PLC environment, such as attenuation along with the transmission distance, frequency selective fading and coloured background noise. In order to remedy the defects of the PLC transmission, relay aided transmission protocols are proposed in this chapter. Relays, which has been discussed exhaustively in wireless communications are used to increase the network coverage, data transmission capacity and system robustness. Considering the frequency selective fading in PLC network, a relay node between transmitter and receiver may make up the loss in data rate caused by deep fading. There are already some papers that discuss specific relay schemes in PLC networks. But there is no comprehensive investigation on how relay options, such as amplify-and-forward (AF), decode-and-forward (DF) along with the number of the nodes, and data stream direction, impact the performance. Thus, in this work, the performance of different relay options are investigated to help the later researcher focusing on the option which has better performance in PLC networks.

The structure of this chapter is as follows: The relay protocols are described in Subsection 5.2.1, The relay protocols cover the topics such as forward mode, number of the relay nodes, and direction of data stream. In Subsection 5.2.2, the protocol performance with channel estimation error is studied. Section 5.3 summarises the chapter.

5.1 Review of Relay on PLC

So far, communications over powerline is still quite an open topic compared with the communications over other medium like wireless channel. Many aspects of the PLC are still under investigation. There are even fewer papers on relay aided PLC networks. In this section, current research on relay aided PLC networks carried out by other researchers is reviewed. The first paper on introducing relay concepts for PLC is by Lampe in [106] in 2006. In [106], the relay nodes which are termed as repeaters retransmitting the received signal using a distributed space-time block coding (DSTBC) scheme with a pre-assigned unique signature sequence. With the proposed DSTBC scheme, the transmit power and multi-hop delay are reduced. In [78] and [107], Zou proposed dynamic spectrum and power allocation schemes for DF aided PLC relay in view of the selective frequency fading nature of the PLC channel. With the proposed resource allocation schemes, the data transmission capacity of the relay aided PLC network is increased. In [108], a multi-relay node multi-hop AF scenario is investigated, and cooperative diversity gain is first used to evaluate the PLC performance. In [109] and [110], an opportunistic relay scheme is proposed based on a realistic channel model. The proposed opportunistic relay scheme selects the best candidate and optimises the time duration for both source-relay and relay-destination transmissions in DF relay PLC networks. The numerical results in the paper show that the optimised opportunistic DF scheme can achieve power saving or coverage extension. In [111], the authors discussed the system capacity of a AF relay scheme for long distance data transmission over a power cable. Then, in [112], the same authors further involved the optimal power allocation between the transmitting nodes and the optimal power distribution over the signal frequency band in the AF aided PLC network. Besides the relay application in the broadband PLC networks, flooding relay schemes can be used in the single-frequency networks as proposed in [113] for the large-scale PLC automation control which is identified as a narrowband PLC application. The simulation results show that the robustness and transmission delay performance are increased by the proposed flooding transmission. For narrowband PLC applications, a space-time coding (STC) criterion is proposed in [114] [115] for the purpose to increase the data rate.

In this work, we focus our scope on the broadband PLC networks. As can be seen from the review, the works on the relay aided PLC network so far are fragmental and not systematical. Each work only focuses on one or two aspects of PLC networks. For example, both [108] and [111] only investigate the AF aided PLC, but they did not mention why AF is chosen for

the work. Similarly in [78], [106], [107] [109] and [110], they did not explain why DF is picked out as research object. Also, some of the conclusion in the papers are contradictory. For example, cooperative diversity gain is emphasised in [108], but diversity gain in PLC networks is disputed in [78] because of the correlation between $S \rightarrow R$ and $R \rightarrow D$ channels. Also, in these papers, only [109] and [110] clearly showed that valid channel and noise models are used for conducting results. In the other papers, they do not demonstrate that the proper channel and noise models are used. Researchers have not presented clear consistent conclusions on what is the main impact factors in PLC and which relay technology is the suitable for the PLC in the above papers. Thus, a detailed investigation of relay aided PLC is given in our work. The data forwarding approaches (DF/AF), the number of relay nodes, relay working duplex mode, and channel estimation impact are thoroughly studied. Based on the results of our work, the reader can easily figure out the most suitable technology for relay PLC network.

5.2 Relay for Broadband PLC Network

5.2.1 Relay Protocols and Performance for PLC Network

In papers on relay enhanced networks, techniques such as the forwarding mechanism, the number of relay nodes, the validity of the direct link and duplex mode of relay node, are often discussed for different communications systems. As the power grid as a new medium for relay communications, there is still not clear conclusions about which option will potentially benefit data transmission. In this section, the relay protocols that cover all the mentioned facts are investigated for finding out proper principles for PLC network.

5.2.1.1 Uni-direction Decode-and-Forward

To discuss Decode-and-Forward (DF) relay aided PLC transmission, the first issue needing to be studied is the location of the relay node. Unlike the situation in wireless communications where the relay can be deployed in an arbitrary location between the data source and the destination. In PLC networks, the relay node can usually only be placed on the power sockets, the deviation box or in a transformer station. Since the focus of the broadband PLC network is mainly about indoor, inter houses and transform station to house scenarios, thus, here we only consider the socket and deviation box as the candidate relay position. In this work, single relay and multiple relays scenarios are discussed due to the fact that there are more then one locations

in PLC network that can be used as relay node,

Single Relay In Figure 5.1, two abstracted relay channel are given for the single relay PLC network. Figure 5.1 (a) shows that the relay is located on the main path from data source to destination. Figure 5.1 (b) shows that the relay located at the terminal of a branch. In

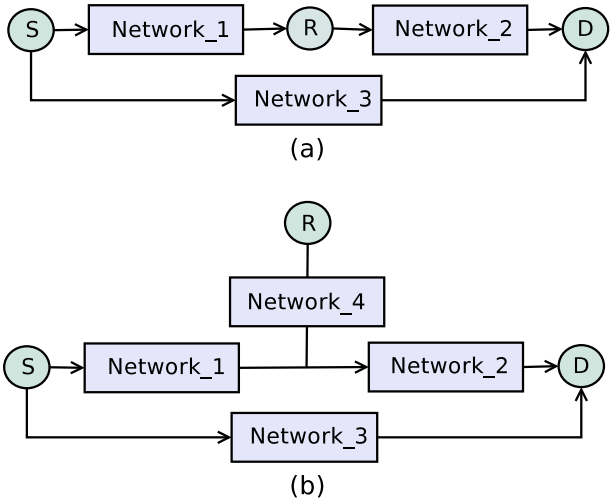

Figure 5.1: *The abstracted single relay node channel for PLC network*

scenario (a), the transfer function of Network_3 can be considered as the product of the tansfer functions of Network_1 and Network_2 as shown in equation (3.36). In scenario (b), equation (3.35) is required because the product relation does not hold since there is a shunt network (Network_4) is connected between the two networks. The capacity of the single relay uni-direction DF protocol is discussed under the assumptions that transmission via Network_3 is valid/invalid. The Network_X is one part of the PLC network. In the case shown in Figure 5.1, Network_3 is denotes the network for the direct propagation, Network_1 and Network_2 are the networks of S$\rightarrow$ R and R$\rightarrow$ D links. The situation can be demonstrated as Figure 5.2.

Though (a) and (b) are used to present different scenarios, they can use the same process to evaluate the system capacity by following equations (5.1) to (5.5). As a multi-path transmission environment, discrete multi-tone (DMT) is utilised to combat the frequency selective fading channel. Assume there are K subcarriers in total over the available bandwidth. First, we consider the situation that the Network_3 is invalid. The achievable spectrum efficiency for source-relay ($S \rightarrow R$) link and relay-destination ($R \rightarrow D$) link

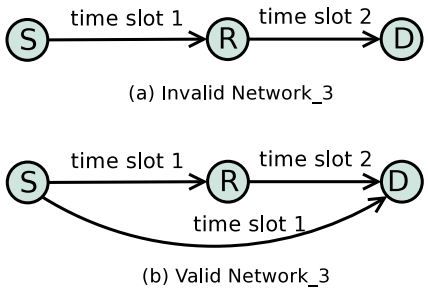

Figure 5.2: *The transmission situations when $S \rightarrow D$ link is invalid (a) and valid (b)*

can be written as:

$$R_{sr} = \frac{1}{K}\sum_{k=1}^{K}\log_2\left(1+\frac{SNR_{sr}^{k}\cdot \mid h_{sr}^{k} \mid^2}{\Gamma}\right) \tag{5.1}$$

Similarly, the spectrum efficiency for $R \rightarrow D$ link is:

$$R_{rd} = \frac{1}{K}\sum_{k=1}^{K}\log_2\left(1+\frac{SNR_{rd}^{k}\cdot \mid h_{rd}^{k} \mid^2}{\Gamma}\right) \tag{5.2}$$

where, $SNR_{sr}^{k} = \frac{P_s}{\sigma_r^2}$, $SNR_{rd}^{k} = \frac{P_r}{\sigma_d^2}$, h_{sr}^{k} and h_{rd}^{k} are the SNR and channel gains for $S \rightarrow R$ and $R \rightarrow D$ links on the kth subcarrier respectively. P_s and P_r are are the transmit power level at the source node and the relay node. Γ is the SNR gap introduced in 2.3.1.3. Here, we assume that all the PLC devices have the same transmission power. σ_r^2 and σ_{dr}^2 are the noise power level at the relay node and the destination node. According to [116], regardless of the delay caused by buffering, the overall spectrum efficiency for the single relay uni-directional link scenario DF protocol can be maximised by full buffer operation on relay node is:

$$R_{uni\_DF}^{single\_invalid} = \frac{R_{sr}\cdot R_{rd}}{R_{sr}+R_{rd}} \tag{5.3}$$

The buffering method is used for balance the S→ R and R→ D links when the transmission capacities of these two links are too unbalanced. The balance is achieved by adjusting the transmission durations of the S→ R and R→ D phase according to the capacity of the links, which is described in [116] in detail.

When the $S \rightarrow D$ link is considered, the spectrum efficiency for the second time slot

should be modified as:

$$R_{2nd}^{valid} = \frac{1}{K}\sum_{k=1}^{K}\log_2\left(1+\frac{SNR_{sd}^{k}\cdot \mid h_{sd}^{k} \mid^2 + SNR_{rd}^{k}\cdot \mid h_{rd}^{k} \mid^2}{\Gamma}\right) \tag{5.4}$$

$SNR_{sd}^{k} = \frac{P_s}{\sigma_d^2}$ is the SNR for $S \rightarrow D$ link on kth subcarrier. We assume that a buffer is not used in the relay when the $S \rightarrow D$ link is available, the overall spectrum efficiency for the valid $S \rightarrow D$ link situation can be written as:

$$R_{uni\_DF}^{single\_valid} = \frac{1}{2}\min\left\{R_{sr}, R_{2nd}^{valid}\right\} \tag{5.5}$$

This result assumes that the slot duration of two phase are equal for $S \rightarrow R$ and $R \rightarrow D$ links because data source should use the same transmission scheme for the $S \rightarrow R$ and $S \rightarrow D$ link in two time slots . Thus factor $\frac{1}{2}$ is used. Based on the above analysis, the achievable spectrum efficiencies for the single relay DF protocol are given in Figure 5.3. From the simulation results, we can see that the capacity of the direct

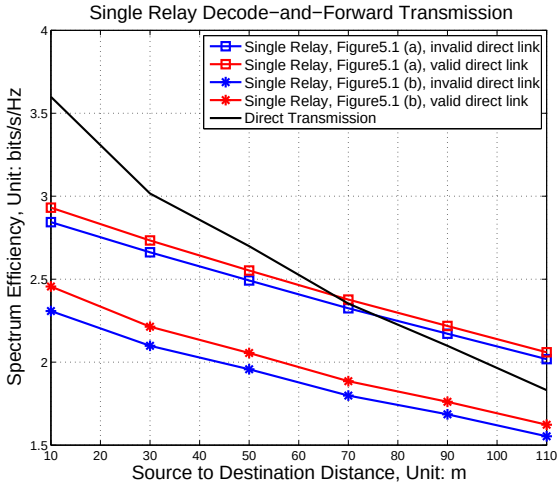

Figure 5.3: *The achievable spectrum efficiencies for the uni-directional single relay DF transmission*

transmission decreases faster then the DF aided transmission schemes as a decreased with source to destination distance increasing. It means that the link quality can be improved by the DF operation when the channel attenuation becomes significant, for example, when the distance is longer than 70m. Another important conclusion can be seen from Figure 5.3 is that the relay will bring more benefit to the system when the relay node

is located at the main path. This indicates that the transformer or deviation box will be better candidate for deploying relay nodes comparing with the terminal socket. Also, the validity of the $S \rightarrow D$ link will also bring extra gain due to the SNR gain but not significant.

Multiple Relay Multi-relay transmission is possible in a PLC network since all the sockets, transform station and deviation box can be used as relay nodes. Thus, the multi-relay scenario can be described as Figure 5.4 The multi-relay uni-direction DF protocol is

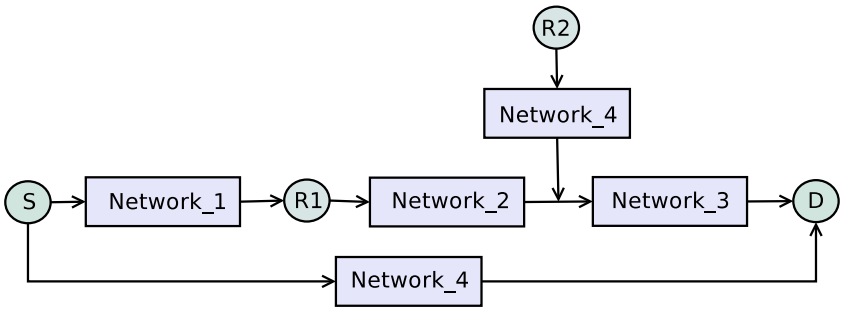

Figure 5.4: *The subtracted multi-relay DF transmission channel model*

discussed under the assumptions that transmission through Network_4 is valid/invalid. The situation can be demonstrated as Figure 5.5. In the multi-relay DF scenario, all the

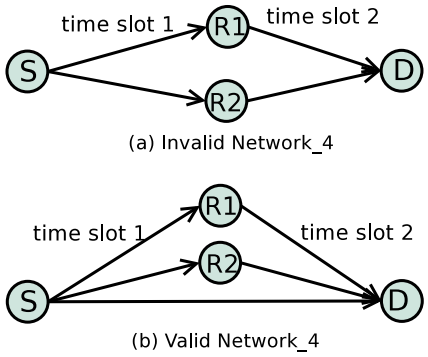

Figure 5.5: *The multi-relay transmission situations when $S \rightarrow D$ link is invalid and valid*

relay nodes need to decode the message sent by source node, then forward to destination. In order to make the all the relay nodes have the ability to decode the message, the data transmission capacity for the 1st data transmission phase are limited by the minimum capacities of the $S \rightarrow R_1$ and $S \rightarrow R_2$ link:

$$R_{1st}^{multi} = \min\{R_{sr_1}, R_{sr_2}\} \tag{5.6}$$

Thus, the overall capacity for the multi-relay DF protocol can be written as:

$$R_{uni\_DF}^{multi} = \frac{1}{2}\min\{R_{1st}, R_{2nd}\} \tag{5.7}$$

where:

$$R_{2nd}^{multi} = \frac{1}{K}\sum_{k=1}^{K}\log_2\left(1+\frac{SNR_{r_1d}^k + SNR_{r_2d}^k}{\Gamma}\right) \tag{5.8}$$

and $SNR_{r_1d}^k$ and $SNR_{r_2d}^k$ are the SNR of $R_1 \rightarrow D$ and $R_2 \rightarrow D$ links which has already taken account the SNR gap Γ which is introduced in 2.3.1.3. From (5.6) and (5.7), we can see that the performance of multi-relay DF protocol is limited by the worse case of the $S \rightarrow R_1$ and $S \rightarrow R_2$ links. But considering the fact that data transmission in the 2nd phase will be enhanced due to the SNR gain, the overall data transmission can be improved when the capacity of 1st phase is enhanced. Thus, we can conclude that when the relay nodes are close to the data Source, the performance will be significantly improved. Based on the above analysis, the performance of the two relay DF scheme is given and compared with the single relay DF scheme in Figure 5.6 For the two relay

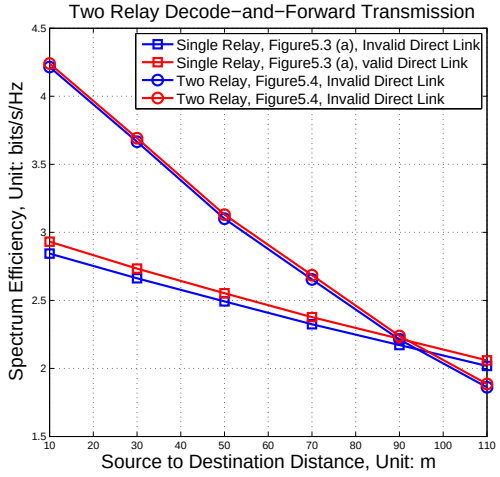

Figure 5.6: *The achievable spectrum efficiencies for the two relay uni-directional DF transmission*

simulation, we assume there are two relay nodes randomly located on the main path or a branch respectively. From the result in Figure 5.6, we can see that the extra relay brought significant performance gain when the transmission distance is short. But the performance deteriorates quickly compared with the single relay DF schemes. This is because the performance of the two relay nodes DF protocol is deeply limited by the

relay which has the faster degeneration in channel quality. Relay selection schemes can be applied to combat this shortcoming, and an initial study of the relay selecting method has been done in [109] and [110]. Thus, if there are more relay nodes in a PLC network, to select a best node is a better choice then taking all the nodes in the transmission.

5.2.1.2 Uni-directional Amplify-and-Forward

Similar to the uni-directional DF relay transmission, the amplify-and-forward relay schemes can be also discussed with single relay and multiple relay situation.

Single Relay The relay node location and the validity of the $S \rightarrow D$ link can be also demonstrated by Figure 5.1 and Figure 5.2. Here the capacity analysis is given in following. The receiving signal on the kth subcarrier at the relay node can be expressed as:

$$y_r^k = x^k \cdot h_{sr}^k + n_r^k \tag{5.9}$$

Then, the receiving signal at the destination is:

$$y_d^k = y_r^k \cdot g^k \cdot h_{rd}^k + n_d^k \tag{5.10}$$

Assume the transmit power at both the data source and thee relay node are the same. Thus the amplification factor on the kth subcarrier can be written as:

$$g^k = \left[\mid h_{sr}^k \mid^2 + (SNR_{sr}^k)^{-1} \right]^{-\frac{1}{2}} \tag{5.11}$$

$g_k d$ is a constraint for the relay node, which ensures the output power of the relay node equals to 1. Then the receive SNR on kt subcarrier at the destination for the $S \rightarrow D$ link invalid situation can be written as:

$$\begin{aligned} SNR_{AF_{invalid}}^k &= \frac{(g^k)^2 \cdot P_s \mid h_{rd}^k \mid^2 \mid h_{sr}^k \mid^2}{(g^k)^2 \cdot \mid h_{rd}^k \mid^2 \cdot (\sigma_r^k)^2 + (\sigma_d^k)^2} \\ &= \left(\frac{(SNR_{sr}^k)^{-1}}{\mid h_{sr}^k \mid^2} + \frac{SNR_{rd}^k}{\mid h_{rd}^k \mid^2} + \frac{(SNR_{sr}^k)^{-1} SNR_{rd}^k}{\mid h_{rd}^k \mid^2 \mid h_{sr}^k \mid^2} \right)^{-1} \end{aligned} \tag{5.12}$$

For the $S \rightarrow D$ link valid situation the equivalent received SNR at the destination is:

$$SNR_{AF_{valid}}^k = SNR_{AF_{invalid}}^k + SNR_{sd}^k \cdot \mid h_{sd}^k \mid^2 \tag{5.13}$$

Thus the achievable spectrum efficiency for the single relay uni-directional AF transmission is:

$$R_{uni\_AF}^{single} = \frac{1}{2K} \cdot \sum_{k=1}^{K} log_2 \left(1 + \frac{SNR_{AF_{valid}}^{k}}{\Gamma} \ or \ \frac{SNR_{AF_{invalid}}^{k}}{\Gamma} \right) \tag{5.14}$$

where, Γ is the SNR gap. According to the above analysis, the numeric results of the single relay uni-directional AF are given in Figure 5.7. As can be seen from the simulation

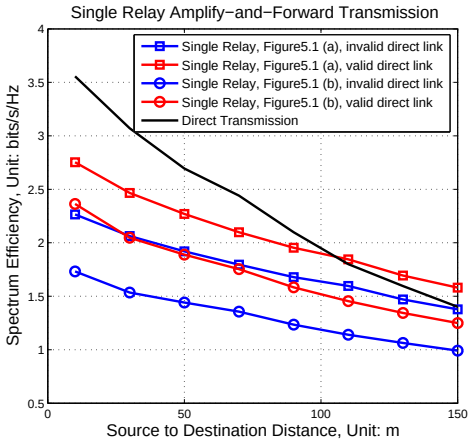

Figure 5.7: *The achievable spectrum efficiencies for the single relay uni-directional AF transmission*

results, the capacity performance is much better if the relay node is located which often on the main path. When the direct link is invalid, the main path location is will bring 30% gain on the achievable spectrum efficiency. If the direct link is valid, the main path location can still being 20% increasing. This phenomenon shows the consistency with the results in DF transmission that the transform station, deviation box, or the socket located on the main path will be the better choice for placing a relay node, and AF scheme is more sensitive to the relay node location. Unlike the DF transmission, adding a valid $S \rightarrow D$ link in AF schemes will bring significant performance benefits. The reason for this phenomenon is that $S \rightarrow D$ link can directly contribute to the destination SNR. Another important point that can be seen from Figure 5.7 is that amplified signal will not necessarily contribute to the SNR since the noise is also amplified during the signal forwading processing. Thus, we can see that the performance of the AF aided PLC link may even be worse than direct transmission in the short range transmission.

Multi Relay The uni-directional AF transmission for multiple relay can be also described by

the Figure 5.4 and Figure 5.5. Assume that the transmit power on data and source relay point are the same. Thus, the amplify factor on ith relay and the kth subcarrier can be written as:

$$g_i^k = \left[\mid h_{sr_i}^k \mid^2 + \left(SNR_{sr_i}^k \right)^{-1} \right]^{-\frac{1}{2}} \tag{5.15}$$

Thus, the receive SNR on the kth subcarrier at the destination when the $S \rightarrow D$ link is invalid situation can be written as:

$$SNR_{AF\_multi}^k = \sum_{i=1}^{N} \left\{ SNR_{AF}^k \right\}_i \tag{5.16}$$

where, $\left\{ SNR_{AF}^k \right\}_i$ is the receive SNR achieved from the ith relay node kth subcarrier. The value of this SNR can be obtained by using (5.12). Notice that (5.16) may not always hold due to channel phase differences between relay nodes. Beamforming is often used to align the phase differences between the relays the and to achieve the performance described by formula (5.16). The principle of the beamforming is already discussed in [117] and [118]. For the scenario when $S \rightarrow D$ link is valid, the SNR can be obtained by following (5.13). Also, the (5.13) holds when beamforming is considered.

To demonstrate the benefits brought by an extra relay node in AF, the following transmission scenario is considered: Two relay nodes are randomly located between data source and destination, either on the main path or a branches. The capacities changing with the increasing of transmission distance are given in Figure 5.8. From the simulation results in Figure 5.8, we can easily see that the SNR gain contributed by the extra relay node will bring a significant gain in capacity. Also, what we can see is that the benefit brought by the extra relay node is more than the benefit brought by the availability of $S \rightarrow D$ link. Compared with the DF transmission scheme, the availability of the direct link has more impact on the AF transmissions for the two relay scenario.

5.2.1.3 Bi-directional Decode-and-Forward I

The relay protocols introduced in the above sections are based on the assumption that the data stream is in one direction only. To further exploit the transmission capacity for the relay enhanced PLC network, the bi-directional relay protocols are induced where the relay node can be equivalently considered in full-duplex working mode. First a 3-step bi-directional protocol is described. The process for the protocol can be demonstrated in Figure 5.9. The blue lines

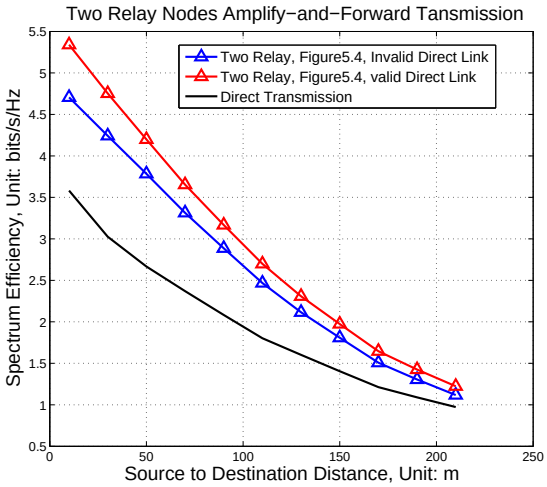

Figure 5.8: *The achievable spectrum efficiencies for the two relay nodes uni-directional AF transmission*

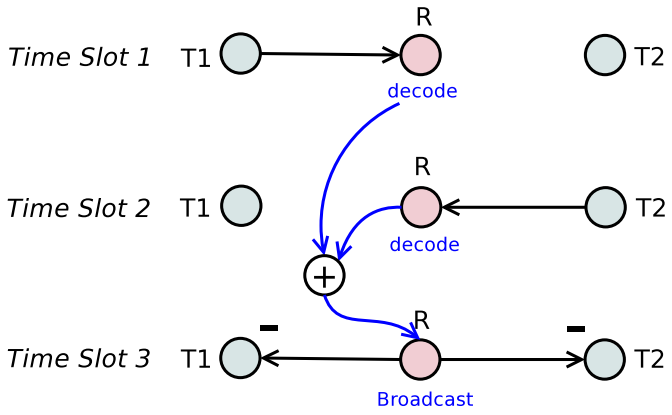

Figure 5.9: *The processing for 3-step bi-directional DF protocol*

in Figure 5.9 show the signal processing applied at the relay node and the black lines show the signal propagation between relay nodes, data sources and destination. Based on papers such as [119] and [120], network coding or superposition modulation can be used to enable the bi-directional transmission in the relay system. Usually the network conding operation is done at the bit level, which limits the transmission capacity because the coding scheme need to designed according to the bit stream which has the lower rate. The superposition modulation concept is considered when evaluating the capacity of the protocol.

For the 3-step bi-directional DF protocol, terminal T_1 transmits data to relay node in the first time slot, and the relay decodes the data to the modulation level. The relay node then receives

the data from terminal T_2 and decodes to the modulation level in the second time slot. Then the superposition modulation in [120] is employed to superpose the modulated data from T_1 and T_2 and broadcast to T_1 and T_2 in the third time slot. T_1 and T_2 substract the their own data from the superposed signal and extract their expected data from the other transmitter. Based on the description, there are two data streams in one transmission. Here $R_{t_1rt_2}$ and $R_{t_2rt_1}$ are used to denote the data rate for the $T_1 \rightarrow T_2$ and $T_2 \rightarrow T_1$ directions. Thus the overall data rate for the protocol can be written as:

$$R_{bi\_DF}^{3step} = \frac{1}{3} \cdot (R_{t_1rt_2} + R_{t_2rt_1}) \tag{5.17}$$

where factor 1/3 denotes the fact that the transmission process should be completed in 3 time-slots due to the half-duplex operation of the relay node, and $R_{t_1rt_2}$ and $R_{t_2rt_1}$ can be achieved by following calculations:

$$\begin{aligned} R_{t_1rt_2} &= \frac{1}{K} \min \left\{ \sum_{k=1}^{K} \log_2 \left(1 + \frac{SNR_{t_1r}^k \cdot \mid h_{t_1r}^k \mid^2}{\Gamma} \right), \right. \\ &\quad \left. \sum_{k=1}^{K} \log_2 \left(1 + \frac{SNR_{rt_2}^k \cdot \mid h_{rt_2}^k \mid^2}{\Gamma} \right) \right\} \end{aligned} \tag{5.18}$$

$$\begin{aligned} R_{t_2rt_1} &= \frac{1}{K} \min \left\{ \sum_{k=1}^{K} \log_2 \left(1 + \frac{SNR_{t_2r}^k \cdot \mid h_{t_2r}^k \mid^2}{\Gamma} \right), \right. \\ &\quad \left. \sum_{k=1}^{K} \log_2 \left(1 + \frac{SNR_{rt_1}^k \cdot \mid h_{rt_1}^k \mid^2}{\Gamma} \right) \right\} \end{aligned} \tag{5.19}$$

where, Γ is the SNR gap which has been introduced in 2.3.1.3.

5.2.1.4 Bi-direction Decode-and-Forward II

In the 3-step bi-directional DF protocol, the terminals send their data in the separate time slots, which we can define these time slots as the multi-access (MA) phase. In this section, we merge the time slots in the MA phase into one time slot to further improve the time efficiency. Thus, a 2-step bi-directional DF protocol is developed for the relay enhanced PLC network. The process for the protocol can be demonstrated as the Figure 5.10. The blue lines in Figure 5.10 show the signal processing at the relay node and the black lines show the signal propagation

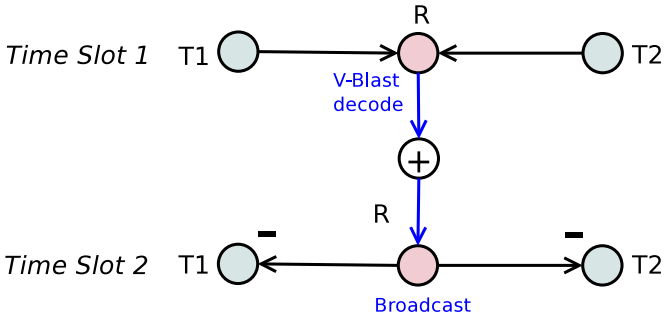

Figure 5.10: *The processing for 2-step bi-directional DF protocol*

between relay nodes and data sources and destination. Though the data arrive at the relay node simultaneously, the signal detection on relay still need to be done step by step. The V-Blast detection is used at the relay node to distinguish the data from T_1 and T_2. The relay node will detect the signal from one terminal first and consider the signal from the other terminal as noise. After removing the detected signal from the receiving signal, the relay node detects the signal from the other terminal from the remaining signal.

In the 2-step bi-directional DF protocol, there are also two data streams. According to the feature of V-Blast that the decoding order will impact the result, here, we assume the relay R detects the data stream from T1 first, by considering the signal from T2 as interference. Thus the spectrum efficiency for the $T1 \rightarrow R1 \rightarrow T2$ link is:

$$R_{t_1rt_2} = \frac{1}{K}\min\left\{\sum_{k=1}^{K}\log_2\left(1+\frac{P \mid h_{t_1r}^k \mid^2}{\left[\left(\sigma_r^k\right)^2 + P \mid h_{t_2r}^k \mid^2\right]\Gamma}\right), \sum_{k=1}^{K}\log_2\left(1+\frac{P \mid h_{rt_2}^k \mid^2}{\left(\sigma_{t_2}^k\right)^2\Gamma}\right)\right\} \tag{5.20}$$

In (5.20), $P \mid h_{t_2r}^k \mid^2$ denotes the received power from T_2 at R which is considered as interference for decoding T_1. Before decoding the message from T_2 , the detected signal should be subtracted. Thus, the spectrum efficiency for the reverse link is:

$$R_{t_2rt_1} = \frac{1}{K}\min\left\{\sum_{k=1}^{K}\log_2\left(1+\frac{P \mid h_{t_2r}^k \mid^2}{\left(\sigma_r^k\right)^2\Gamma}\right), \sum_{k=1}^{K}\log_2\left(1+\frac{P \mid h_{rt_1}^k \mid^2}{\left(\sigma_{t_1}^k\right)^2\Gamma}\right)\right\} \tag{5.21}$$

Thus, the total spectrum efficiency for the case of detecting the T_1 data first is:

$$R_{bi\_DF}^{2step'} = \frac{1}{2} \cdot (R_{t_1rt_2} + R_{t_2rt_1}) \tag{5.22}$$

From the above process, the system capacity when the T_1 can be calculated first is approached. In the same way, the capacity when the T_2 is detected first can be evaluated and demonstrated as as $R_{bi\_DF}^{2step''}$. Thus the achievable capacity for the 2-step bi-directional DF protocol can be written:

$$R_{bi\_DF}^{2step} = \max\left\{R_{bi\_DF}^{2step'}, R_{bi\_DF}^{2step''}\right\} \tag{5.23}$$

The achievable spectrum efficiencies for bi-directional DF protocols are shown in the Figure 5.11. The validity of the direct link in the bi-directional DF protocols is not considered. Intuitively, the 3-step DF protocol may have 30% reduction on the spectrum efficiency com-

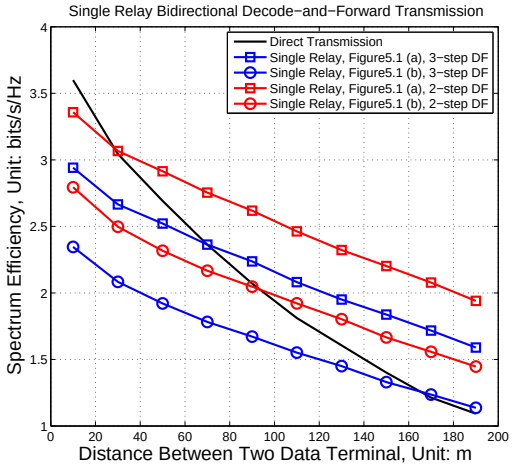

Figure 5.11: *The achievable spectrum efficiency for the bi-directional DF protocols*

pared with the 2-step DF protocol due to the extra time slot that is used. But from the simulation results in Figure 5.11 it is seen that the exact gap is not that big. The reason for this phenomenon is the V-Blast decoding used the 1st time slot in the 2-step bi-directional DF scheme. Under the V-Blast decode scheme, the second signal is treat as noise or interference when decoding the first signal. Thus, this decode scheme causes very poor performance for the first decoded data stream. Compared to the uni-directional relay DF scheme, the performance is more sensitive to the location, whether on the main path or the branch terminal, when the 2-slot bi-directional DF scheme is used.

5.2.1.5 Bi-direction Amplify-and-Forward I

Besides the DF, the bi-directional transmission can be also implemented in the AF protocols, In the AF scenario, the relay node does not decode the signal from T_1 and T_2. In this section, the 3-step bi-directional AF relay is described. In the first time slot T_1 broadcasts the signal to R and T_s, then T_2 broadcasts the signal to R and T_1 in the second time slot. At the third time slot, R broadcasts the superimposed signal to T_1 and T_2. The transmission process can be described by Figure 5.12. The purpose of the decomposed the MA phase into two time slot is that both

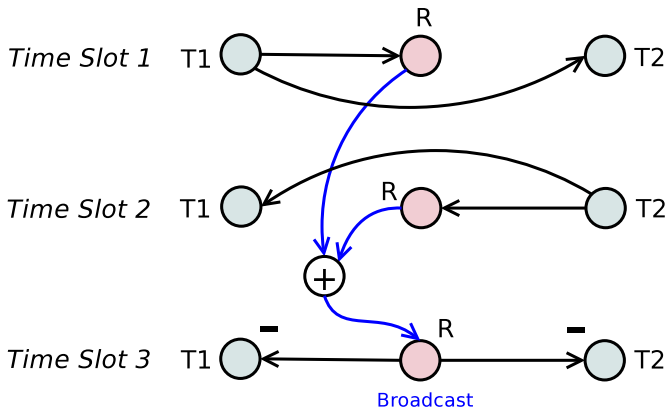

Figure 5.12: *The processing for 3-step bi-directional AF protocol*

T_1 and T_2 can get a copy expecting data before R broadcasting the superposed signal. Thus, the receiver can get extra SNR gain when it decodes the expecting signal. For this protocol, the capacity for $T_1 \rightarrow R \rightarrow T_2$ link and $T_2 \rightarrow R \rightarrow T_1$ link can be written as:

$$R_{bi\_AF}^{t_1rt_{2_{3step}}} = \frac{1}{K}\sum_{k=1}^{K}\log_2\left(1+\frac{P \mid g^k h_{t_1r}^k h_{t_2r}^k \mid^2}{\left[\mid g^k h_{t_2r} \mid^2 \left(\sigma_r^k\right)^2 + \left(\sigma_{t_2}^k\right)^2\right]\Gamma} + \frac{P \mid h_{t_1t_2} \mid^2}{\left(\sigma_{t_2}^k\right)^2 \Gamma}\right) \tag{5.24}$$

$$R_{bi\_AF}^{t_2rt_{1_{3step}}} = \frac{1}{K}\sum_{k=1}^{K}\log_2\left(1+\frac{P \mid g^k h_{t_1r}^k h_{t_2r}^k \mid^2}{\left[\mid g^k h_{t_1r} \mid^2 \left(\sigma_r^k\right)^2 + \left(\sigma_{t_1}^k\right)^2\right]\Gamma} + \frac{P \mid h_{t_1t_2} \mid^2}{\left(\sigma_{t_1}^k\right)^2 \Gamma}\right) \tag{5.25}$$

where g^k can be calculated by using the same principle shown in (5.11). Since in this protocol, a extra time slot is added to achieve the SNR gain at receiver, the overall capacity for the 3-step bi-directional AF protocol should be written as:

$$R_{bi\_AF}^{3step} = \frac{1}{3}\left(R_{bi\_AF}^{t_1rt_{2_{3step}}} + R_{bi\_AF}^{t_2rt_{1_{3step}}}\right) \tag{5.26}$$

5.2.1.6 Bi-directional Amplify-and-Forward II

In the above section, the bi-directional AF relay is implemented in three steps for the purpose of obtaining extra SNR gain. Actually, the bi-directional AF also can be implemented in two steps mode. It simply superposes the signals from both directions which includes impact of the noise and then forwards the amplified signal. The 2-step bi-directional AF can not benefit from the extra SNR gain, while saves the transmission time that also increases the achievable spectrum efficiency. Similarly, the amplification scaling at the kth subcarrier for the bi-directional AF can be written as:

$$g^k_{bi_{2step}} = \left(\mid h^k_{t_1r} \mid^2 + \mid h^k_{t_2r} \mid^2 + \frac{\left(\sigma^k_r\right)^2}{P} \right)^{-\frac{1}{2}} \tag{5.27}$$

Thus, the spectrum efficiency for $T1 \rightarrow R \rightarrow T2$ direction is:

$$R^{t_1rt_{2_{2step}}}_{bi\_AF} = \frac{1}{K} \sum_{k=1}^{K} \log_2 \left(1 + \frac{P \mid g^k h^k_{t_1r} h^k_{t_2r} \mid^2}{\left[\mid g^k h_{t_1r} \mid^2 \left(\sigma^k_r\right)^2 + \left(\sigma^k_{t_1}\right)^2 \right] \Gamma} \right) \tag{5.28}$$

the spectrum efficiency for$T2 \rightarrow R \rightarrow T1$ direction is:

$$R^{t_2rt_{1_{2step}}}_{bi\_AF} = \frac{1}{K} \sum_{k=1}^{K} \log_2 \left(1 + \frac{P \mid g^k h^k_{t_1r} h^k_{t_2r} \mid^2}{\left[\mid g^k h_{t_2r} \mid^2 \left(\sigma^k_r\right)^2 + \left(\sigma^k_{t_2}\right)^2 \right] \Gamma} \right) \tag{5.29}$$

Thus, the achievable spectrum efficiency for bi-directional AF protocol is given by:

$$R^{2step}_{bi\_AF} = \frac{1}{2} \left(R^{t_1rt_{2_{2step}}}_{bi\_AF} + R^{t_2rt_{1_{2step}}}_{bi\_AF} \right) \tag{5.30}$$

The simulation results for the bi-directional AF protocols are shown in Figure 5.13, Since in the AF scenario, the relay node does not decode the signal and forward it directly to the destination, the performance deeply depends on the SNR on the receiver side. In order to achieve higher SNR, the direct link is taken into account in the bi-directional AF. To obtain the SNR gain from the direct link, the first time slot are decomposed into 2 time slots. Thus the 3-step bi-directional AF protocol is developed for the bi-directional AF scenario. From the simulation in Figure 5.13, the gain brought by the SNR can not make up the loss caused by the inefficient use of three time slots. Compared with the 3-step bi-directional AF scheme, the 2-step approach provides higher capacity. But the superiority of the 2-step scheme not as much as for the bi-directional DF schemes. Consistent with the other AF schemes, the bi-directional AF is more

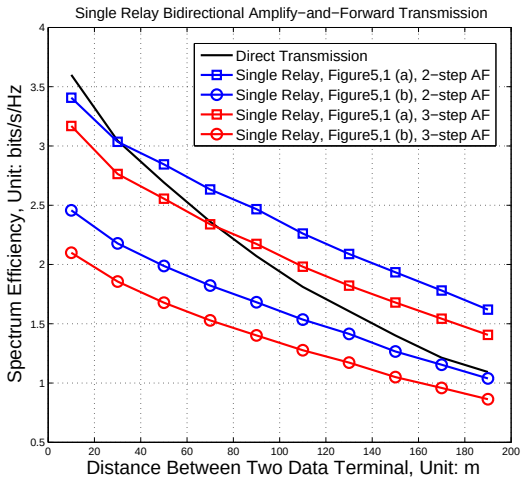

Figure 5.13: *The achievable spectrum efficiency for bi-directional AF protocols*

sensitive to the location of the relay node. Only if the relay node is located on the main path can a the capacity gain can be achieved over direct transmission.

5.2.2 Relay Protocol Performance with Channel Estimation Error

In previous sections, research on relay protocols is based on the assumption that relay nodes know the channel state information (CSI) perfectly. Also, the protocols with decode and forward mechanism are proved more suitable for PLC transmissions. In order to discover the performance of DF protocols more realistic, this section investigates the achievable spectrum efficiencies for single relay uni-directional, 3-step bi-directional and 2-step bi-directional DF schemes. We consider the impact of channel estimation error in the frequency selective fading PLC channel and coloured background noise environment to provide a realistic transmission scenario. A multi-pilot based linear minimum mean square error (LMMSE) channel estimation method is applied for the above relay schemes. A realistic analysis for the achievable spectrum efficiency for the above relay schemes in PLC is given. Finally, the best choice of the number of symbols pilot for DF PLC relay schemes is obtained. The channel estimation impact on OFDM modulate direct data transmission in PLC network is discussed in [121], while in our work we focus on the impact on the relay transmission.

Before the evaluation of the capacity performance, the channel estimation method used in this work is introduced. First assume that the channel estimation operation is done in every N

OFDM symbols and M of them are used as pilot symbols. For each pilot symbol, the LMMSE method proposed in [122] is employed to estimate the frequency domain transfer function. The estimated channel transfer function based on the mth pilot is:

$$\widehat{H}_m = R_{HH}\left(R_{HH} + \Theta_m\left(X_m X_m^H\right)^{-1}\right)^{-1} H_m^{ls} = H + E_m \tag{5.31}$$

where, $H = \left[h_m^1, h_m^2, \cdots, h_m^k\right]$ is the channel vector, $\widehat{H}_m^{ls}{=}X_m^{-1}Y_m{=}[\widehat{h}_m^1, \widehat{h}_m^2, \cdots, \widehat{h}_m^K]$ is the least-square (LS) estimate of H and $\widehat{h}_m^k$ is the estimated channel gain on k_{th} sub-carrier. The matrix $\Theta_m{=}$ diag$[(\sigma_m^1)^2, (\sigma_m^2)^2, \cdots, (\sigma_m^K)^2]$ is the variance matrix of the noise for the mth pilot on the receive terminal, and $(\sigma_m^k)^2$ is the noise power on k_{th} sub-carrier, $R_{HH}{=}E\left\{HH^H\right\}$ is covariance matrix of H, $E_m{=}[\epsilon_m^1, \epsilon_m^2, \cdots, \epsilon_m^K]$ is the channel estimation error vector and ϵ_m^k is the channel estimation error for the mth pilot in the k_{th} sub-carrier.

According to [122], a statistical time domain channel model is needed to evaluate R_{HH} in (5.31). To keep the complexity low but use a realistic channel approximation, in this paper, L randomly generated channels in the frequency domain are employed to calculate R_{HH}. The channel correlation matrix used in (5.31) is then obtained:

$$R_{HH} = [r_{m,n}] = \left[E\left[\left(h_l^m - \mu^m\right)\left(h_l^n - \mu^n\right)\right]\right] \tag{5.32}$$

where, h_l^k is the channel gain of lth randomly generated channel at the k_{th} sub-carrier, and μ^k is the average channel gain at the k_{th} sub-carrier over all the L generated channels.

On the basis of the LMMSE estimation result above, the average value of all the M estimated channel transfer functions is used as the final channel estimation result.

$$\widehat{H} = \frac{1}{M}\sum_{m=1}^{M}\widehat{H}_m = H + \frac{1}{M}\sum_{m=1}^{M}E_m \tag{5.33}$$

here, we define the second term of (5.31) as the channel estimation error $E = [\epsilon^1, \epsilon^2, \cdots, \epsilon^K]$ for the multi-pilot scenario, where $\epsilon^k = \frac{1}{M}\sum_{m=1}^{M}\epsilon_m^k$. Assume the variance of ϵ_m^k is a_m^k which is also can be considered as the noise power induced by the inaccuracy of channel estimation. The estimation noise on each pilot symbol, E_m, is mutually independent and identically distributed. Thus, the variance of ϵ^k is $\frac{1}{M}a_m^k$ which means that using more pilot symbols will lead to a more precise estimation result.

In the following part of this work, we use $\widehat{H}_{xy} = [\widehat{h}_{xy}^1, \widehat{h}_{xy}^2, \cdots, \widehat{h}_{xy}^k]$ and $E_{xy} = [\epsilon_{xy}^1, \epsilon_{xy}^2,$

$\cdots, \epsilon_{xy}^{K}]$ to denote the estimated channel and channel estimation error for the $x \rightarrow y$ link, where $\widehat{h}_{xy}^{k}$ and ϵ_{xy}^{k} denote the estimated channel and channel estimation error on the k_{th} sub-carrier for this link. One further point should be noted. In the perfect channel estimation scenario, the channel transfer function for $x \rightarrow y$ and $y \rightarrow x$ link can be assumed to be the same, the symmetry of the transfer function in PLC has bee proved in [68]. But if the channel estimation error is considered, $\widehat{H}_{xy}$ will not equal to $\widehat{H}_{yx}$ for the reason that the different noise disturbances at x and y will cause different channel estimation results.

5.2.2.1 Single Directional Decode-and-Forward

By using similar calculations in section 5.2.1.1, the capacity for the single uni-directional DF protocol can be computed. The point we need to notice here is that the channel estimation error needs to be considered when calculating the SNR. Then $SNR_{sr}^{k} = \frac{P_s}{\sigma_r^2}$ and $SNR_{rd}^{k} = \frac{P_r}{\sigma_d^2}$ in (5.1) and (5.1) should be re-calculated taking into account the channel estimation error:

$$\overline{SNR}_{sr}^{k} = \frac{P_s}{\sigma_r^2 + P \mid \varepsilon_{sr}^{k} \mid^2} \tag{5.34}$$

where, $P \mid \varepsilon_{sr}^{k} \mid^2$ is the noise induced by channel estimation inaccuracy. Similarly, the SNR_{rd}^{k} and SNR_{sd}^{k} in (5.3) can be recalculated by using a similar approach to (5.34). The channel estimation errors ε_{sr}^{k}, ε_{rd}^{k} and ε_{sd}^{k} can be obtained by using (5.32) and (5.33). Capacities which involved channel estimation error for $S \rightarrow R$, $R \rightarrow D$ and $S \rightarrow D$ links as R_{sr}^{CE}, R_{rd}^{CE} and R_{sd}^{CE} respectively. Thus, the capacity for the single relay uni-directional DF protocol when the $S \rightarrow D$ link is invalid can be written as:

$$\overline{R}_{uni\_DF}^{invalid} = \frac{1}{2}\left(1 - \frac{M}{N}\right)\frac{\overline{R}_{sr} \cdot \overline{R}_{rd}}{\overline{R}_{sr} + \overline{R}_{rd}} \tag{5.35}$$

5.2.2.2 Bi-directional Decode-and-Forward I

In the 3-step bi-directional DF relay schemes, T_1 and T_2 send their pilot sequences on the first M symbols. Then, R_1 transmits the pilot symbols with its data and broadcasts it to T_1 and T_2. The capacity for this protocol can be written in the similar way as (5.17) and with the consideration of information loss caused by pilot symbol occupation as shown in (5.35).

$$\overline{R}_{uni\_DF}^{3step} = \frac{1}{3}\left(1 - \frac{M}{N}\right)\left(\overline{R}_{t_1rt_2} + \overline{R}_{t_2rt_1}\right) \tag{5.36}$$

where, the factor $1/3$ denotes the fact that the transmission process should be completed in 3 time-slots due to the half-duplex operation of the relay node, and:

$$\overline{R}_{t_1rt_2} = \frac{1}{K}\min\left\{\sum_{k=1}^{K}\log_2\left(1+\frac{P \mid \widehat{h}_{t_1r}^{k} \mid^2}{\left[P \mid \epsilon_{t_1r}^{k} \mid^2 + \left(\sigma_r^k\right)^2\right]\Gamma}\right), \sum_{k=1}^{K}\log_2\left(1+\frac{1}{2}\frac{P \mid \widehat{h}_{rt_2}^{k} \mid^2}{\left[P \mid \epsilon_{rt_2}^{k} \mid^2 + \left(\sigma_{t_2}^k\right)^2\right]\Gamma}\right)\right\} \tag{5.37}$$

$$\overline{R}_{t_2rt_1} = \frac{1}{K}\min\left\{\sum_{k=1}^{K}\log_2\left(1+\frac{P \mid \widehat{h}_{t_2r}^{k} \mid^2}{\left[P \mid \epsilon_{t_2r}^{k} \mid^2 + \left(\sigma_r^k\right)^2\right]\Gamma}\right), \sum_{k=1}^{K}\log_2\left(1+\frac{1}{2}\frac{P \mid \widehat{h}_{rt_1}^{k} \mid^2}{\left[P \mid \epsilon_{rt_1}^{k} \mid^2 + \left(\sigma_{t_1}^k\right)^2\right]\Gamma}\right)\right\} \tag{5.38}$$

stand for spectrum efficiencies of the $T_1 \rightarrow R_1 \rightarrow T_2$ link and the opposite link, respectively.

5.2.2.3 Bi-direction Decode-and-Forward II

For the channel estimation process in the 2-step single relay bi-directional DF protocol, at the first phase, T_1 and T_2 send mutually orthogonal pilot sequences to ensure that the estimation processes for $T_1 \rightarrow R$ and $T_2 \rightarrow R$. links do not impact on each other. Then R1 transmits pilot symbols with its data and forwards the signal to T_1 and T_2 . Thus the spectrum efficiency for $T_1 \rightarrow R \rightarrow T_2$ link is:

$$\overline{R}_{t_1rt_2}^{2S} = \frac{1}{K}\min\left\{\sum_{k=1}^{K}\log_2\left(1+\frac{P \mid \widehat{h}_{t_1r}^{k} \mid^2}{\left[P \mid \epsilon_{t_1r}^{k} \mid^2 + \left(\sigma_r^k\right)^2 + P \mid h_{t_2r}^{k} \mid^2\right]\Gamma}\right), \sum_{k=1}^{K}\log_2\left(1+\frac{\frac{1}{2}P \mid \widehat{h}_{rt_2}^{k} \mid^2}{\left[P \mid \epsilon_{rt_2}^{k} \mid^2 + \left(\sigma_{t_2}^k\right)^2\right]\Gamma}\right)\right\} \tag{5.39}$$

In (5.39), $P \mid h_{t_2r}^{k} \mid^2$ denotes the received power from T_2 at R which is considered as interference for R decoding T_1. Before decoding the message from T_2, X_1 should be subtracted out.

Thus, the spectrum efficiency for the reverse link is:

$$\overline{R}_{t_2rt_1}^{2S} = \frac{1}{K}\min \left\{ \sum_{k=1}^{K} \log_2 \left(1 + \frac{P \mid \widehat{h}_{t_2r}^{k} \mid^2}{\left[P \mid \epsilon_{t_2r}^{k} \mid^2 + (\sigma_r^k)^2 + P \mid \epsilon_{t_1r}^{k} \mid^2 \right] \Gamma} \right), \sum_{k=1}^{K} \log_2 \left(1 + \frac{\frac{1}{2} P \mid \widehat{h}_{rt_1}^{k} \mid^2}{\left[P \mid \epsilon_{rt_1}^{k} \mid^2 + \left(\sigma_{t_1}^{k}\right)^2 \right] \Gamma} \right) \right\} \tag{5.40}$$

Thus, the total spectrum efficiency for the case of detecting the data for T_1 rst is:

$$\overline{R}_{bi\_DF}^{2step'} = \frac{1}{2} \left(\overline{R}_{t_1rt_2}^{2S} + \overline{R}_{t_2rt_1}^{2S} \right) \tag{5.41}$$

In the same way, the spectrum efficiency $R_{bi\_DF}^{2step''}$ which denotes the spectrum efficiency for detecting the T_2 data stream rst can be obtained. Therefore, the achievable spectrum efficiency for 2-step bi-directional DF protocol is given by:

$$\overline{R}_{uni\_DF}^{2step} = \left(1 - \frac{M}{N} \right) \cdot \max \left\{ \overline{R}_{bi\_DF}^{2step'}, \overline{R}_{bi\_DF}^{2step''} \right\} \tag{5.42}$$

5.2.2.4 Simulation of Channel Estimation Error Impact on Performance

As described by (5.31) and (5.33), the channel estimation error ϵ^k will reduce with the pilot symbol numbers M. Predictably, the achievable spectrum efficiencies for each protocol will also be variable and will generally reduce with increasing numbers of pilot symbols. Here, we define the information loss as the the difference between the evaluated capacity under the perfect channel estimation scenario and the capacity calculated with the channel estimation error included.

$$\Delta R = R_{imp\_channel} - R_{p\_channel} \tag{5.43}$$

Intuitively, ΔR will relate with one factor, the number of the pilot symbols. Large numbers of pilot symbols will cause the a more accurate channel estimation which will lead to a closer approach to the capacity with perfect channel knowledge. However it is also easy to observe, from equation (5.30) that the use of the pilot symbols will cause some information loss. Thus, the choice of a proper pilot symbol quantity is important for optimised performance. In the following Figure 5.14, the information losses for each protocol are shown. From Figure 5.14, we can see that direct transmission has an obviously larger gap than the relay schemes. The reason is that without the help of the relay, the received signal at T_2 is weaker due to the larger

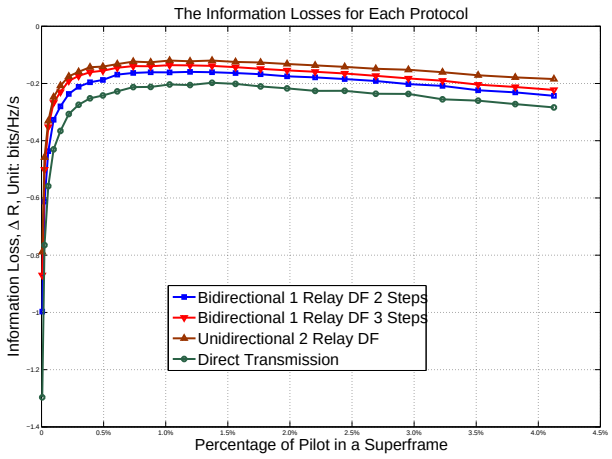

Figure 5.14: *The Information Loss for Each Protocol*

channel attenuation. Thus, a less accurate channel estimation is obtained which leads to higher information loss. By using a relay node to decode and forward the transmission, the signal can be detected more reliably at the receiver. Thus, the information gap of an uni-directional single relay DF protocol is much smaller than the direct transmission case. For the bi-directional protocols, they can benefit from the DF signal reconstruction operation but are limited by the power split operation in the broadcasting phase. In particular, for the 2-step bi-directional DF protocol, the V-Blast detection process is vulnerable when channel estimation errors are present. For example, due to the inaccuracy of channel estimation of $T_1 \rightarrow R$ link, after decoding the signal X_1 from T_1, the impact of X_1 can not be totally subtracted, and the residual interference will limit the capacity of detecting X_2 from T_2. Therefore, the 2-step bi-directional protocol has a larger performance loss than the 3-step bi-directional protocol.

5.3 Conclusion and Discussion

From the simulation results in this chapter, we can see that the introduction of the relay nodes may not always help to increase the system performance. But if we properly deploy the relay nodes and choose the right signal forwarding method, the system capacity can be increased with the aid of one or more relay nodes. In this section, some conclusions for relay aided PLC networks are given based on the simulation results.

The first conclusion can been seen from Figure 5.3, Figure 5.6, Figure 5.7, Figure 5.11 and

Figure 5.13, is that if the relay nodes are deployed on the main path, it will bring more capacity gain compared with locating it on a branch. This consistency is shown in the simulation results indicates that the derivation boxes or transformers are better candidates for placing relay nodes in practice. Also, from the capacity simulation results of the AF schemes, another interesting phenomenon is that amplify-and-forward operation on relay schemes are more sensitive to the relay node location than DF schemes.

The second conclusion that can be summarised from the simulation results is that DF protocols generally have better performance than the AF protocols. The reason for this phenomenon is determined by the frequency selective fading nature of PLC channels. In the AF protocols, the relay node only forwards the received signal with a certain amplification factor, and does not consider the channel gain on a specific subcarrier. Thus, if the channel gain $S \rightarrow R$ or $R \rightarrow D$ link on a subcerrier is low, there is no effective mechanism to make up the data rate loss caused by the fading. By contrast, the receive information on the relay nodes are decoded and re-organised at the relay node in the DF scenario. The decoding and re-encoding operation makes it is possible to reallocate the data onto different sub-carriers. Thus, the frequency selective fading impact on the DF protocols is much less. Another advantage of the single relay uni-directional DF protocol is that the system can adjust the time duration allocated for $S \rightarrow R$ and $R \rightarrow D$ links to maximum the overall data transmission capacity.

In the simulations, multiple relay nodes scenarios are discussed. Interestingly, the extra relay node will bring more benefits in the AF scheme then for then DF scheme. Though the DF operation has a clear advantage in the frequency selective fading channel, the situation is reversed in the multi-relay node scenario. In the multi-relay AF scheme, the extra node will contribute extra SNR directly. For the multi-relay DF scheme, the extra relay node only bring extra SNR in the second time slot. But in the first time slot, the transmission capacity is limited by the weakest source to relay link. Thus, only if the transmission distance is short can the impact of the weak source to relay link can be ignored. For the multiple relay nodes DF transmission, selecting a best node among the candidates is a better choice then taking all the nodes in the transmission.

Another important topic related to uni-directional and bi-directional relays in this chapter. The most obvious advantage of bi-directional relay schemes is time efficiency. Comparing with uni-directional schemes, the bi-directional schemes save up 50% or 33% of the time to finish a two direction transmission between two data terminals. However the drawback is that the data

rate for each data stream may be unbalanced since relay node needs to detect the signals from both sides by using the V-Blast method, where the data stream from one direction should be considered as interference in the first detection stage of V-Blast method. The simulation results shown in Figure 5.11 and Figure 5.13 indicate that the bi-directional mode helps to increase the system capacity performance. From the simulations in Figure 5.14, the bi-directional 2-step DF protocol shows superiority over all the other protocols in transmission capacity, but is vulnerable to noise disturbance which will impact the channel estimation accuracy. With accurate channel estimation using multiple pilot symbols, the 2-step protocol will minimise such deterioration. The 3-step protocol shows more robustness then the 2-step protocol when channel estimation errors are present.

Based on the simulation results, some basic criteria for selecting a relay method can be stated. First, for any possible relay protocols, it is better to deploy the relay node in deviation box or transformer, but not on terminating socket. Second, the AF scheme performs best if only one relay node is considered for either uni-directional or bi-directional transmission. If a multi-relay system is taken into account, AF protocols will present superiority since AF protocols will contribute to overall SNR directly and not be limited by the weak source-relay links. Then, bi-directional schemes increase the system performance significantly by the reducing the time duration of the data transmission. Based on the above primary conclusions, we can select a proper relay scheme that is suitable for a given scenario.

Chapter 6
Conclusion and Future Work

In previous chapters, the general history, background as well as current development of PLC are introduced. To fit two important challenges in the PLC networks - channel modelling and adaptivity in diverse application scenarios, a new statistical channel modelling method and relay protocols for PLC networks are proposed and described in detail in Chapter 3, 4 and 5 respectively. As an open research area, the works on PLC is far from finished. Thus, in this chatper the previous works are summarised and future works are proposed based.

6.1 Conclusion

In this thesis, the consistency of the transmission line theory approach and multipath approach is first verified with a set of PLC parameters in Chapter 3. In Chapter 4, the procedure of the statistical channel modelling method is described and the modelling result is compared with the other modelling method. The relay protocols and the capacity performances of each protocol are given in Chapter 5. Here, the contributions and conclusion of this work are summarised.

6.1.1 Channel Model

Unlike the previous deterministic channel modelling methods, the proposed channel model focuses on the statistical characteristics of multipath propagation in PLC network, for example, the path magnitude distribution, path interval distribution, path number and cable loss effects. The simulation result of the proposed model shows high consistency with the traditional TLT channel model. The first advantage of the proposed channel model is that it exempts the necessity of collecting and evaluating the network topology information which are time-consuming work. In the statistical channel model, the randomness of the multipath caused by topology variations is indirectly represented by the random distribution of the multipath parameters. Thus, with statistical channel model, the communication research for powerline is no longer confined to a limited number of topologies, and the performance evaluation based on statistical channels

is provides better insight into a range of deployment scenarios. Also, the time domain channel is more convenient for some application, for example: the correlated impulse noise modelling in PLC networks.

6.1.2 Relay for PLC

In this thesis, the relay concept is introduced to powerline communications for the purpose of enhance the capacity and coverage. With the benefits brought by the relay nodes, the PLC may be applied in more application scenarios. In this work, a series of relay protocols are proposed for PLC networks, which cover signal forwarding mechanism including forwarding mechanism, single/multiple relay nodes and the full/half duplex mode for the relay. The capacity performance shows that not all the relay techniques can help to improve performance. According to the results in Chapter 5, some conclusion can be drawn: first, the deviation box or transforming station are better locations than the terminal sockets for placing the relay nodes. Second, DF forward mechanism shows more gain in capacity performance when compared with AF forward mechanism in the PLC environment. Another interesting result shown in the Chapter 5 is that extra relay nodes may not necessary help the network improve the performance, especially in DF scenarios. Finally it is seen that bidirectional relay schemes present better capacity results, which benefit from the effective time slot sharing strategy. From this chapter, we can say that if properly choosing the location and signal forwarding mode, relay will be a promising technology for the future powerline communications. In addition, the protocol performance with channel estimation error is investigated and the mechanism of choosing proper pilot length is given based on the simulation.

6.2 Future Work

Though we have discussed two challenges in the powerline communications, the PLC is still an open area for research. Even for the channel modelling and relay, there are still some interesting topics to study. In this section, some future research suggestions on channel modelling and relay aided PLC are given.

6.2.1 Unit Based Statistical Channel Modelling

The statistical multipath properties of PLC channel are investigated in detail in Chapter 5. The channel can be modeled according to the extracted properties. Though the proposed statistical model is based on the random branch density, if the branch density of the target networks varies over a very large range, the model can not fully present the channel characteristics. To overcome this drawback, an initial idea of a new statistical channel model is described here.

The new channel modelling method is based on the fact introduced in Section 4.2.2.1 to 4.2.2.5 in Chapter 4. We intend to decompose the PLC network to basic network unit which can present the channel characteristics of 4.77 meters length. Since the new channel model is designed to present diverse channel conditions, the network unit should have the ability to demonstrate different channel conditions of for a network 4.77 meters length. As known from previous chapters, the deep fading points are mainly caused by reflected signals on the branches. Thus, the density of the branches is used as an indicator of the channel conditions. Higher branch density implies worse channel condition and vice verse. In order to obtain the channel properties of different branch densities, the following points should be studied by using the similar methods in Chapter 4:

1. path magnitude distribution, and distribution parameters trends with the branch density in a network unit
2. Path interval distribution and distribution parameters trends with the branch density in a network unit
3. Path loss for each 4.77 meters transmission distance

With the above steps, the channel properties of one network unit for different branch densities can be obtained. With the network unit, we can evaluate the channel response of a long distance transmission by cascading a certain number of network units. For example, if a channel response of about 100 meters is required, we can cascade 21 network units. The channel response of the expecting link can be obtained by using :

$$h = h_1 \otimes h_2 \otimes \cdots \otimes h_n \tag{6.1}$$

where $\otimes$ is convolution operation, h_i is the time domain channel impulse response of the ith

network unit. With the network unit properties and the cascading operation in (6.1), a channel response with arbitrary distance in any channel condition can be obtained.

6.2.2 Multiple User Node Relay for PLC

In Chapter 5, relay protocols for P2P transmission and the corresponding capacity performance evaluation are given. This work describes suitable relay options for the PLC environment. But when considering practical network connections, there may often be more then two PLC device connected to one deviation box where used to deploy the relay node. Thus, the relay transmission scenario in practice can be demonstrated in Figure 6.1: As can be seen, the relay

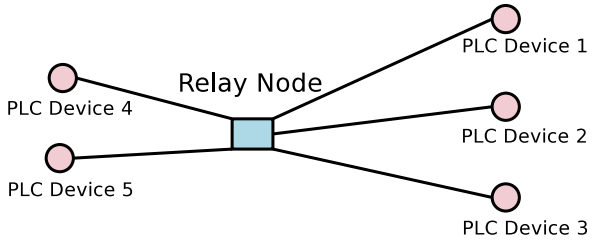

Figure 6.1: *The multiple point to multiple point relay scenario in a practical PLC environment*

node is not specifice deployed for one relay link but for multiple PLC devices. Based on this fact, following issues will be promising topics:

1. The first issue for the multi-user is the multiple access (MA) mechanism. In general we may consider three MA patterns: frequency division (DF), time division (TD) and spatial division (SD). Spatial division may be difficult to achieve in PLC networks due to the limit of channel correlation in PLC network. so the advantages of FD and TD should be investigated in detail. Considering that PLC channels are often highly frequency selective, FDMA may provide enough flexibility for the system.

2. Related to the MA patterns, resource allocation is a major problem for multi-user relay systems. In the relay aided PLC system, the available allocating resources include: spectrum, power and time slots. These resources can be allocated to different users according to different criteria such as maximising the total capacity, providing equal data rates for each user or according to different priorities of the users. Thus, the dynamic power and spectrum allocations schemes for the relay aid multi-user PLC network will be important option for pushing PLC to more applications scenarios.

3. As described in Chapter 5, the bidirectional relay mode shows superiority over other techniques. But in multi-user scenarios, the V-Blast detection method is no longer an effective way to detect and distinguish the signals from different PLC devices. In order to benefit from the full duplex working mode, network coding and frequency division multiple access patterns can be used to help the relay node working in full duplex mode. For example, the specific codeword or spectrum segment can be allocated to given pair of PLC devices pair.

6.2.3 Relay for Narrowband Automation Control

As reported in many papers, Smart Grid will attract lot of attention in the near future. Thus, the demand for communications in Smart Grid will continue growing. Unlike broadband communications, the communications in Smart Grid will require wide area coverage, with robustness data transmission over narrowband channels, which have some special characteristics, for example, the channel may experience deep flat fading due to the narrowband coverage that may lead to channel outage. Also, the data stream in Smart Grid will include both data collection and control signal distribution, which will require a two-way communication solution over narrow bandwidth. Based on the special requirements of Smart Grid communications, following topics may be interesting for investigating:

1. In order to cover larger area, the two hop relay may not enough, thus multi-hop data transmission in the physical layer will be quite a promising direction, for example space time coding scheme designs for multi-hop narrowband PLC.

2. For the purpose of compensating outages caused by deep fading links, it is necessary to develop multi-hop route protocols for the narrowband PL network which covers large area. This will mean that there is more than one path for the signal to reach the destination. If any one path is faded, the signal can still arrive from the other paths. Thus, the adaptive relay scheme will be applied to fit the dynamic route. Thus, it will be a cross layer design challenge for researchers.

Appendix A
Construction and Geometric Parameters of the Cable

Figure A.1. shows the construction of a common power cable which is used in [18], Table A.1. and Table A.2. show the geometric parameters and the electromagnetic parameters of NAYY150 and NAYY35 cables.

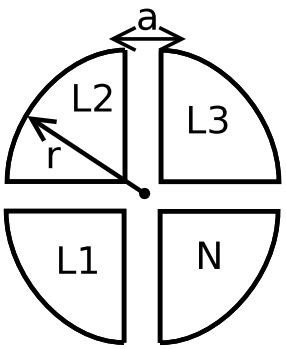

Figure A.1: *The Cross-Section of a Four Conductor Power Cable*

The insulator between conductors is PVC. When feeding signals into two adjacent conductors, most of the electric field is concentrated between these two conductors. The parameters of the cable can be estimated by the geometric dimensions and some material properties.

Lumped Parameter Calculation

Following the steps introduced in [18], the lumped parameters such as capacitance, inductance,

	NAYY150 (mm)	NAYY35 (mm)
a	1.8	1.2
r	6.9099	5.9161

Table A.1: *Geometry information of NAYY cable*

Conductivity of Cooper	κ	58×10^6 S/m
Dissipation of PVC	tanδ	0.025
relative permittivity of PVC	ε_r	4
free space permittivity	ε_0	$8.541878176 \times 10^{-12}$ [F/m]
relative permeability of Cooper	μ_r	1
free space permeability	μ_0	1.2566290×10^{-6} [H/m]

Table A.2: *Electrical parameters of NAYY cable*

resistance and conductance per unit length can be calculated.

$$C' = \varepsilon_0 \varepsilon_r \frac{r}{a} \tag{A.1}$$

$$L' = \mu_0 \mu_r \frac{r}{a} \tag{A.2}$$

$$R' = \sqrt{\frac{\pi \mu_0}{\kappa r^2} f} \tag{A.3}$$

$$G' = 2\pi f C' \tan\delta \tag{A.4}$$

Appendix B
Statistical Channel Model Parameter

B.1 Parameters for Number of Paths Distribution

The number of the paths for the channel of ith Class and kth Cluster can be described by a Gussian distribution as (4.3):

$$N_{i,k} = [\mathcal{N}(\mu_{i,k}, \sigma_{i,k})] \tag{B.1}$$

where $[\cdot]$ means to round towards the nearest integer, parameters $\mu_{i,k}$ and $\sigma_{i,k}$ are the expectation and variance of the Gaussian distribution. The value μ and σ in each Class increase as power function of Cluster Index. The Power function can be written as:

$$\mu_{i,k} = p_{i1} k^{p_{i2}} + p_{i3} \tag{B.2}$$

$$\sigma_{i,k} = q_{i1} k^{q_{i2}} + q_{i3} \tag{B.3}$$

where i and k are the class index and cluster index respectively. The parameters p_{i1}, p_{i2}, p_{i3}, q_{i1}, q_{i2} and q_{i3} are shown in Table B.1

i=2	$p_{i1} = 1.623$ $q_{i1} = -0.3818$	$p_{i2} = 0.08596$ $q_{i2} = -0.8461$	$p_{i3} = 0$ $q_{i3} = 1.592$
i=3	$p_{i1} = 3.913$ $q_{i1} = -0.005983$	$p_{i2} = 0.0968$ $q_{i2} = 1.033$	$p_{i3} = 0$ $q_{i3} = 1.783$
i=4	$p_{i1} = 6.169$ $q_{i1} = -0.4401$	$p_{i2} = 0.09686$ $q_{i2} = -0.6989$	$p_{i3} = 0$ $q_{i3} = 2.007$
i=5	$p_{i1} = 8.684$ $q_{i1} = -8.725$	$p_{i2} = 0.1688$ $q_{i2} = -0.06764$	$p_{i3} = 0$ $q_{i3} = 10.98$

Table B.1: *The parameters for calculating expectation and variance value of path number distribution*

i=1	$a_i^M = 0.4815$	$b_i^M = -0.0821$	$c_i^M = 0.4103$	$d_i^M = -0.02408$
i=2	$a_i^M = 0.2601$	$b_i^M = -0.1214$	$c_i^M = 0.4948$	$d_i^M = -0.03241$
i=3	$a_i^M = 0.1841$	$b_i^M = -0.1246$	$c_i^M = 0.3628$	$d_i^M = -0.03334$
i=4	$a_i^M = 0.1221$	$b_i^M = -0.1515$	$c_i^M = 0.2736$	$d_i^M = -0.03445$
i=5	$a_i^M = 0.1721$	$b_i^M = -0.1517$	$c_i^M = 0.0905$	$d_i^M = -0.01979$

Table B.2: *The double exponential parameters for first arrival path magnitude*

B.2 Parameters for Magnitude Distribution

B.2.1 First Arrival Path

For the channels in a particular Class, the magnitude of the first arrival path of follows the double exponential decay with the Cluster Index k increasing. The double exponential decay can be written as (4.4):

$$I_{i,k} = a_i^M e^{b_i^M k} + c_i^M e^{d_i^M k} \tag{B.4}$$

where i and k are the class index and cluster index respectively. The parameters a_i^M, b_i^M, c_i^M and d_i^M are the double exponential parameters, and are shown in Table B.2.

B.2.2 Other paths

The magnitude of the other paths are deeply depended on the arriving time of the path. The decay profile with the time sampling index can be also demonstrated by double exponential function (4.5):

$$I_{k,j} = a_k^o e^{b_k^o j} + c_k^o e^{d_k^o j} \tag{B.5}$$

where k and j are the cluster index and sampling index respectively. The parameters a_k^o, b_k^o, c_k^o and d_k^o are shown in Table B.3.

B.3 Parameters for Path Interval Distribution

For the channels in a particular Class, the path intervals can be described by a Generalised Extreme Value (GEV) distribution. The PDF of GEV distribution for ith Class and kth Cluster

k=1	$a_k^o = 0.4194$	$b_k^o = -0.1270$	$c_k^o = 0.0328$	$d_k^o = -0.0083$
k=2	$a_k^o = 0.4388$	$b_k^o = -0.1355$	$c_k^o = 0.0487$	$d_k^o = -0.0207$
k=3	$a_k^o = 0.4647$	$b_k^o = -0.1353$	$c_k^o = 0.0502$	$d_k^o = -0.0206$
k=4	$a_k^o = 0.4542$	$b_k^o = -0.1329$	$c_k^o = 0.0562$	$d_k^o = -0.0235$
k=5	$a_k^o = 0.4381$	$b_k^o = -0.1244$	$c_k^o = 0.0521$	$d_k^o = -0.0229$
k=6	$a_k^o = 0.4632$	$b_k^o = -0.1253$	$c_k^o = 0.0571$	$d_k^o = -0.0249$
k=7	$a_k^o = 0.4677$	$b_k^o = -0.1163$	$c_k^o = 0.0422$	$d_k^o = -0.0196$
k=8	$a_k^o = 0.5124$	$b_k^o = -0.1200$	$c_k^o = 0.0457$	$d_k^o = -0.0213$
k=9	$a_k^o = 0.4262$	$b_k^o = -0.1032$	$c_k^o = 0.0327$	$d_k^o = -0.0171$
k=10	$a_k^o = 0.4419$	$b_k^o = -0.1004$	$c_k^o = 0.0287$	$d_k^o = -0.0151$
k=11	$a_k^o = 0.5116$	$b_k^o = -0.1046$	$c_k^o = 0.0292$	$d_k^o = -0.0149$
k=12	$a_k^o = 0.4604$	$b_k^o = -0.0964$	$c_k^o = 0.0257$	$d_k^o = -0.0140$
k=13	$a_k^o = 0.4501$	$b_k^o = -0.0925$	$c_k^o = 0.0223$	$d_k^o = -0.0126$
k=14	$a_k^o = 0.4968$	$b_k^o = -0.0946$	$c_k^o = 0.0238$	$d_k^o = -0.0134$
k=15	$a_k^o = 0.5187$	$b_k^o = -0.0950$	$c_k^o = 0.0243$	$d_k^o = -0.0136$
k=16	$a_k^o = 0.5242$	$b_k^o = -0.0915$	$c_k^o = 0.0207$	$d_k^o = -0.0116$
k=17	$a_k^o = 0.5355$	$b_k^o = -0.0896$	$c_k^o = 0.0188$	$d_k^o = -0.0109$
k=18	$a_k^o = 0.6164$	$b_k^o = -0.0934$	$c_k^o = 0.0224$	$d_k^o = -0.0125$
k=19	$a_k^o = 0.5288$	$b_k^o = -0.0852$	$c_k^o = 0.0180$	$d_k^o = -0.0108$
k=20	$a_k^o = 0.5829$	$b_k^o = -0.0864$	$c_k^o = 0.0175$	$d_k^o = -0.0099$

Table B.3: *The double exponential parameters for magnitudes of other paths*

Expression	Detail
$\xi_{5,k} = ak^b + c$	$a = 0.4063$, $b = 0.2886$, $c = 1.061$
$\delta_{5,k} = ak^b + c$	$a = 1.246$, $b = 0.1702$, $c = -1.892$
$\mu_{5,k} = ak + b$	$a = 0.0002687$, $b = 0.2033$

Table B.4: *GEV parameters of Class V*

can be written as (4.6):

$$f_{gev}\left(x;\epsilon_{i,k},\eta_{i,k},\xi_{i,k}\right)=\frac{1}{\eta_{i,k}}\left(1+\xi_{i,k}\left(\frac{x-\epsilon_{i,k}}{\eta_{i,k}}\right)\right)^{-\frac{1}{\xi_{i,k}}-1}\cdot e^{-\left(1+\xi_{i,k}\left(\frac{x-\epsilon_{i,k}}{\eta_{i,k}}\right)\right)^{-\frac{1}{\xi_{i,k}}}} \tag{B.6}$$

where i and k are the class index and cluster index respectively.. Parameter ξ and η in Class V should be described by power function of Cluster Index. Except these two special cases, the other parameters can be demonstrated by linear function of Cluster Index. The calculation parameters for $epsilon_{i,k}$, $\eta_{i,k}$ and $\xi_{i,k}$ are given in Table B.4 to Table B.7.

Expression	Fitted Result
$\xi_{4,k} = ak + b$	$a = 0.000972$, $b = 2.734$
$\eta_{4,k} = ak + b$	$a = 0.0009786$, $b = 0.9539$
$\epsilon_{4,k} = ak + b$	$a = 0.0001653$, $b = 0.3061$

Table B.5: *GEV parameters of Class IV*

Expression	Fitted Result
$\xi_{3,k} = ak + b$	$a = 0.0006167$, $b = 2.537$
$\eta_{3,k} = ak + b$	$a = 0.0005993$, $b = 0.8095$
$\epsilon_{3,k} = ak + b$	$a = -0.00009132$, $b = 0.571$

Table B.6: *GEV parameters of Class III*

B.4 Parameters for Cable Losses

The cable loss can be demonstrated as:

$$A\left(f,d\right) = e^{-\left(a_0 + a_1 \cdot f^k\right)} e^{-jb_0 f} \tag{B.7}$$

The parameters a_0, a_1, k and b_0 are the functions of the path propagation distance:

$$a_0 = 0.00020860 \cdot d + 0.00087386 \tag{B.8}$$

$$a_1 = 0.000026440 \cdot d - 0.000046444 \tag{B.9}$$

$$k = -0.000090980 \cdot d + 0.8876 \tag{B.10}$$

$$b_0 = -0.0006432 \cdot d - 0.0000011264 \tag{B.11}$$

where, d is the path propagation distance.

Expression	Fitted Result
$\xi_{2,k} = ak + b$	$a = 0.001143$, $b = 2.211$
$\eta_{2,k} = ak + b$	$a = 0.0008684$, $b = 0.6979$
$\epsilon_{2,k} = ak + b$	$a = -0.00003362$, $b = 0.5586$

Table B.7: *GEV parameters of Class II*

Appendix C
Publications

C.1 Conference Papers

1. B. Tan, J.S. Thompson, ”Relay Transmission Protocols for In-Door Powerline Communications Networks,” 2011 IEEE International Conference on Communications (ICC) Workshop on Smart Grid Communications, vol.1, no.5, pp.5-9 Kyoto, Japan, June 2011

2. B. Tan, J.S. Thompson, ”Capacity evaluation with channel estimation error for the decode-and-forward relay PLC networks,” 2011 European Signal Processing Conference, Barcelona, Spain, September 2011

C.2 Journal Papers

1. H. Sun, A. Nallanathan, B. Tan, J.S. Thompson, J. Jiang, H.V. Poor,, ”Relaying technologies for smart grid communications,” Wireless Communications, IEEE , vol.19, no.6, pp.52-59, December 2012

2. B. Tan, J.S. Thompson, ”Statistical Characteristics of Multipath Channel in Indoor Powerline Communications,” submitted to IET Communications, 2013

Relay Transmission Protocols for In-door Powerline Communications Networks

Bo Tan
Institute for Digital Communications
The University of Edinburgh
Edinburgh, EH9 3JL, UK
Email: b.tan@ed.ac.uk

John Thompson
Institute for Digital Communications
The University of Edinburgh
Edinburgh, EH9 3JL, UK
Email: john.thompson@ed.ac.uk

***Abstract*—In this paper, relay protocols for one or more relay nodes, employing either Amplify-and-Forward (AF) or Decode-and-Forward (DF) are discussed for frequency selective fading channel environment and coloured background noise in power-line communications (PLC) networks. Also, the performance of beamforming aided multi-relay protocols and bidirectional single relay protocols are analysed. The achievable information rate and the Cumulative Distribution Function (CDF) of achievable information rates for each protocol are obtained through the simulations. The difference among relay protocols are given in the simulation results. The work shows that relay has the potential of resolving the resource scarcity problem for some resource demonding applications in the indoor PLC networks, and helps enlarge the coverage of power grid.**

I. Introduction

To use the power grid as the data transmission network, termed Powerline Communications (PLC), has been proved feasible in [1]. With the spread of the Smart Grid concepts, PLC has drawn the attention of many researchers because of its wide distribution and low infrastructure build cost. As a broadband communications technology, PLC has been considered a candidate for the Smart Home [2]. For narrowband communications, PLC has also been proposed as a solution for Automatic Mater Reading (AMR)/Advanced Metering Infrastructure (AMI), vehicle-togrid (V2G) communications and in-home energy management, which are the important applications of the low-voltage Smart Grid (SG) [3]. Considering the the data rate and QoS requirements in broadband transmission and coverage issues in SG, relay/repeaters have been proposed to enhance the PLC network.

There are already some discussions on embedding relays in the PLC networks. In [4], decode-and-forward (DF) schemes and corresponding sub-carrier and power allocation schemes are investigated. In [5], space-time coding are proposed for the multi-hop PLC networks, and, the impact of repeater location is also studied. However, there is still no comprehensive study and comparison on how different techniques, such as Amplify-and-Forward (AF), Decode-and-Forward (DF), beamforming and bidirectional, enhance relay transmission in PLC. In this paper, a serial of protocols and corresponding information rate are comprehensively studied in the frequency band ranging up to 30MHz defined in Homeplug AV. The contributions of this paper include the following points. First, it constructs a realistic PLC simulation environment according to the cable parameters and network topology. Second, it studies the capacity trends of different relay protocols and determines suitable conditions for applying relay in PLC. Third, the techniques which are suitable for PLC relay network are figured for deciding the research focuses in relay PLC networks.

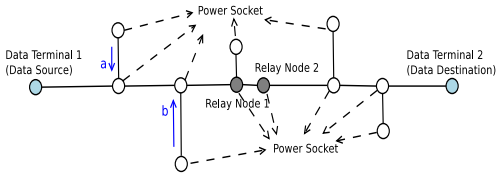

Fig. 1. Typical In-door PLC Network Topology

The paper is organised as follows. Section II describes the channel, noise characteristics and modelling methods and system definition. In Section III, the performance of different relay schemes is analysed. Numerical results are provided to demonstrate the achievable information rate for each scheme in Section IV. Finally, conclusions and future research directions are given in Section V.

II. Channel and Noise Modelling, System Definition

A. Channel, Noise Characteristics and Modelling

In Fig. 1 a typical in-door PLC network includes a cluster of sockets, where PLC modems can be plugged in as transmitter/receiver or relay nodes is given. Because of the existence of reflect signals a and b which is shown in Fig. 1 power cable represents as a typical frequency selective fading channel in frequency domain, and multi-path channel in time domain. But it is hard to evaluate the impact of the infinitely reflected signals from sockets when the network topology becomes complex. A method based on the Transmission Line Theory is proposed in [6], which abstracts each segment as 2-port-network. The whole network can be considered as a series of concatenated 2-port-networks. The transfer functions for the Data Terminal 1 to Data Terminal 2 ($T_1 \rightarrow T_2$), Data Terminal 1 to Relay Node ($T_1 \rightarrow R_1$) and Relay Node 1 to Data Terminal 2 ($R_1 \rightarrow T_2$) links in Fig. 1 are shown in Fig. 2. As can be seen from Fig. 2, the channels suffer deep fading

978-1-61284-955-3/11/$26.00 ©2011 IEEE

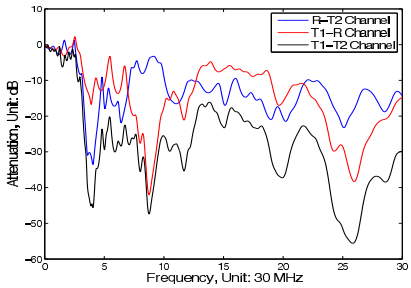

Fig. 2. Transfer Functions for the Data Source to Relay nodes link, Data Source to Data Destination link and Relay node1 to Data Destination link

on some frequency points which may cause low information rate.

The noise in PLC appears as coloured background noise blended with impulse noise. The source of the noise has been studied and classified into 5 categories in [7]. Noise types 1 and 2 in [7] that are sum of several low power noise sources and narrowband interference induced by medium and short wave broadcasts, often have a stable power spectral density over seconds, minutes and even hours. Thus, they are considered as background noise. The others three sources may change rapidly within microseconds and milliseconds, therefore, are considered to be as impulse noise. In this paper, we only consider the impact of the background noise. A synthesis process in [8] that passes White Gaussian Noise (WGN) through a coloured filter is used to model the background noise.

B. System Definition

Based on the frequency selective fading fact of PLC channel and harsh noise condition in frequency domain, Orthogonal Frequency-Division Multiplexing (OFDM) is used to combact these obstacles. Assume that the bandwidth is portioned into K orthogonal subcarriers in the frequency domain.

Here, we use $H_{t_1t_2} = \left[h^1_{t_1t_2}, h^2_{t_1t_2}, \cdots, h^K_{t_1t_2}\right]$ to denote frequency domain channel transfer function for the $T_1 \rightarrow T_2$ link, where, $h^k_{t_1t_2}$ $(k \in [1, 2, \cdots, K])$ denotes the channel gain on the kth sub-carrier. The vectors $H_{t_1r_1}$, $H_{t_1r_2}$, $H_{r_1t_2}$ and $H_{r_2t_2}$ for the $T_1 \rightarrow R_1$, $T_1 \rightarrow R_2$, $R_1 \rightarrow T_2$ and $R_2 \rightarrow T_2$ links are defined in the same way. In addition, $N_{t_2} = \left[n^1_{t_2}, n^2_{t_2}, \cdots, n^K_{t_2}\right]$ stands for the noise samples at T_2, where $n^k_{t_2}$ denotes noise on the k_{th} sub-carrier with power $\left(\sigma^k_{t_2}\right)^2$. Similarly, N_{t_1}, N_{r_1} and N_{r_2} denote the noise samples on T_1, R_1 and R_2 with power $\left(\sigma^k_{t_1}\right)^2$, $\left(\sigma^k_{r_1}\right)^2$ and $\left(\sigma^k_{r_2}\right)^2$ on the k_{th} subcarrier, respectively. Furthermore P is defined as the data transmit power on each sub-carrier. Thus, data transmission on the $T_1 \rightarrow T_2$ link with sequence $X = \left[x^1, x^2, \cdots, x^K\right]$ can be modelled as (1):

$$Y_{t_2} = \sqrt{P} \cdot H_{t_1t_2} \cdot X + N_{t_2} \tag{1}$$

Where, $Y_{t_2} = \left[y^1_{t_2}, y^2_{t_2}, \cdots, y^K_{t_2}\right]$ is the received signal sequence on the receive side. The data communication processes through other links can also be modelled in the same way as (1).

III. ACHIEVABLE INFORMATION RATE OF DIFFERENT RELAY PROTOCOLS

In this section, achievable information rates of 5 relay protocols in PLC are analysed. It is assumed that the source can not reach destination without the help of relay, and the relays work in half-duplex mode. The signal-to-noise ratio (SNR) for both single relay and multi-relay scenarios, and the constraint conditions for each relay protocol are analysed.

A. Two Relays Unidirectional Protocols

Theoretically, all the available sockets between data source and destination, for example R_1 and R_2 in Fig. 1, can be considered as potential relay nodes. Thus, multi-relay operation is possible in a PLC network. Due to the physical distribution of power sockets we assume that sockets often appear in pairs, which means we can often find two sockets which are closely located. Based on this assumption, unidirectional relay protocols with 2 relay nodes are discussed. The performance analysis of multi-relay AF scheme with beamforming in wireless communications and the scheme which applies beamforming in the second hop in DF are introduced in [9] and [10], here we investigate its performance in the PLC channel environment.

Protocol 1). 2Relay-1Way DF with Beamforming

T_1 transmits messages to T_2 with the help of R_1 and R_2. R_1 and R_2 decode the messages independently in the 1st phase, then forward the re-encoded messages to T_2. The received signal on R_1 and R_2 in the 1st phase are:

$$Y_{r_1} = \sqrt{P} \cdot H_{t_1r_1} \cdot X + N_{r_1} \tag{2}$$

$$Y_{r_2} = \sqrt{P} \cdot H_{t_1r_2} \cdot X + N_{r_2} \tag{3}$$

The signal at T_2 in the 2nd phase is:

$$Y_{t_2} = \sqrt{P} \cdot H_{r_1t_2} \cdot X' + \sqrt{P} \cdot H_{r_2t_2} \cdot X'' + N_{t_2} \tag{4}$$

where X' and X'' are the re-encoded message on R_1 and R_2 respectively based on Y_{r_1} and Y_{r_2}. In order to make sure that both R_1 and R_2 can fully decode the message, the information rate for the 1st phase should be limited by:

$$R_{t_1r_1r_2} = \sum_{k=1}^{K} \log_2 \left(1 + \min\left\{ \frac{P \mid h^k_{t_1r_1} \mid^2}{\left(\sigma^k_{r_1}\right)^2 \Gamma}, \frac{P \mid h^k_{t_1r_2} \mid^2}{\left(\sigma^k_{r_2}\right)^2 \Gamma} \right\}\right) \tag{5}$$

When combining the signal at the receiver, the amplitude of the received signal will not be always enhanced due to the existence of phase differences, θ between the two links. Based on the fact that channel is stationary for long periods of time and the fact that Time division duplex (TDD) modes will be used in PLC, we can assume that the transmitter knows channel phase information. Thus, transmit beamforming can be employed to compensate the phase difference, thus θ always equals 0, which means the superposed signal is always coherently combined. The information rate for the 2nd phase thus is given by:

$$R_{r_1r_2t_2}=\sum_{k=1}^{K}\log_2\left(1+\frac{P\left(|\,h_{r_1t_2}^k\,|+|\,h_{r_2t_2}^k\,|\right)^2}{\left(\sigma_{t_2}^k\right)^2\Gamma}\right) \quad (6)$$

where, Γ denotes SNR gap which is used to indicate the information rate loss caused by link protect manners such as channel coding, synchronising overhead. From the statement in [11], for the uncoded modulation system, the achievable information rate is often $10dB$ less than the Shannon capacity. If convolution code is applied, the performance will be improved by 7 to $8dB$. Thus, here we make the assumption that $\Gamma=3dB$ is reasonable. By DF, the overall information rate for this scheme is given by:

$$R_{2R1W\_BF}^{DF}=\frac{1}{2}\min\{R_{t_1r_1r_2},R_{r_1r_2t_2}\} \quad (7)$$

where, the factor $\frac{1}{2}$ denotes the half-duplex working mode of relay.

Protocol 2). 2Relay-1Way AF with Beamforming

In this scheme, the received signals on relays in the 1st phase are the same as shown in (2) and (3). But, here AF is used instead of DF in the 2nd phase. In order to avoid the offsetting of signal, transmit beamforming is also applied in this scheme. Thus, a new combined signal format can be obtained:

$$Y_{t_2}=G_{r_1}\cdot H_{r_1t_2}\cdot Y_{r_1}+G_{r_2}\cdot H_{r_2t_2}\cdot Y_{r_2}+N_{t_2} \quad (8)$$

where $G_{r_i}=\left[g_{r_i}^1,g_{r_i}^2,\cdots,g_{r_i}^K\right],i=1$ and 2 is the amplify factor vector on R_1 and R_2 respectively, and $g_{r_i}^k=\sqrt{\frac{P}{P|h_{t_1r_i}^k|^2+\left(\sigma_{r_i}^k\right)^2}},i=1$ or 2. In consequence, the information rate for this protocol is given by:

$$R_{2R1W\_BF}^{AF}=\frac{1}{2}\sum_{k=1}^{K}\log_2\left(1+\frac{\left(SNR_{BF}^{AF}\right)_k}{\Gamma}\right) \quad (9)$$

where, $\left(SNR_{BF}^{AF}\right)_k$ is the SNR on k_{th} sub-carrier at T_2 when beamforming is applied:

$$\left(SNR_{BF}^{AF}\right)_k=\frac{P\left(|\,g_{r_1}^k h_{t_1r_1}^k h_{r_1t_2}^k|+|\,g_{r_2}^k h_{t_1r_2}^k h_{r_2t_2}^k|\right)^2}{(g_{r_1}^k)^2\left(\sigma_{r_1}^k\right)^2+(g_{r_1}^k)^2\left(\sigma_{r_2}^k\right)^2+\left(\sigma_{t_2}^k\right)^2} \quad (10)$$

B. Single Relay Bidirectional Protocols

Due to the half-duplex mode on relay nodes, all the unidirectional relay protocols suffer the information rate loss. We consider a bidirectional schemes which will help the system increase its spectral efficiency. Assume that T_1 and T_2 have messages to send to each other. In bidirectional protocols, relay nodes collect the messages from both directions and forward the superposed signal in a broadcast manner. Then T_1 and T_2 extract their expected message from the superposed signal by removing their own message first. As discussed in [12] and [13], bidirectional relay operation can be implemented in both AF and DF scenarios. In this paper the performance of bidirectional relay protocols in PLC channel environment is investigated.

Protocol 3). 1Relay-2Way-3Step DF

In this protocol, the whole data transmission is accomplished in 3 time-slots. First, T_1 sends X_1 to R_1, which is decoded and stored on R_1. Second, T_2 sends X_2 to R_1, which is also decoded and stored. At R_1, the two decoded messages are superposed into $X_3=[x_3^1,x_3^2,\cdots,x_3^K]$, where, $x_3^k=\sqrt{\frac{1}{2}P}x_1^k+\sqrt{\frac{1}{2}P}x_2^k$. In the third phase, R_1 broadcasts X_3, T_1 and T_2 then receive X_3 and extract their expected messages. The received signals in 1st phase and 2nd phase at R_1 can be written as:

$$Y_{r_1\_A}=\sqrt{P}\cdot H_{t_1r_1}\cdot X_1+N_{r_1} \quad (11)$$

$$Y_{r_1\_B}=\sqrt{P}\cdot H_{t_2r_1}\cdot X_2+N_{r_1} \quad (12)$$

the receive signals on T_1 and T_2 in the 3rd phase are:

$$Y_{t_1}=\sqrt{\frac{1}{2}P}\cdot H_{r_1t_1}\cdot X_1+\sqrt{\frac{1}{2}P}\cdot H_{r_1t_1}\cdot X_2+N_{t_1} \quad (13)$$

$$Y_{t_2}=\sqrt{\frac{1}{2}P}\cdot H_{r_1t_2}\cdot X_1+\sqrt{\frac{1}{2}P}\cdot H_{r_1t_2}\cdot X_2+N_{t_2} \quad (14)$$

As the total information rate is the sum of the data streams $T_1\rightarrow R_1\rightarrow T_2$ and $T_2\rightarrow R_1\rightarrow T_1$, the sum-rate of this protocol is given by:

$$R_{1R2W\_3S}^{DF}=\frac{1}{3}\left(R_{t_1r_1t_2}+R_{t_2r_1t_1}\right) \quad (15)$$

where, the factor $1/3$ denotes the fact that the transmission process should be completed in 3 time-slots due to the half-duplex operation of the relay node, and:

$$R_{t_1r_1t_2}=\min\left\{\sum_{k=1}^{K}\log_2\left(1+\frac{P\,|\,h_{t_1r_1}^k\,|^2}{\left(\sigma_{r_1}^k\right)^2\Gamma}\right),\sum_{k=1}^{K}\log_2\left(1+\frac{1}{2}\frac{P\,|\,h_{r_1t_2}^k\,|^2}{\left(\sigma_{t_2}^k\right)^2\Gamma}\right)\right\} \quad (16)$$

$$R_{t_2r_1t_1}=\min\left\{\sum_{k=1}^{K}\log_2\left(1+\frac{P\,|\,h_{t_2r_1}^k\,|^2}{\left(\sigma_{r_1}^k\right)^2\Gamma}\right),\sum_{k=1}^{K}\log_2\left(1+\frac{1}{2}\frac{P\,|\,h_{r_1t_1}^k\,|^2}{\left(\sigma_{t_1}^k\right)^2\Gamma}\right)\right\} \quad (17)$$

stand for information rates of the $T_1\rightarrow R_1\rightarrow T_2$ link and the reverse link, respectively.

Protocol 4). 1Relay-2Way-2Step DF

Merging the first and second phases in Protocol 3 into one phase and using V-Blast detection at R_1, a 2-step bidirectional DF relay protocol is constructed. The step in which T_1 and T_2 transmit concurrently to R_1 is called the $Multi-Access$ (MA) phase. According to the feature of V-Blast that the decoding order will impact the result, here, we assume R_1 detects the data stream from T_1 first, by considering the signal from T_2 as interference. Thus the information rate for $T_1\rightarrow R_1\rightarrow T_2$ link is:

$$R_{t_1r_1t_2\_2S}=\min\left\{\sum_{k=1}^{K}\log_2\left(1+\frac{P\,|\,h_{t_1r_1}^k\,|^2}{\left((\sigma_{r_1}^k)^2+P\,|\,h_{t_2r_1}^k\,|^2\right)\Gamma}\right),\sum_{k=1}^{K}\log_2\left(1+\frac{\frac{1}{2}P\,|\,h_{r_1t_2}^k\,|^2}{\left(\sigma_{t_2}^k\right)^2\Gamma}\right)\right\} \quad (18)$$

In (18), $P \mid h_{t_2r_1}^k \mid^2$ denotes the received power from T_2 at R_1 which is considered as interference for R_1 decoding. Before decoding message from T_2, X_1 should be substract. Thus, the information rate for the reverse link is:

$$R_{t_2r_1t_1\_2S} = \min \left\{ \sum_{k=1}^{K} \log_2 \left(1 + \frac{P \mid h_{t_2r_1}^k \mid^2}{\left(\sigma_{r_1}^k\right)^2 \Gamma} \right), \sum_{k=1}^{K} \log_2 \left(1 + \frac{\frac{1}{2} P \mid h_{r_1t_1}^k \mid^2}{\left(\sigma_{t_1}^k\right)^2 \Gamma} \right) \right\} \quad (19)$$

Thus, the total information rate for the case of detecting the data for T_1 first is:

$$R_{1R2W\_2S}^{DF'} = \frac{1}{2} \left(R_{t_1r_1t_2\_2S} + R_{t_2r_1t_1\_2S} \right) \quad (20)$$

In the same way, the information rate $R_{1R2W\_2S}^{DF''}$ which denotes the information rate for detecting the T_2 data stream first can be obtained. Therefore, the achievable information rate for 2-step bidirectional DF protocol is given by:

$$R_{1R2W\_2S}^{DF} = \max \left\{ R_{1R2W\_2S}^{DF'}, R_{1R2W\_2S}^{DF''} \right\} \quad (21)$$

Protocol 5). 1Relay-2Way AF

If AF is used to replace DF in the Protocol 4, a new protocol is obtained as the following. In the 1st phase, T_1 and T_2 send messages to R_1. R_1 receives signal Y_{r_1}, shown as:

$$Y_{r_1} = \sqrt{P} \cdot H_{t_1r_1} \cdot X_1 + \sqrt{P} \cdot H_{t_2r_1} \cdot X_2 + N_{r_1} \quad (22)$$

The receive signals on T_1 and T_2 are:

$$Y_{t_1} = G \cdot H_{t_1r_1} \cdot Y_{r_1} + N_{t_1} \quad (23)$$

$$Y_{t_2} = G \cdot H_{t_2r_1} \cdot Y_{r_1} + N_{t_2} \quad (24)$$

where, $g^k = \sqrt{\frac{P}{P|h_{t_1r_1}^k|^2 + P|h_{t_2r_1}^k|^2 + \left(\sigma_{r_1}^k\right)^2}}$ forms $G = [g^1, g^2, \cdots, g^K]$. Thus, the information rate for $T_1 \rightarrow R_1 \rightarrow T_2$ link is:

$$R_{t_1r_1t_2}^{AF} = \sum_{k=1}^{K} \log_2 \left(1 + \frac{P|g^k h_{t_1r_1}^k h_{t_2r_1}^k|^2}{\left(|g^k h_{t_1r_1}^k|^2 \left(\sigma_{r_1}^k\right)^2 + \left(\sigma_{t_1}^k\right)^2\right)\Gamma} \right) \quad (25)$$

Similarly, the information rate for reverse link is:

$$R_{t_2r_1t_1}^{AF} = \sum_{k=1}^{K} \log_2 \left(1 + \frac{P|g^k h_{t_1r_1}^k h_{t_2r_1}^k|^2}{\left(|g^k h_{t_2r_1}^k|^2 \left(\sigma_{r_1}^k\right)^2 + \left(\sigma_{t_2}^k\right)^2\right)\Gamma} \right) \quad (26)$$

Thus, the achievable information rate for bidirectional AF protocol is given by:

$$R_{1R2W}^{AF} = \frac{1}{2} \left(R_{t_1r_1t_2\_AF} + R_{t_2r_1t_1\_AF} \right) \quad (27)$$

IV. Simulation and Numerical Results

In this part we take the PVC-insulated cables that are widely used in low-voltage power distribution grid which is also used in [1] to emulate the network shown in Fig. 1. Treat T_1 as data source, and T_2 as destination in the unidirectional scenario, while in the bidirectional protocols, both T_1 and T_2 are treated as the terminals which need to exchange data with each other. For the single relay protocols, R_1 is used as relay node located in the middle region between T_1 and T_2, while for the multi-relay protocols, both R_1 and R_2 are used as relay nodes closely located in the middle region between T_1 and T_2. Further assume that each terminal in the system can transmit signal on the same power level with equal power allocation on each sub-carrier. Power spectral density (PSD) of -60 dBm/Hz which is used for many PLC devices in market is quoted from [14] to make simulation more realistic,.

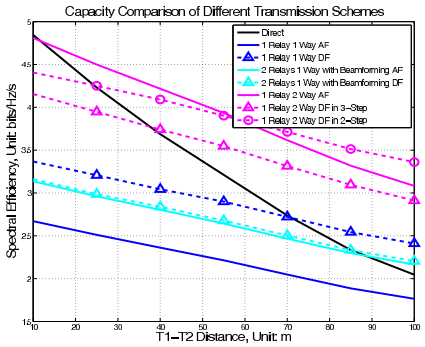

Fig. 3. Spectral efficiency as function of distance

Here, we use the frame structure in [15] where each frame contains 256 OFDM symbols and 64 frames form a superframe which lasts $1.92s$. Due to the fact that PLC channel is stationary for a long time, often seconds or tens of seconds, one generated channel can be used during a whole superframe. According to the background noise characteristics described in Section II, the noise PSD on a node can be assumed to be unchanged during a superframe. Further suppose that background noise PSDs on R_1 and R_2 are the same due to the very close location of these two nodes. In order to make the simulation realistic, channel transfer functions are re-generated by using a group of randomly located branches with random branch length and a new group of background noise PSDs on T_1, T_2, R_1 and R_2 are re-generated according to [8] for a new superframe.

Besides the 5 protocols studied in Section III, the performance of direct transmission, unidirectional DF/AF with single relay schemes is also shown here as benchmarks. From Fig. 3, we can see that direct transmission has better performance, but is most vulnerable with increasing of channel attenuation. For the unidirectional AF protocols, performance is not as good as expected since during the forwarding processes, noise is also amplified. With help of beamforming, the unidirectional 2 relays AF protocol has better performance than the single relay unidirectional AF schemes, but the performance gain of adding a extra relay node into system may not be worthwhile if the complexity of designing for multi-relay system is taken into account. Beamformng is not necessarily helpful in unidirectional 2 relays DF protocol, because in this protocol the overall information rate deeply depend on the worse channel condition between $T_1 \rightarrow R_1$ and $T_1 \rightarrow R_2$ links. This limitation can be

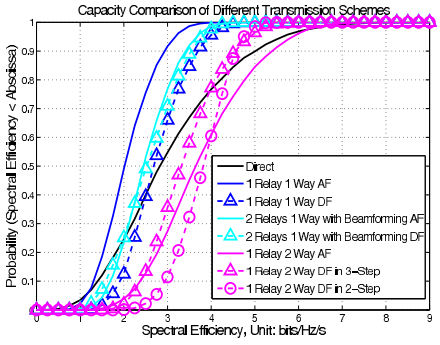

Fig. 4. Spectral efficiency CDF When $T_1 \leftrightarrow T_2$ distance is 55m

seen clearly in (5) and (7). By observing Fig. 3, unidirectional DF protocols have a significantly better performance than the AF protocols because of the signal reconstruction operation at relay nodes. Bidirectional protocols have the best performance among all the investigated protocols, since they make up the spectral efficiency loss of half duplex relays by adding a reverse data stream. Intuitively, 3-step DF and 2-step DF bidirectional schemes could probably increase the information rate by 67% and 100% respectively compare with unidirectional single relay DF scheme. But due to the power spliting operation on relay in the 2nd phase in these schemes, as shown in (13) to (19), the benefit may not reach expectation. Especially, for the 1st phase in the 2-step DF scheme, the V-Blast principle treats the signal from other link as interference. This operation severely impact the rate for the data stream which is detected first. For the bidirectional AF protocol, it has the best performance among all the schemes for short range, because in this scheme both data flows are transmitted without power spliting. However, the spectral efficiency drops sharply when the channel attenuation become large and the amplified noise impact becomes noticable.

The spectral efficiency CDF when $D_{t_1 \leftrightarrow t2} = 55$m is given in Fig. 4. We can see that the bidirectional AF scheme has same performance as the 2-step DF scheme when $D_{t_1 \leftrightarrow t2} = 55$m in Fig. 3, but, the slope of CDF curve of the 2-step is more steeper than the bidirectional AF scheme. It means that 2-step DF scheme is more robust. The bidirectional AF can reach some higher information rate occasionally. This phenomenon is more obvious in the direct transmission protocol. It can be seen that direct protocol can achieve 6bits/Hz/s or 7bits/Hz/s occasionally where 3-step DF and 2-step DF schemes can not reach, but the average rate is still less then the other two schemes. Therefore, the conclusion is that direct transmission and bidirectional AF protocol are more sensitive to channel and noise condition than bidirectional DF protocols. The DF schemes appear to give more robust performance, no matter how the channel condition changes.

V. Conclusion and Future Work

From the achievable information rate analysis and the numerical simulation results, we can see that relay technology can certainly help improve the performance when the transmission distance is long. Furthermore, the bidirectional relay protocols are better than direct transmission even when the transmission distance is as short as 20m or 30m. Additionally, the simulation show that in bidirectional relay protocols DF operation is more robust than AF operation in PLC environment. The work in this paper proved that relay technology can help the PLC network enlarge the coverage and improve the data transmission rate. Future work for this reseach may consider the impact of channel estimation error in bidirectional protocols, dynamic sub-carriers and power allocation for nodes in the multi-user PLC network.

References

[1] M. Zimmermann, K. Dostert, "A multipath model for the powerline channel," IEEE Transactions on Communications, vol.50, no.4, pp.553-559, Apr 2002

[2] A. Majumder and J. Caffery Jr, Power lines communications: an overview, IEEE Potentials, vol. 23, pp. 4-8, Oct./Nov. 2004.

[3] S. Galli, A. Scaglione, Zhifang Wang, "Power Line Communications and the Smart Grid," Smart Grid Communications (SmartGridComm), 2010 First IEEE International Conference on , vol., no., pp.303-308, 4-6 Oct. 2010

[4] Hao Zou, A. Chowdhery, S. Jagannathan, J.M. Cioffi, J. Le Masson, "Multi-User Joint Subchannel and Power Resource-Allocation for Powerline Relay Networks," IEEE International Conference on Communications, 2009. ICC '09. pp.1-5, 14-18 June 2009

[5] L. Lampe, R. Schober, Simon Yiu, "Distributed space-time coding for multihop transmission in power line communication networks," IEEE Journal on Selected Areas in Communications , vol.24, no.7, pp. 1389-1400, July 2006

[6] S. Galli, T. Banwell, "A novel approach to the modeling of the indoor power line channel-Part II: power line transmission medium," IEEE Communications Magazine , vol.41, no.4, pp. 41- 47, April 2003

[7] M. Zimmermann, K. Dostert, "Analysis and modeling of impulsive noise in broad-band powerline communications," IEEE Transactions on Electromagnetic Compatibility , vol.44, no.1, pp.249-258, Feb 2002 transfer function and its properties," IEEE Transactions on Power Delivery , vol.20, no.3, pp. 1869- 1878, July 2005

[8] D. Benyoucef, "A New Statistical Model of the Noise Power Density Spectrum for Powerline Communications" in 2005 International Symposium on Power Line Communications and Its Applications, pp. 136-141, Kyoto, Japan, Mar. 2003.

[9] Yindi Jing; H. Jafarkhani, "Network Beamforming Using Relays With Perfect Channel Information." IEEE Transactions on Information Theory, vol.55, no.6, pp.2499-2517, June 2009

[10] Junwei Zhang, M.C. Gursoy, "Relay beamforming strategies for physical-layer security," 2010 44th Annual Conference on Information Sciences and Systems (CISS), pp.1-6, 17-19 March 2010

[11] John G. Proakis, "Digital Communications", 4th Edition, McGraw Hill Higher Education, 2000

[12] B. Rankov; A. Wittneben; , "Spectral efficient protocols for half-duplex fading relay channels," IEEE Journal on Selected Areas in Communications , vol.25, no.2, pp.379-389, February 2007

[13] P. Popovski, H. Yomo, "Physical Network Coding in Two-Way Wireless Relay Channels," IEEE International Conference on Communications, 2007. ICC '07, pp.707-712, 24-28 June 2007

[14] A. schwager, L. Stadelmeier and M. Zumkeller, " Potential of Broadband Power Line Home Network" in *Consumer Communications and Networking Conference, 2005*, pp. 359–363, Jan. 2005.

[15] Gault, S.; Ciblat, P.; Hachem, W.; , "An OFDMA based modem for powerline communications over the low voltage distribution network," 2005 International Symposium on Power Line Communications and Its Applications, pp. 42- 46, 6-8 April 2005

19th European Signal Processing Conference (EUSIPCO 2011) Barcelona, Spain, August 29 - September 2, 2011

CAPACITY EVALUATION WITH CHANNEL ESTIMATION ERROR FOR THE DECODE-AND-FORWARD RELAY PLC NETWORKS

Bo Tan, John Thompson

Institute for Digital Communications, The University of Edinburgh
Edinburgh, EH9 3JL, UK
phone: +(44) 131 650 5659, email: b.tan@ed.ac.uk

ABSTRACT

In this paper, the achievable information rates of three Decode-and-Forward (DF) relay protocols are investigated with linear minimum mean square error (LMMSE) channel estimation in powerline communications (PLC) networks. Analysis of how the channel estimation errors impact the performance of unidirectional and bidirectional relay protocols is given. Realistic simulations are performed to evaluate the performance for varying the number of pilot Orthogonal Frequency-Division Multiplexing (OFDM) symbols and the robustness of different protocols is discussed. Solutions for how to mitigate the impact of channel and noise on the protocol to maximise performance are also discussed.

1. INTRODUCTION

Powerline Communications (PLC) which uses the existing power grid as the data transmission medium draws increasing attention with the spread of the Smart Grid concept. In [1], it has been proved that to use power cables as a broadband communications channel is feasible. A variety of potential applications, such as High-Definition Television (HDTV), Voice over IP (VoIP) and Smart Energy have been proposed in the Homeplug AV and AV2 standards. However, research to optimise the data transmission capacity of PLC is still on going. Relays, or repeaters, are one technique that will help increase network capacity and coverage in PLC environments.

Among the current discussions on relays in PLC networks, Decode-and-forward (DF) schemes and corresponding sub-carrier and power allocation schemes are investigated in [2]. Space-time coding schemes are proposed for the multi-hop PLC networks in [3], where the impact of repeater location is also studied. A series of relay protocols which involve beamforming and bidirectional techniques in PLC relay transmission have been studied in [4], where DF has been shown to have significant advantages in PLC environments. Previous research on relays is usually based on the assumption that relay nodes know the channel state information (CSI) perfectly. This paper investigates the achievable information rates for multi-relay unidirectional, 3-step bidirectional and 2-step bidirectional DF schemes. We consider the impact of channel estimation error in frequency selective fading PLC channel and coloured background noise environment. The contributions of this paper are: First, a multi-pilot based linear minimum mean square error (LMMSE) channel estimation method is proposed for the above relay schemes. Second, in Section 3 a realistic analysis for the achievable information rate for the above relay schemes in PLC is given. Finally, the best choice of the number of pilot for DF PLC relay schemes is obtained.

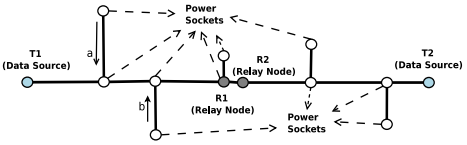

Figure 1: Typical In-door PLC Network Topology.

The remaining parts of this paper are organised as follows. In Section 2, channel, noise characteristics and modelling in PLC are introduced. Also, the notation used in this paper are defined. The basic LMMSE estimation method and the channel estimation method used in this paper are described in Section 2.2. Analysis of achievable information rates for 3 DF relay protocols is given in Section 3. In section 4, the simulation results are plotted and the reasons for the results are discussed. Finally, Section 5 concludes the paper and gives future research direction.

2. SYSTEM MODEL AND CHANNEL ESTIMATION

2.1 System Model

Fig. 1 shows a typical in-door PLC network including a group of power sockets where PLC modems can be plugged in as data transmitters/receivers or relay nodes. Because of the existence of reflections such as a and b which are shown in Fig. 1, the power cable presents as a typical frequency selective fading channel in the frequency domain, and a multipath channel in the time domain. Here, a method based on the Transmission Line Theory which is proposed in [5] and [15] is employed to model the PLC channel. The transfer functions for the Data Terminal 1 to Data Terminal 2 ($T_1 \rightarrow T_2$), Data Terminal 1 to Relay Node 1 ($T_1 \rightarrow R_1$) and Relay Node 1 to Data Terminal 2 ($R_1 \rightarrow T_2$) links in Fig. 1 are shown in Fig. 2. In this paper, the house connection cable of type NAYY35 which is also used in [13] is employed to model the channel. As can be seen from Fig. 2 the channels suffer deep fading at some frequencies which will cause low information rate.

The noise in PLC appears as coloured background noise blended with impulse noise. The source of the noise has been studied and classified into 5 categories in [6]. Noise types 1 and 2 in [6] that are the sum of several low power noise sources and narrowband interference induced by medium and short wave broadcasts often have a stable power spectral density over seconds, minutes and even hours, thus, they are considered as background noise. The others three sources may change rapidly within microseconds and milliseconds, therefore, are considered to be as impulse noise. In this pa-

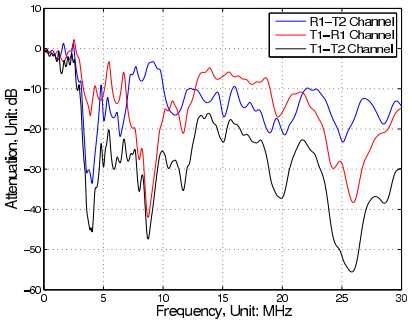

Figure 2: Transfer Functions for the Data Source to Relay nodes link, Data Source to Data Destination link and Relay node to Data Destination link, here, Distance of $T_1 \longleftrightarrow T_2$ is 100 m, and Relay node is at the middle point between T_1 and T_2

per, we only consider the impact of the background noise. A synthesis process in [7] that passes White Gaussian Noise (WGN) through a coloured filter is used to model the background noise.

Based on the frequency selective fading property of the PLC channel and the harsh noise conditions in the frequency domain, Orthogonal Frequency-Division Multiplexing (OFDM) is used to combat these issues. Assume that the bandwidth is divided into K orthogonal subcarriers in the frequency domain. Here, we use the vector $H_{t_1t_2}=[h^1_{t_1t_2},h^2_{t_1t_2},\cdots,h^K_{t_1t_2}]$ to denote the frequency domain channel transfer function for the $T_1 \rightarrow T_2$ link, where, $h^k_{t_1t_2}$ $(k \in [1,2,\cdots,K])$ denotes the channel gain on the k_{th} subcarrier. The vectors H_{t_1r} and H_{rt_2} for the $T_1 \rightarrow R$ and $R \rightarrow T_2$ links are defined in the same way. In addition, $N_{t_2}=[n^1_{t_2},n^2_{t_2},\cdots,n^K_{t_2}]$ stands for the noise samples at T_2, where $n^k_{t_2}$ denotes noise on the k_{th} sub-carrier with power $\left(\sigma^k_{t_2}\right)^2$. Similarly, N_{t_1}, N_r denote the noise samples on T_1 and R with power $\left(\sigma^k_{t_1}\right)^2$ and $\left(\sigma^k_r\right)^2$ on the k_{th} subcarrier, respectively. Furthermore P is defined as the data transmit power on each sub-carrier. Thus, data transmission on the $T_1 \rightarrow T_2$ link with sequence $X=[x^1,x^2,\cdots,x^K]$ can be modelled as (1):

$$Y_{t_2} = \sqrt{P} \cdot H_{t_1t_2} \cdot X + N_{t_2} \tag{1}$$

Where, $Y_{t_2}=[y^1_{t_2},y^2_{t_2},\cdots,y^K_{t_2}]$ is the received signal sequence on the receive side. The data communication processes through other links can also be modelled in the same way as (1).

2.2 Channel Estimation

Generally, in DF protocols, the terminal at the receive side should estimate the CSI based on the pilot OFDM symbols sent by the adjacent terminal which sends the signal. We use the frame structure in [8] where each frame contains 256 OFDM symbols and 64 frames form a superframe. Thus, there are a total of $N = 16384$ symbols in a superframe. Assume that there are M OFDM symbols used as pilot symbols per superframe. For each pilot symbol, the LMMSE method proposed in [9] is employed to estimate frequency domain transfer function. The estimated channel transfer function based on the m_{th} pilot is:

$$\widehat{H}_m = R_{HH}\left(R_{HH}+\Theta_m\left(X_m X_m^H\right)^{-1}\right)^{-1} H^{ls}_m = H + E_m \tag{2}$$

where, $\widehat{H}^{ls}_m = X_m^{-1} Y_m = [\widehat{h}^1_m, \widehat{h}^2_m, \cdots, \widehat{h}^K_m]$ is the least-square (LS) estimate of H and $\widehat{h}^k_m$ is the estimated channel gain on k_{th} sub-carrier. The matrix $\Theta_m = diag[(\sigma^1_m)^2, (\sigma^2_m)^2, \cdots, (\sigma^K_m)^2]$ is the variance matrix of the noise for the m_{th} pilot on the receive terminal, and $(\sigma^k_m)^2$ is the noise power on k_{th} sub-carrier, $R_{HH} = E\left\{HH^H\right\}$ is covariance matrix of H, $E_m = [\varepsilon^1_m, \varepsilon^2_m, \cdots, \varepsilon^K_m]$ is the channel estimation error vector and ε^k_m is the channel estimation error for the m_{th} pilot in the k_{th} sub-carrier.

According to [9], a statistical time domain channel model is needed to evaluate R_{HH} in (2). To keep the complexity low but use a realistic channel approximation, in this paper, L randomly generated channels in the frequency domain are employed to calculate R_{HH}. The channel correlation matrix used in (2) is then obtained:

$$R_{HH} = [r_{m,n}] = [E[(h^m_l - \mu^m)(h^n_l - \mu^n)]] \tag{3}$$

where, h^k_l is the channel gain of l_{th} randomly generated channel at the k_{th} sub-carrier, and μ^k is the average channel gain at the k_{th} sub-carrier over all the L generated channels.

On the basis of the LMMSE estimation result above, the average value of all the M estimated channel transfer functions is used as the final channel estimation result.

$$\widehat{H} = \frac{1}{M}\sum_{m=1}^{M}\widehat{H}_m = H + \frac{1}{M}\sum_{m=1}^{M} E_m \tag{4}$$

here, we define the second phase of (4) as the channel estimation error $E = [\varepsilon^1, \varepsilon^2, \cdots, \varepsilon^K]$ for the multi-pilot scenario, where $\varepsilon^k = \frac{1}{M}\sum_{m=1}^{M}\varepsilon^k_m$. Assume the variance of ε^k_m is a^k_m which is also can be considered as the noise power induced by the inaccuracy of channel estimation. The estimation noise on each pilot symbol, E_m, is mutually independent and identically distributed. Thus, the variance of ε^k is $\frac{1}{M}a^k_m$ which means that using more pilot symbols will lead to a more precise estimation result.

In the following part of this paper, we use $\widehat{H}_{xy} = [\widehat{h}^1_{xy}, \widehat{h}^2_{xy}, \cdots, \widehat{h}^K_{xy}]$ and $E_{xy} = [\varepsilon^1_{xy}, \varepsilon^2_{xy}, \cdots, \varepsilon^K_{xy}]$ to denote the estimated channel and channel estimation error for the $x \rightarrow y$ link, where $\widehat{h}^k_{xy}$ and ε^k_{xy} denote the estimated channel and channel estimation error on the k_{th} sub-carrier for this link. One further point should be noted. In the perfect channel estimation scenario, the channel transfer function for $x \rightarrow y$ and $y \rightarrow x$ link can be assumed the same, but if the channel estimation error is considered, $\widehat{H}_{xy}$ will not equal to $\widehat{H}_{yx}$ for the reason that the different disturbance situations on x and y will cause different channel estimation results.

3. ACHIEVABLE INFORMATION RATE OF DIFFERENT RELAY PROTOCOLS

The conclusion in [4] shows that in PLC environments the DF protocols often provide more robustness and higher capacity performance than AF protocols. Therefore, in this paper, 3 DF protocols are investigated with the existence of channel estimation error.

3.1 Protocol 1: 2Relay-1Way DF with Beamforming

Theoretically, all the available sockets between data source and destination, for example R_1 and R_2 in Fig. 1., can be considered as potential relay nodes. Thus, multi-relay operation is possible in a PLC network. Due to the physical distribution of power sockets we made the assumption that sockets often appear in pairs, which means we can often find two sockets which are closely located. Though applying the transmit beamforming technique in the 2nd hop in a DF relay scheme with perfect channel estimation has been discussed in [16] for wireless communications, here the focus is the achievable information rate with channel estimation error in PLC channel environment.

As described in [4], in this protocol, T_1 transmits messages to T_2 with the help of R_1 and R_2. R_1 and R_2 decode the message independently in the 1st phase, then the relays forward the re-encoded message to T_2. Further define the first M OFDM symbols in a super frame as the pilot symbols. During the channel estimation period, R_1 and R_2 estimate the channel transfer functions for $T_1 \rightarrow R_1$ and $T_1 \rightarrow R_2$ links respectively, then apply beamforming to forward the signal to T_2 Thus, the information rate for the 1st phase can be written as:

$$R_{t_1r_1r_2} = \sum_{k=1}^{K} \log_2\left(1+\min\left\{SNR^k_{t_1\rightarrow r_1}, SNR^k_{t_1\rightarrow r_2}\right\}\right) \quad (5)$$

where, $SNR^k_{t_1\rightarrow r_1} = \frac{P|\widehat{h}^k_{t_1r_1}|^2}{\left(\left(\sigma^k_{r_1}\right)^2+P|\varepsilon^k_{t_1r_1}|^2\right)\Gamma}$ and $SNR^k_{t_1\rightarrow r_2} = \frac{P|\widehat{h}^k_{t_1r_2}|^2}{\left(\left(\sigma^k_{r_1}\right)^2+P|\varepsilon^k_{t_1r_2}|^2\right)\Gamma}$ are the SNRs for $T_1 \rightarrow R_1$ and $T_1 \rightarrow R_2$ links at k_{th} sub-carrier.

Considering the existence of the difference on the channel phases and local oscillators, there always phase differences between $R_1 \rightarrow T_2$ and $R_2 \rightarrow T_2$ channel. Here, the complex channels are written as $|\, h^k_{r_1t_2} \,| e^{j\theta_1}$ and $|\, h^k_{r_2t_2} \,| e^{j\theta_2}$. If $\theta = \mid \theta_1 - \theta_2 \mid$ falls in $[\frac{-\pi}{2}, \frac{\pi}{2}]$, the amplitude of simple superposed signal as $|\, \sqrt{P}h^k_{r_1t_2} + \sqrt{P}h^k_{r_2t_2} \,|$ will be increased at receive side. If θ falls in $[\frac{\pi}{2}, \frac{3\pi}{2}]$, the received amplitude will reduce rather than increase. Taking account the fact that channel status keeps stationary and the Time Division Duplex (TDD) work mode in PLC, wen can assume that transmitter fully knows channel status. Thus, transmit beamforming can be employed to compensate the phase difference, thus θ always equals 0, which means the superposed signal is always enhanced. Then information rate for the 2nd phase thus is given by:

$$R_{r_1r_2t_2} = \sum_{k=1}^{K} \log_2\left(1+\frac{P\left(|\,\widehat{h}^k_{r_1t_2}\,|+|\,\widehat{h}^k_{r_1t_2}\,|\right)^2}{\left(\left(\sigma^k_{t_2}\right)^2+P|\,\varepsilon^k_{r_1t_2}|^2+P|\,\varepsilon^k_{r_2t_2}|^2\right)\Gamma}\right) \quad (6)$$

where, Γ denotes SNR gap which is used to indicate the information rate loss caused by link protection techniques such as channel coding, synchronising overhead. From the statement in [11], for the uncoded modulation system, the achievable information rate is often 10 dB less than the Shannon capacity. If convolutional coding is applied, the performance will be improved by 7 to 8 dB. Thus, here we make the assumption that $\Gamma = 3$ dB is reasonable. Then the overall achievable information rate for this protocol is given by:

$$R^{DF}_{2R1W\_BF} = \frac{1}{2}\left(1-\frac{M}{N}\right)\min\{R_{t_1r_1r_2}, R_{r_1r_2t_2}\} \quad (7)$$

where, the factor $\frac{1}{2}$ denotes the half-duplex operation of the relay, and the factor $\frac{M}{N}$ denotes the overhead loss caused by pilot symbols.

3.2 Protocol 2: 1Relay-2Way-3Step DF

Due to the half-duplex mode on relay nodes, all the unidirectional relay protocols suffer information rate loss. We consider bidirectional schemes which will help the system increase its spectral efficiency. Assume that T_1 and T_2 have messages to send to each other. In bidirectional protocols, relay nodes collect the messages from both directions and forward the superposed signal in a broadcast manner. Then T_1 and T_2 extract their expected message from the superposed signal by removing their own message first. As discussed in [12] and [14], bidirectional relay operation can be implemented in both AF and DF scenarios. In this paper the performance of bidirectional relay protocols in PLC channel environment with channel estimation error is investigated.

First a 3-Step protocol is discussed. In this protocol, the whole data transmission is accomplished in 3 steps. First, T_1 sends X_1 to R_1, which is decoded and stored at R_1. Second, T_2 sends X_2 to R_1, which is also decoded and stored. At R_1, the two decoded messages are superposed into $X_3 = [x^1_3, x^2_3, \cdots, x^K_3]$, where, $x^k_3 = \sqrt{\frac{1}{2}P}x^k_1 + \sqrt{\frac{1}{2}P}x^k_2$. In the third phase, R_1 broadcasts X_3, T_1 and T_2 then receive X_3 and extract their expected messages. For the pilot symbols, T_1 and T_2 send their pilot sequences on the first M symbols. Then, R_1 fills the pilot symbols with its own sequence. This sequence is broadcasted to T_1 and T_2.

In this protocol, the achievable information rate consists of 2 data streams: $T_1 \rightarrow R_1 \rightarrow T_2$ and $T_2 \rightarrow R_1 \rightarrow T_1$. The sum-rate of this protocol is given by:

$$R^{DF}_{1R2W\_3S} = \frac{1}{3}\left(1-\frac{M}{N}\right)(R_{t_1r_1t_2} + R_{t_2r_1t_1}) \quad (8)$$

where, the factor $1/3$ denotes the fact that the transmission process should be completed in 3 time-slots due to the half-duplex operation of the relay node, and:

$$R_{t_1r_1t_2} = \min\left\{\sum_{k=1}^{K}\log_2\left(1+\frac{P\,|\,\widehat{h}^k_{t_1r_1}\,|^2}{\left(\left(P\,|\,\varepsilon^k_{t_1r_1}\,|^2+\sigma^k_{r_1}\right)^2\right)\Gamma}\right), \sum_{k=1}^{K}\log_2\left(1+\frac{1}{2}\frac{P\,|\,\widehat{h}^k_{r_1t_2}\,|^2}{\left(P|\,\varepsilon^k_{r_1t_2}|^2+\left(\sigma^k_{t_2}\right)^2\right)\Gamma}\right)\right\} \quad (9)$$

$$R_{t_2r_1t_1} = \min\left\{\sum_{k=1}^{K}\log_2\left(1+\frac{P\,|\,\widehat{h}^k_{t_2r_1}\,|^2}{\left(P\,|\,\varepsilon^k_{t_2r_1}\,|^2+\left(\sigma^k_{r_1}\right)^2\right)\Gamma}\right), \sum_{k=1}^{K}\log_2\left(1+\frac{1}{2}\frac{P\,|\,\widehat{h}^k_{r_1t_1}\,|^2}{\left(P|\,\varepsilon^k_{r_1t_1}|^2+\left(\sigma^k_{t_1}\right)^2\right)\Gamma}\right)\right\} \quad (10)$$

stand for information rates of the $T_1 \rightarrow R_1 \rightarrow T_2$ link and the reverse link, respectively.

3.3 Protocol 3: 1Relay-2Way-2Step DF

Merging the first and second phases in Protocol 3 into one phase and using V-BLAST detection at R_1, a 2-step directional DF relay protocol is constructed. The step in

which T_1 and T_2 transmit concurrently to R_1 is called the *Multi−Access* (MA) phase. Here, we assume R_1 detects the data stream from T_1 first, by considering the signal from T_2 as interference. Then R_1 subtracts out the detected signal and decodes T_2. For the channel estimation process in this protocol, at the first phase, T_1 and T_2 send the mutual orthogonal pilot sequences on pilot symbols to ensure that the estimation processes for $T_1 \rightarrow R_1$ and $T_2 \rightarrow R_1$. links do not impact each other. Then R_1 fills the pilot symbols into superframe and forwards the signal to T_1 and T_2. Thus the information rate for $T_1 \rightarrow R_1 \rightarrow T_2$ link is:

$$R^{2S}_{t_1 r_1 t_2} = \min \left\{ \sum_{k=1}^{K} \log_2 \left(1 + \frac{P \mid \widehat{h}^k_{t_1 r_1} \mid^2}{\left(P \mid \varepsilon^k_{t_1 r_1} \mid^2 + \left(\sigma^k_{r_1}\right)^2 \right) \Gamma} \right), \right.$$
$$\left. \sum_{k=1}^{K} \log_2 \left(1 + \frac{\frac{1}{2} P \mid \widehat{h}^k_{r_1 t_2} \mid^2}{\left(P \mid \varepsilon^k_{r_1 t_2} \mid^2 + \left(\sigma^k_{t_2}\right)^2 \right) \Gamma} \right) \right\} \quad (11)$$

In (11), $P \mid h^k_{t_2 r_1} \mid^2$ denotes the received power from T_2 at R_1 which is considered as interference for R_1 decoding T_1. Before decoding the message from T_2, X_1 should be subtracted out. Thus, the information rate for the reverse link is:

$$R^{2S}_{t_2 r_1 t_1} = \min \left\{ \sum_{k=1}^{K} \log_2 \left(1 + \frac{P \mid \widehat{h}^k_{t_2 r_1} \mid^2}{\left(P \mid \varepsilon^k_{t_2 r_1} \mid^2 + \left(\sigma^k_{r_1}\right)^2 \right) \Gamma} \right), \right.$$
$$\left. \sum_{k=1}^{K} \log_2 \left(1 + \frac{\frac{1}{2} P \mid \widehat{h}^k_{r_1 t_1} \mid^2}{\left(P \mid \varepsilon^k_{r_1 t_1} \mid^2 + \left(\sigma^k_{t_1}\right)^2 \right) \Gamma} \right) \right\} \quad (12)$$

Thus, the total information rate for the case of detecting the data for T_1 first is:

$$R^{DF'}_{1R2W\_2S} = \frac{1}{2} \left(R_{t_1 r_1 t_2 \_2S} + R_{t_2 r_1 t_1 \_2S} \right) \quad (13)$$

In the same way, the information rate $R^{DF''}_{1R2W\_2S}$ which denotes the information rate for detecting the T_2 data stream first can be obtained. Therefore, the achievable information rate for 2-step bidirectional DF protocol is given by:

$$R^{DF}_{1R2W\_2S} = \left(1 - \frac{M}{N} \right) \cdot \max \left\{ R^{DF'}_{1R2W\_2S}, R^{DF''}_{1R2W\_2S} \right\} \quad (14)$$

4. SIMULATION AND NUMERICAL RESULTS

The PVC-insulated cables that are widely used in low-voltage power distribution grid are used in [13] to simulate the network shown in Fig 1. One generated channel can be used during a superframe since the PLC channel is considered stationary for seconds or tens of seconds. According to the background noise characteristics described in [6], the noise power spectral density (PSD) on a node can be assumed to be unchanged during a superframe. In order to make the simulation realistic, channel transfer functions are re-generated by using a group of randomly located branches with random branch length and a new group of background noise PSDs for T_1, T_2, R_1 and R_2 are re-generated according to [7] for each new superframe. It is assumed that each terminal in the system transmits a signal at the same power level with equal power allocation on each sub-carrier. Pilot symbols are transmitted with the same power level as the data symbols. A transmit power spectral density (PSD) of −60 dBm/Hz which is used for many actual PLC products [1] is used in this paper.

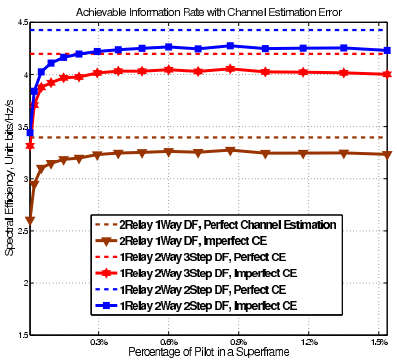

Figure 3: Data rate trends with increasing numbers of pilot symbols, when the $T_1 \leftrightarrow T_2$ distance is 10m.

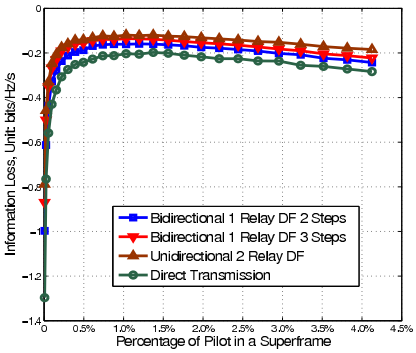

Figure 4: Information gaps between perfect channel estimation scenario and scenario with channel estimation error when the $D_{T_1 \leftrightarrow T_2}$ distance is 10m.

Fig. 3 shows the trend of achievable information rates by increasing the number of pilot symbols. When there is only 1 pilot symbol, the information rate for bidirectional 3-step DF and 2-step is almost the same. But with increasing numbers of pilot symbols, the 2-step protocol improves throughput faster than 3-step protocol. This phenomenon means that 2-step protocol is more sensitive to CSI errors than the 3-step protocol. To utilise the benefit of bidirectional 2-step scheme, precise channel estimation procedures should be guaranteed.

The information gap, which is difference of rate between the estimated CSI data rate and the rate with prefect CSI, is defined here to measure the performance of protocols. From Fig. 4, we can see that direct transmission has an obviously larger gap than the relay schemes. The reason is that without the help of the relay the received signal at T_2 is weaker due to the larger channel attenuation. Thus, a less accurate channel estimation is obtained which leads to higher information loss. By using a relay node to decode and forward the transmission, the signal can be detected more reliably at

the receiver. Thus, the information gap of unidirectional single relay DF protocol is smaller than the direct transmission. For the bidirectional protocols, they can benefit from the DF signal reconstruction operation but are limited by the power split operation in the broadcasting phase. In particular, for the 2-step bidirectional DF protocol, the performance of V-BLAST detection degraded when channel estimation errors are present. For example, due to the inaccuracy of channel estimation of $T_1 \rightarrow R$ link, after decoding the signal X_1 from T_1, the impact of X_1 can not be totally subtracted, and the residual interference will limit the capability to detect X_2 from T_2. Therefore, the 2-step bidirectional protocol has a larger information gap than the 3-step bidirectional protocol.

In Fig. 3 and Fig. 4, we can see that performance does not always increase with number of the pilots because the pilots reduce the available data payload in a superframe. From the simulation results, when the number of pilot occupies 0.5% of the total the symbols in a superframe, the protocols have the best performance. From the simulation of [4], the average channel attenuation incerase with the increasing of $T_1 \leftrightarrow T_2$ distance. Thus, more pilot symbols are required for accurate channel estimation. In practical system, the length of pilot symbols is a trade-off design. In addition, considering the slow channel varying of PLC, an adaptive pilot control mechanism can be developed for keeping relay PLC system always in optimal status without frequently update.

5. CONCLUSION AND FUTURE WORK

From the analysis and simulation above, the achievable information rates for unidirectional single direction DF, bidirectional 3-step DF and 2-step DF are given with consideration of channel estimation error in the PLC environment. The results of the simulation proved that DF technique can help PLC transmission system to combat the hostile noise and channel conditions to improve throughput. The bidirectional 2-step DF protocol shows superiority in transmission capacity, but is vulnerable to noise disturbance which will impact the channel estimation accuracy. With accurate channel estimation using multiple pilot symbols, the 2-step protocol will minimise such deterioration. The 3-step protocol show more robustness then the 2-step protocol when channel estimation errors are present. This paper showed that bidirectional relay techniques can be a good choice for PLC transmission. In future work, the impact of impulse noise and methods to mitigate it will be studied, and the a relation between the average channel gain and optimal pilot length will be investigated in detail.

REFERENCES

[1] A. Schwager, L. Stadelmeier and M. Zumkeller, " Potential of Broadband Power Line Home Network" in *Consumer Communications and Networking Conference, 2005*, pp. 359–363, Jan. 2005.

[2] Z. Hao; A. Chowdhery, S. Jagannathan, J.M. Cioffi, J. Le Masson, "Multi-User Joint Subchannel and Power Resource-Allocation for Powerline Relay Networks," IEEE International Conference on Communications, 2009. ICC '09. pp.1-5, 14-18 June 2009

[3] L. Lampe; R. Schober, Y. Simon, "Distributed space-time coding for multihop transmission in power line communication networks," IEEE Journal on Selected Areas in Communications , vol.24, no.7, pp. 1389- 1400, July 2006

[4] B. Tan, J.S. Thompson, "Relay Transmission Protocols for In-door Powerline Communications Networks" IEEE International Conference on Communications, Workshop on Smart Grid Communications, Kyoto, Japan, Jun. 2011.

[5] S. Galli, T. Banwell, "A novel approach to the modeling of the indoor power line channel-Part II: power line transmission medium," IEEE Communications Magazine , vol.41, no.4, pp. 41- 47, April 2003

[6] M. Zimmermann, K. Dostert, "Analysis and modeling of impulsive noise in broad-band powerline communications," IEEE Transactions on Electromagnetic Compatibility , vol.44, no.1, pp.249-258, Feb 2002 transfer function and its properties," IEEE Transactions on Power Delivery , vol.20, no.3, pp. 1869- 1878, July 2005

[7] D. Benyoucef, "A New Statistical Model of the Noise Power Density Spectrum for Powerline Communications" in 2005 International Symposium on Power Line Communications and Its Applications, pp. 136-141, Kyoto, Japan, Mar. 2003.

[8] S. Gault, P. Ciblat, W. Hachem, "An OFDMA based modem for powerline communications over the low voltage distribution network," 2005 International Symposium on Power Line Communications and Its Applications, pp. 42- 46, 6-8 April 2005

[9] O. Edfors, M. Sandell, J.-J. van-de-Beek, S.K. Wilson, P.O. Borjesson, "OFDM channel estimation by singular value decomposition," Communications, IEEE Transactions on , vol.46, no.7, pp.931-939, Jul 1998

[10] A. Leke, J.M. Cioffi, "Impact of imperfect channel knowledge on the performance of multicarrier systems," Global Telecommunications Conference, 1998. GLOBECOM 98. The Bridge to Global Integration. IEEE , vol.2, no., pp.951-955 vol.2, 1998

[11] John G. Proakis, "Digital Communications", 4th Edition, McGraw Hill Higher Education, 2000

[12] A. Boris, W. Armin, "Spectral efficient protocols for half-duplex fading relay channels," IEEE Journal on Selected Areas in Communications , vol.25, no.2, pp.379-389, February 2007

[13] M. Zimmermann, K. Dostert, "A multipath model for the powerline channel," IEEE Transactions on Communications, vol.50, no.4, pp.553-559, Apr 2002

[14] P. Popovski, H. Yomo, "Physical Network Coding in Two-Way Wireless Relay Channels," IEEE International Conference on Communications, 2007. ICC '07, pp.707-712, 24-28 June 2007

[15] H. Meng, S. Chen, Y.L. Guan, C.L. Law; P.L. So, E. Gunawan, T.T. Lie, "Modeling of transfer Characteristics for the broadband power line communication channel," IEEE Transactions on Power Delivery , vol.19, no.3, pp. 1057- 1064, July 2004

[16] Zh. Junwei; M.C. Gursoy , "Relay beamforming strategies for physical-layer security," 2010 44th Annual Conference on Information Sciences and Systems (CISS), pp.1-6, 17-19 March 2010

ACCEPTED FROM OPEN CALL

RELAYING TECHNOLOGIES FOR SMART GRID COMMUNICATIONS

HONGJIAN SUN AND ARUMUGAM NALLANATHAN, KING'S COLLEGE LONDON
BO TAN AND JOHN S. THOMPSON, UNIVERSITY OF EDINBURGH
JING JIANG, UNIVERSITY OF SURREY
H. VINCENT POOR, PRINCETON UNIVERSITY

ABSTRACT

Wireless technologies can support a broad range of smart grid applications including advanced metering infrastructure and demand response. However, there are many formidable challenges when wireless technologies are applied to the smart gird, such as the trade-offs between wireless coverage and capacity, the high reliability requirement for communication, and limited spectral resources. Relaying has emerged as one of the most promising candidate solutions for addressing these issues. In this article, an introduction to various relaying strategies is presented, together with a discussion of how to improve spectral efficiency and coverage in relay-based information and communications technology infrastructure for smart grid applications. Special attention is paid to the use of unidirectional relaying, collaborative beamforming, and bidirectional relaying strategies.

INTRODUCTION

There is a widely recognized need to upgrade existing electricity grids in order to improve power delivery, reduce operating costs, and support renewable energy sources. Due to the dependence of these goals on data acquisition and control, such smart grids must combine existing electricity grids with advanced information and communications technology (ICT) infrastructure. A mature smart grid will consist of a number of applications, such as supervisory control and data acquisition (SCADA), advanced metering infrastructure (AMI), and demand response (DR). As different applications require distinct degrees of coverage, capacity, reliability, security, and latency, the implementation of ICT infrastructure for smart grid networks raises many challenging design issues [1].

Most smart grid applications (e.g., SCADA and AMI) should exhibit high reliability, large coverage, and high security, while requiring different scales of latency and data rates (e.g., 0.1~1 s latency and 100 kb/s data rate for SCADA, and 10~20 s latency and 1 Mb/s data rate for AMI). Considering neighborhood area networks (NANs), both wireline and wireless technologies can be used to meet these requirements. In the former case, power line communications (PLC) is a natural solution [1]. Using PLC, relatively small equipment investment is needed because it uses existing power lines as the data transmission medium. Nevertheless, there are a number of challenges with PLC (e.g., low capacity).

In the latter case, either ZigBee or Wi-Fi can be employed to enable AMI and DR applications due to their good capacity and low transmit power [2, 3]. However, because of their low transmit power levels, both technologies have limited coverage. A wireless mesh network that consists of various nodes (e.g., WiFi and ZigBee) organized in a mesh topology can enhance the coverage [4–7]. In addition, wireless mesh networks are inherently more reliable as they can take advantage of self-forming and self-healing network concepts.

Wireless mesh architectures are usually implemented at the network layer or data link layer. Relevant research focuses on protocol design for transferring data between network entities [5–7]. The performance of a wireless mesh network depends on the quality, reliability, and efficiency of communications between different nodes in the network. Taking advantage of spatial diversity, relaying technologies can improve the performance of wireless links between neighboring nodes to meet the communication quality requirements of a wireless mesh network. However, conventional relaying technologies such as amplify-and-forward (AF) and decode-and-forward (DF) enhance the capacity at the expense of consuming resources such as radio frequency (RF) spectrum. Inefficient use of these resources could lead to low spectral efficiency. Thus, it is critical to study advanced relaying technologies to improve the spectral efficiency while retaining the advantages of relaying transmission.

In the remainder of this article, we first ana-

1536-1284/12/$25.00 © 2012 IEEE

lyze the challenges of wireless technologies for the smart grid, and then introduce conventional relaying transmission strategies. Some advanced relaying strategies are then discussed. The aim of this study is to identify relaying strategies that can achieve greater spectral efficiency, extended transmission range, and improved reliability.

Challenges of ICT for Smart Grid

The smart grid ICT infrastructure should allow utilities to interact with their electrical devices as well as with the customers on a near-real-time basis. However, for any wireless technology, there are several challenges that still need to be addressed before their deployment on the smart grid. These challenges are described in the following subsections.

Coverage and Capacity Trade-off

Some smart grid applications (e.g., SCADA and AMI) require the access network to cover a large area. Unfortunately, since the interference level increases as the number of nodes increases, the coverage of a wireless network has an inverse relationship with the channel capacity; therefore, there is a trade-off between coverage and capacity in conventional direct transmission systems.

One potential solution is to use relaying technologies, whereby one long wireless link is broken into two or more shorter lower-power links. Due to the inherent broadcast nature of the communications from the source, it may be possible for one or more nodes receiving strong signals from the source to forward them to the destination. Therefore, relaying transmission is an important technique to widen the coverage and enhance the capacity [8].

Reliability

The reliability of a network can be defined in terms of its robustness, survivability, and sufficiency of its connectivity to support a prescribed level of performance. Most smart grid applications (e.g., AMI) require reliable communications paths from the customers back to the high-speed core network. However, radio propagation in wireless communications is affected by several factors, such as multipath fading, which may result in a temporary failure of the communication due to a severe drop in the received signal-to-noise ratio (SNR). Furthermore, wireless networks may suffer disruptions caused by adverse weather conditions (e.g., thunderstorms) that could attenuate the transmission ability of the wireless network.

Using relaying technologies, the transmit signal can be passed through both the direct communication channel and the relay channel(s). With the aid of a receiver combining strategy, the multipath fading effects can be averaged or even removed. Under adverse weather conditions, a direct transmission link may be blocked. It is feasible to build alternate links using the rest of the nodes, thus offering capabilities of self-forming and self-healing to the ICT infrastructure.

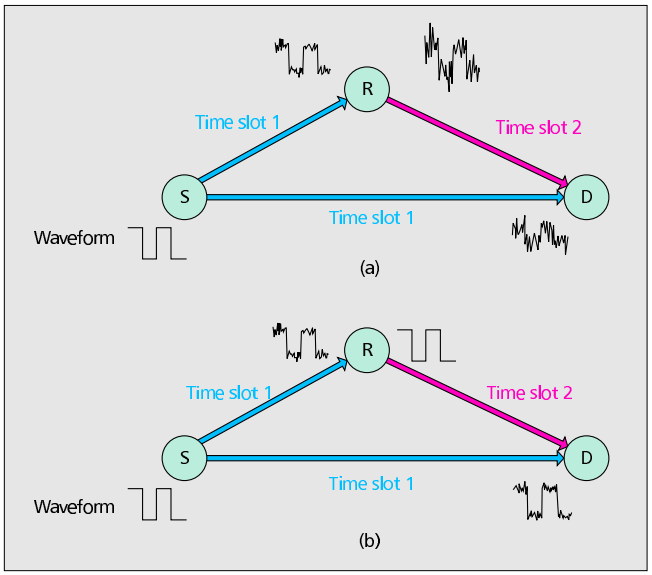

Figure 1. *Demonstration of conventional relaying protocols: a) amplify-and-forward (AF); b) decode-and-forward (DF).*

Spectrum Issues

RF spectrum is the lifeblood of wireless communication systems. However, current ICT for the smart grid has access to limited numbers of frequencies, which are primarily designated for SCADA and AMI. Using current transmission techniques, it is very challenging to support additional demands from certain new smart grid applications, such as video surveillance. The efficient use of RF spectrum is therefore a critical issue that needs to be addressed before the deployment of extensive wireless networking in the smart grid.

The spectral utilization efficiency is often measured by spectral efficiency, which is defined as the number of bits that can be communicated over a given bandwidth within a unit of time (in bits per second per Hertz).

Due to the contributions of relay channels, which can boost the signal strength at the destination, relaying technologies can achieve higher spectral efficiency than direct transmission.

Conventional Relaying Strategies

Based on the above discussion, there is a common need for applying relaying technologies in wireless networks. We consider such a relay-based wireless system, where one or more relays working in the half-duplex mode are used to retransmit the signals to the destination (D). In this relay-based system, the data communication can be divided into two time slots. This is required due to the half-duplex constraint, which means that the relays are unable to receive and transmit data simultaneously. In the first time slot, the source (S) broadcasts its information to both D and one or more relays. In the second time slot, the relays forward the received data to

The main challenge in the relay-based system is how to use the relays efficiently, which requires study of how to use the relay(s) and also how many relays are needed. When we consider a single-relay system, the relaying protocol at the relay could significantly affect the system performance.

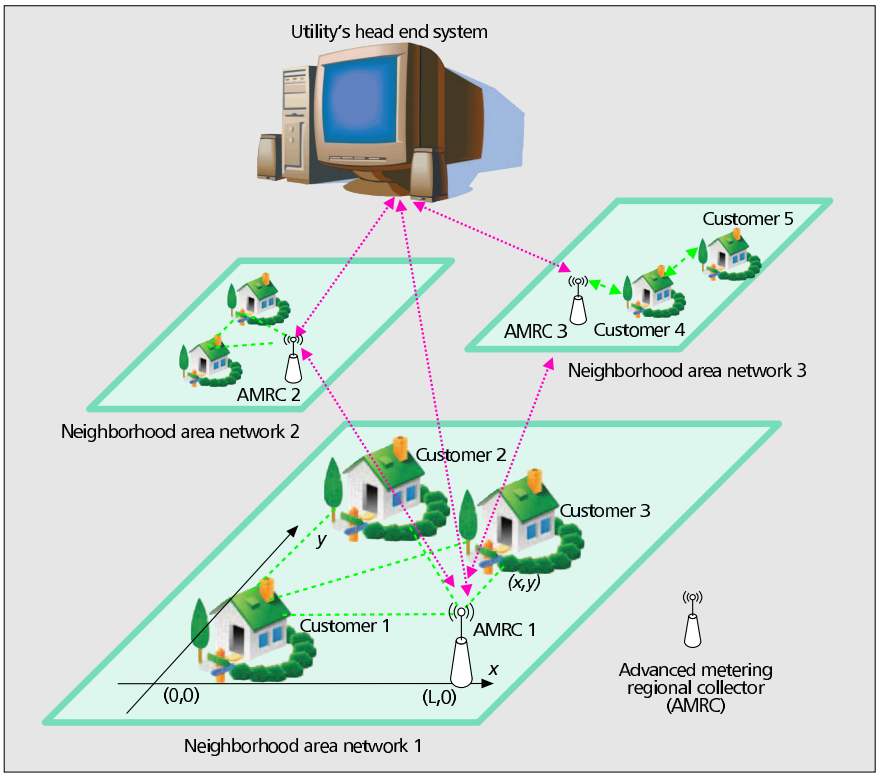

Figure 2. *An example of relaying technology implementation in the smart grid: relaying technology-based advanced metering infrastructure.*

D. By using relays, D could achieve much higher reliability in decoding the information from S by taking advantage of spatial diversity.

The main challenge in the relay-based system is how to use the relays efficiently, which requires study of how to use the relay(s) and also how many relays are needed. When we consider a single-relay system, the relaying protocol at the relay could significantly affect the system performance. Here, we present a brief overview of conventional relaying protocols (i.e., AF and DF). As illustrated in Fig. 1a, after the first time slot, one relay receives a noisy version of the transmitted signal from the source. The AF relaying protocol allows the relay to amplify and retransmit these noisy data to D.

Another simple relaying protocol is DF. As shown in Fig. 1b, the DF protocol allows the relay to decode the received signals from S and then re-encode and forward them to D. The performance of DF heavily depends on whether the relay can successfully decode the transmitted signals. If the relay fails to decode the signal correctly, it may be able to detect this through a cyclic redundancy check and not transmit the data. If the errors are not detected, they will be propagated to the destination and lead to even worse performance than for direct transmission. In either case, the relay is unable to improve detection performance at D. On the other hand, if the signal is correctly decoded at the relay, the destination will receive a stronger signal and thus obtain improved performance.

Case Studies for Improving Spectral Efficiency of Relaying Transmission

It is noteworthy that the RF spectrum in the smart grid is a very valuable resource, as noted in the discussion earlier. Unfortunately, conventional relaying technologies (i.e., AF and DF) boost the signals at the destination at the expense of consuming extra resources (e.g., the time and spectrum allocated to the relay). Inefficient use of these resources leads to low spectral efficiency. The spectral efficiency loss in a multiple-relay system (e.g., a wireless mesh network) could be even worse if either multiple time slots or frequency bands are exclusively allocated to different relays. In order to improve the spectral efficiency while retaining the advantages of relaying transmission, it is necessary to study advanced relaying technologies. In the following subsections, we present two case studies that investigate two potential strategies: a two-relay system using beamforming concepts and a bidirectional relaying strategy for a two-way information exchange system.

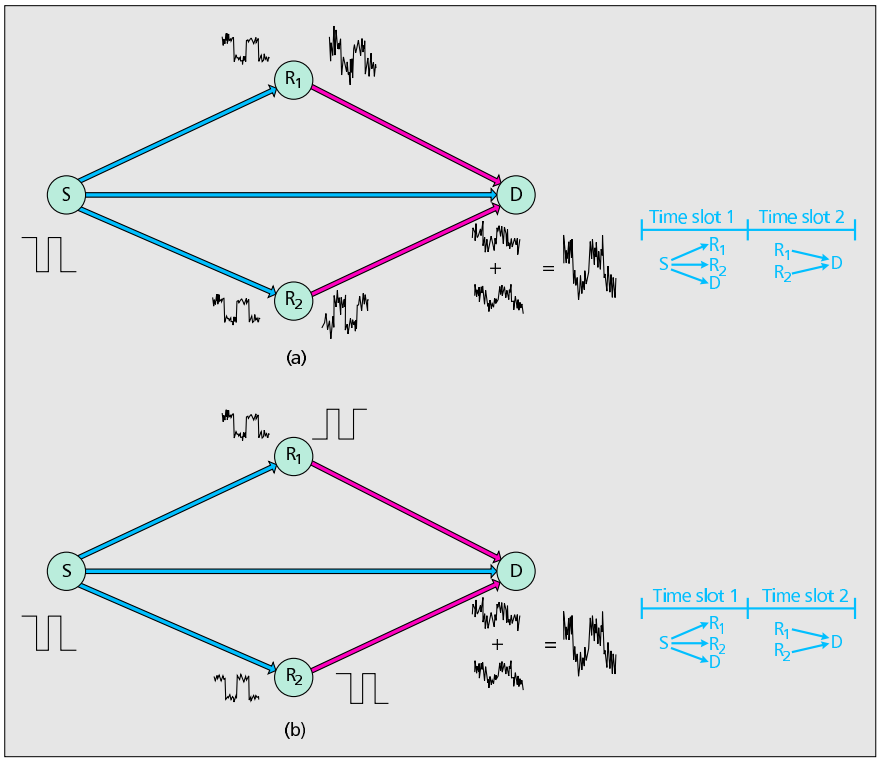

Figure 3. *Relaying protocols combined with 2-relay beamforming: a) unidirectional AF relaying protocol plus beamforming, and b) unidirectional DF relaying protocol plus beamforming.*

DR applications in the smart grid require high data-rate two-way communications between the customers and the UHES. Using conventional unidirectional relaying strategies in NAN, four time slots are needed to accomplish the information exchange process, leading to low spectral efficiency.

The Overall Setting

Considering AMI in the smart grid, the aim is to upload energy consumption data to the utility for DR applications. An example of a wireless network for implementing AMI is shown in Fig. 2. There are two scenarios in which relaying technologies can be used. In a NAN, customers 2 and 3 could act as relays that help customer 1 to transmit data to the advanced metering regional collector (AMRC). Furthermore, AMRCs can help each other to transmit data to the utility's head-end system (UHES). In the following, we discuss the implementation of relaying technologies in NANs.

Suppose that a NAN is implemented using wireless technology based on the ZigBee standard, and the channel center frequency is chosen to be $2405 + 5(k - 11)$ MHz, where the channel index k is a random integer in the range $k \in [11, 26]$. The bandwidth is assumed to be 2 MHz, and the channels between the relay and the end nodes are assumed to suffer frequency-flat Rayleigh fading. Considering the path loss, we adopt the International Telecommunication Union (ITU) indoor propagation model [10], in which the distance power loss coefficient is set to be 28 dB/decade. The transmit power is set to be 0 dBm, and the antenna gain is 2.5 dB. Additive white Gaussian noise (AWGN) is added to the communication channels with the power level of –110 dBm. Without significant loss of generality, all customers are assumed to be located on the x–y plane. Customer 1 is located at the origin (0,0), and the AMRC is at the coordinates $(L, 0)$. The coordinates of the relay (either customer 2 or 3) are denoted by (x, y), where x and y are uniformly distributed values with ranges $x \in [0, L]$ and $y \in [-L/2, L2]$. To emulate the interference from other unlicensed spectrum users (e.g., WiFi or ZigBee), we assume that 1~3 users (with 3 dBm transmit power) are using the same frequency band, with random locations in the ranges $x \in [0, L]$ and $y \in [-L/2, L/2]$.

Case Study 1: Unidirectional Two-Relay System with Collaborative Beamforming

Suppose that one smart meter of customer 1 (source) is uploading the data to the AMRC (destination) while two neighboring customers (relays) could assist the data transmission procedure. Using conventional relaying strategies, two relays forward certain versions of the received signals to the destination, as shown in Fig. 3a for AF and Fig. 3b for DF. No matter which relaying protocol is used, AF or DF, the two-relay system faces a challenge: Because of different channel phases at the two relays, the correlation properties of the received signals at the destination will be distorted. This means

a superposition of the signals at the destination will not necessarily strengthen the intended signals.

Collaborative beamforming [11] can be introduced to adaptively adjust the transmit signal phases and amplitudes at the two relays. For example, as shown in Fig. 3, the signal phase at relay 2 is adjusted. Taking advantage of collaborative beamforming, the received signals at the destination can be constructively added at the destination to improve SNR. To enable collaborative beamforming, the relays are assumed to be synchronized by the use of reference signals from a positioning system such as the global positioning system (GPS). In addition, we assume that the relays are sufficiently separated so that any mutual coupling effects among their antennas are negligible.

The spectral efficiencies of different relaying strategies are compared in Figs. 4a and 4b, where the *x*-axis denotes the distance between two end nodes and the *y*-axis denotes the system spectral efficiency. As shown in Fig. 4a, when direct transmission is available, relaying strategies yield spectral efficiency (also coverage) gain over direct transmission for any transmission distance. Beamforming in the unidirectional two-relay AF system results in marginal improvement compared to the single-relay AF strategy, while adding an extra relay node also increases system complexity. Meanwhile, the performance of the two-relay DF system with collaborative beamforming is similar to the single-relay DF strategy. This is because the overall information rate of the system is, in fact, limited by the channel conditions between the source and the two relays in the first time slot. One poorly conditioned channel from the source to one of the relays will eventually impair the overall spectral efficiency of the two-relay DF strategy. In Fig. 4b, we can see that if direct transmission is blocked, relaying technologies can still achieve satisfactory spectral efficiency.

The empirical cumulative distribution function (CDF) of spectral efficiency is shown in Figs. 4c and 4d, where the *x*-axis denotes the

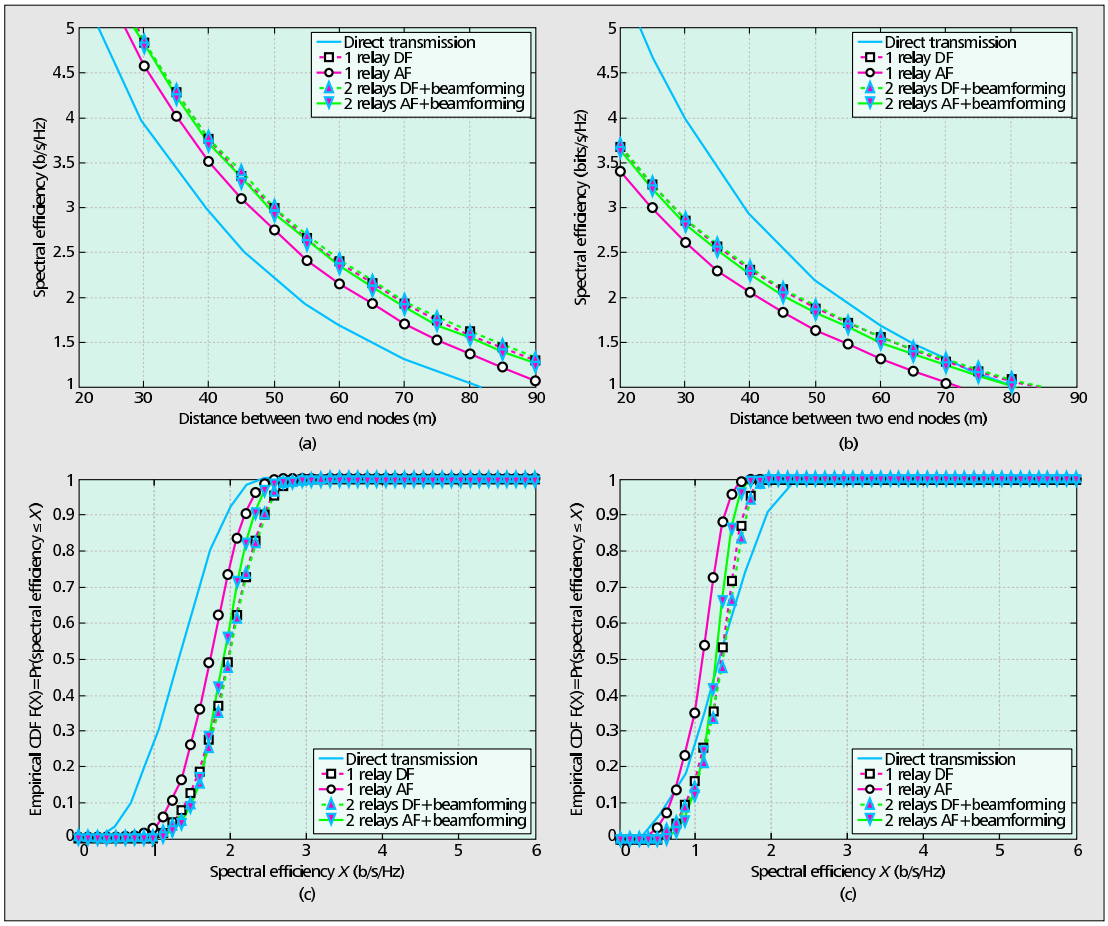

Figure 4. *Comparisons of relaying technologies with direct transmission: a) spectral efficiency when direct transmission is available; b) spectral efficiency when direct transmission is blocked; c) empirical spectral efficiency cumulative distribution function when direct transmission is available; d) empirical spectral efficiency cumulative distribution function when direct transmission is blocked.*

spectral efficiency X and the *y*-axis denotes the empirical CDF F(X). The spectral efficiency CDF F(X) is defined as the percentage of systems having a spectral efficiency less than or equal to X. The simulation results are based on an assumption that the distance between the two end nodes is 70 m. The CDF shows results for 10,000 different channel conditions for a given distance between the two end nodes. It should be emphasized that the steeper the curve, the more robust the system can be. In addition, shifting the curve to the right implies that it can obtain higher spectral efficiency. In Figs. 4c and 4d, we can see that all relaying strategies are more reliable than direct transmission.

Case Study 2: Bidirectional Relaying for Information-Exchange System

DR applications in the smart grid require high-data-rate two-way communications between the customers and the UHES. Using conventional unidirectional relaying strategies in NAN, four time slots are needed to accomplish the information exchange process, leading to low spectral efficiency.

As shown in Fig. 5, the bidirectional relaying strategy requires only two time slots to complete an information exchange process. In the first time slot, two end nodes (e.g., customer 5 and AMRC 3 in Fig. 2) send their information to the relay (e.g., customer 4) using the same frequency band, leading to a superposition of the received signals at the relay. Note that because we assume that all nodes are working in the half-duplex mode, two end nodes cannot decode the signals in the first time slot. Using the AF relaying protocol, the relay directly forwards its received signals to both end nodes. Because these two end nodes have their own copies of transmitted signals, they can subtract their own signals and obtain the information transmitted from the other node. We note that the channel state information between the relay and two end nodes can be estimated by using a channel estimation scheme, such as pilot symbol insertion or training bits [12, 13]. In this way, a higher spectral efficiency can be achieved, since the information at the two nodes is exchanged using fewer time slots.

If the bidirectional relaying strategy is applied together with the DF relaying protocol, the relay needs to decode the superposed signals. Optimal performance can be achieved using a maximum likelihood (ML) detection algorithm. Using ML, the detection error can be minimized but at the expense of high complexity. With lower computational cost, other approaches can obtain near ML performance. One approach is the so-called vertical Bell Labs layered space time (V-BLAST) detection algorithm [14]. Using V-BLAST, we first detect the signal from one node by treating the signal from another node as interference. We then subtract the detected signal vector from the received signal vector, and perform detection on the resulting signal vector. The advantage of the V-BLAST algorithm is that its computational complexity is low and fixed for the whole range of SNRs. Therefore, we consider the V-BLAST detection algorithm at the relay for the bidirectional DF relaying system.

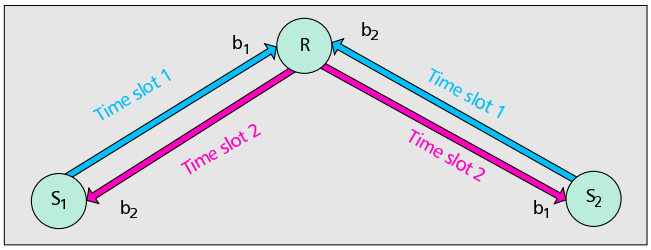

Figure 5. *A bidirectional relaying strategy that uses only two time slots when two end nodes exchange information.*

It can be seen from Figs. 6a and 6b that despite the blocked direct transmission, the bidirectional relay strategies are always superior to direct transmission when the transmission distance is relatively long. This phenomenon arises from the facts that bidirectional relay strategies exchange information using fewer time slots than unidirectional relay strategies do, and that the bidirectional relay strategies do not use the direct link for transmitting information as the two end nodes are working in the half-duplex mode. Bidirectional DF is inferior to direct transmission when the transmission distance L is less than 35 m. This is because, when using V-BLAST, we treat the signal from another node as interference (it becomes stronger as the transmission distance becomes shorter), thereby decreasing the information rate of the whole system. Furthermore, we can see from Figs. 6c and 6d that even though the bidirectional relay strategies are not as reliable as the conventional relaying strategies, they can achieve higher spectral efficiency regardless of the availability of a direct transmission link.

Conclusions

In this article, we have discussed the challenges of wireless communication technologies when applied to the smart grid. In order to improve the coverage, spectral efficiency, and reliability of smart grid communications, we have investigated several potential relaying strategies (e.g., collaborative beamforming for multiple-relay systems and bidirectional relaying for information exchange systems). It has been shown that all relaying strategies can improve the reliability of smart grid communications thanks to spatial diversity. For DR applications, which require two-way information flow, the spectral efficiency and coverage of smart grid communications can be improved by using bidirectional relaying strategies. For SCADA applications where the data flow is mostly in one direction, two-relay systems can only achieve marginal improvement over a single-relay system at the expense of increased implementation complexity.

Acknowledgment

H. Sun and A. Nallanathan acknowledge the support of the U.K. Engineering and Physical Sciences Research Council (EPSRC) with Grant No.

EP/I000054/1. B. Tan, J. Jiang, and J. S. Thompson acknowledge support from the Scottish Funding Council for the Joint Research Institute in Signal and Image Processing between the University of Edinburgh and Heriot-Watt University, as part of the Edinburgh Research Partnership in Engineering and Mathematics (ERPem). H. V. Poor acknowledges the support of the U.S. National Science Foundation under Grants CNS-09-05086, CNS-09-05398, and CCF-10-16671.

References

[1] Trilliant Inc., *Wireless WAN for the Smart Grid: Distribution Networking for Today's (and Tomorrow's) Smart Grid Communications Infrastructure*, Redwood City, CA, Mar. 2010.
[2] P. P. Parikh, M. G. Kanabar, and T. S. Sidhu, "Opportunities and Challenges of Wireless Communication Technologies for Smart Grid Applications," *Proc. IEEE Power and Energy Society General Meeting*, Minneapolis, MN, USA, July 2010, pp. 1–7.
[3] J. Wang and V. C. M. Leung, "Comparisons of Home Area Network Connection Alternatives for Multifamily Dwelling Units," *Proc. 4th IFIP Int'l. Conf. New Technologies, Mobility and Security*, Paris, France, Feb. 2011, pp. 1–5.
[4] V. C. Gungor, B. Lu, and G. P. Hancke, "Opportunities and Challenges of Wireless Sensor Networks in Smart Grid," *IEEE Trans. Industrial Electronics*, vol. 57, no. 10, Oct. 2010, pp. 3557–64.
[5] B. Lichtensteiger *et al.*, "RF Mesh Systems for Smart Metering: System Architecture and Performance," *Proc. IEEE Int'l. Conf. Smart Grid Commun.*, Gaithersburg, MD, Oct. 2010, pp. 379–84.
[6] G. Iyer *et al.*, "Performance Analysis of Wireless Mesh Routing Protocols for Smart Utility Networks," *Proc. IEEE Int'l. Conf. Smart Grid Commun.*, Brussels, Belgium, Oct. 2011, pp. 114–19.
[7] T. Iwao *et al.*, "Dynamic Data Forwarding in Wireless Mesh Networks," *Proc. IEEE Int'l. Conf. Smart Grid Commun.*, Gaithersburg, MD, Oct. 2010, pp. 385–90.
[8] B. Tan and J. S. Thompson, "Relay Transmission Protocols for In-Door Powerline Communications Networks," *Proc. IEEE Int'l. Conf. Commun. Wksps.*, Kyoto, Japan, June 2011, pp. 1–5.
[9] H. A. Suraweera *et al.*, "Amplify and Forward (AF) Relaying with Optimal and Suboptimal Transmit Antenna Selection," *IEEE Trans. Wireless Commun.*, vol. 10, no. 6, June 2011, pp. 1874–85.
[10] ITU-R Recs., "Propagation Data and Prediction Methods for the Planning of Indoor Radio Communication Systems and the Radio Local Area Networks in the Frequency Range 900 MHz to 100 GHz," Geneva, Switzerland, 2001.
[11] H. Ochiai *et al.*, "Collaborative Beamforming for Dis-

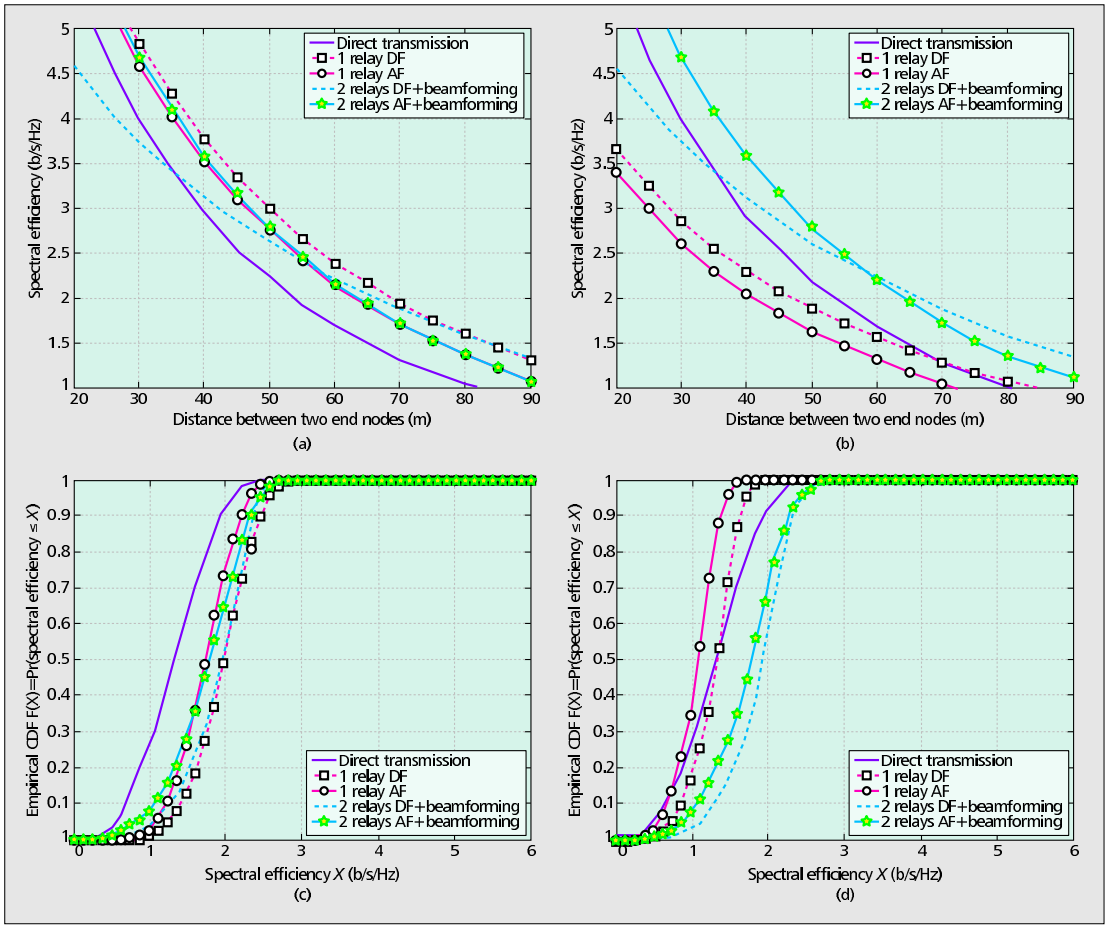

Figure 6. *Comparisons of relaying technologies with direct transmission: a) spectral efficiency when direct transmission is available; b) spectral efficiency when direct transmission is blocked; c) empirical spectral efficiency cumulative distribution function when direct transmission is available, d) empirical spectral efficiency cumulative distribution function when direct transmission is blocked.*

tributed Wireless Ad Hoc Sensor Networks," *IEEE Trans. Signal Proc.*, vol. 53, no. 11, Nov. 2005, pp. 4110–24.
[12] B. Jiang *et al.*, "Channel Estimation and Training Design for Two-Way Relay Networks with Power Allocation," *IEEE Trans. Wireless Commun.*, vol. 9, no. 6, June 2010, pp. 2022–32.
[13] T.-H. Pham *et al.*, "Optimal Training Sequences for Channel Estimation in Bi-Directional Relay Networks with Multiple Antennas," *IEEE Trans. Commun.*, vol. 58, no. 2, Feb. 2010, pp. 474–79.
[14] C. Z. W. H. Sweatman *et al.*, "Comparison of Detection Algorithm Including BLAST for Wireless Communication Using Multiple Antennas," *Proc. IEEE PIMRC*, vol. 1, London, U.K., Sept. 2000, pp. 698–703.

Biographies

HONGJIAN SUN (mrhjsun@hotmail.com) is a postdoctoral research associate in the Institute of Telecommunications at King's College London, United Kingdom. In 2010 he obtained his Ph.D. degree from the University of Edinburgh, United Kingdom, where he received a Wolfson Microelectronics Scholarship. From September 2011 to January 2012, he was a visiting postdoctoral research associate at Princeton University, New Jersey. His recent research interests include smart grid, cognitive radio, power line communications, cooperative communication, compressive sensing, and femtocells.

BO TAN (b.tan@ed.ac.uk) received his B.Eng. and M.Sc. degrees from Beijing University of Posts and Telecommunications (BUPT), China, in 2004 and 2008, respectively. He is currently a Ph.D. candidate at the University of Edinburgh. Meanwhile he is a research associate in the Department of Electronic & Electrical Engineering, University College London since February 2012. His research interests include power line communications and its applications in smart grid, passive radar, and hardware approaches for signal processing.

JING JIANG (jing.jiang@surrey.ac.uk) received B.Eng. and M.Sc. degrees from Harbin Institute of Technology, China, in 2005 and 2007, respectively, and a Ph.D. degree in electronic engineering from the University of Edinburgh in 2011. Since June 2011, she has been a research fellow with the Centre for Communication Systems Research, University of Surrey, United Kingdom. Her research interests include multiple-input multiple output (MIMO) and virtual-MIMO systems, cognitive radio systems, relay and cooperation techniques, and energy-efficient system design.

JOHN S. THOMPSON (john.thompson@ed.ac.uk) was appointed as a lecturer at what is now the School of Engineering at the University of Edinburgh in 1999. He was recently promoted to a personal chair in Signal Processing and Communications. His research interests currently include energy-efficient communications systems, antenna array techniques, and multihop wireless communications. He has published over 200 papers to date including a number of invited papers, book chapters, and tutorial talks, as well as co-authoring an undergraduate textbook on digital signal processing. He is also the academic deputy leader for the EPSRC/Mobile VCE Green Radio project, which involves a number of international communication companies. He was the Founding Editor-In-Chief of *IET Signal Processing* and was a technical programme co-chair for the GLOBECOM conference in Miami in December 2010.

ARUMUGAM NALLANATHAN (nallanathan@ieee.org) is the head of graduate studies in the School of Natural and Mathematical Sciences and a Reader in Communications at King's College London. From August 2000 to December 2007, he was an assistant professor in the Department of Electrical and Computer Engineering at the National University of Singapore. His research interests include smart grid, cognitive radio, and relay networks. He has authored nearly 200 journal and conference papers. He is an Editor for *IEEE Transactions on Communications*, *IEEE Transactions on Vehicular Technology*, *IEEE Wireless Communications Letters*, and *IEEE Signal Processing Letters*. He served as an Editor for *IEEE Transactions on Wireless Communications* (2006–2011).

H. VINCENT POOR [F] (poor@princeton.edu) is Dean of Engineering and Applied Science at Princeton University, where he is also the Michael Henry Strater University Professor. His interests include statistical signal processing and information theory, with applications in several fields. He is a member of the NAE, the NAS, and the RAE. Recent recognition includes the 2010 IET Fleming Medal, the 2011 IEEE Sumner Award, and honorary doctorates from Aalborg University, the Hong Kong University of Science and Technology, and the University iof Edingburgh.

References

[1] M. Schwartz, "Carrier-wave telephony over power lines: Early history," *2007 IEEE Conference on the History of Electric Power*, pp. 244 – 254, 3-5 Aug. 2007.

[2] A. Haidine and R. Lehnert, "Analysis of the channel allocation problem in broadband power line communications access networks," in *IEEE International Symposium on Power Line Communications and Its Applications*, pp. 192 –197, Mar. 2007.

[3] J. Sanchez-Martinez, J. Cortes, L. Diez, F. Canete, and L. Torres, "Performance analysis of ofdm modulation on indoor plc channels in the frequency band up to 210 mhz," in *2010 IEEE International Symposium on Power Line Communications and Its Applications*, pp. 38 –43, Mar. 2010.

[4] L. Zbydniewski and T. Zielinski, "Ofdm vs wavelet-ofdm and circular wavelet-ofdm in high speed communication over power lines," in *Signal Processing Algorithms, Architectures, Arrangements, and Applications Conference Proceedings (SPA), 2009*, pp. 76 –81, Sept. 2009.

[5] A. Haidine, B. Adebisi, A. Treytl, H. Pille, B. Honary, and A. Portnoy, "High-speed narrowband plc in smart grid landscape; state-of-the-art," in *2011 IEEE International Symposium on Power Line Communications and Its Applications*, pp. 468 –473, Apr. 2011.

[6] H. Hrasnica, A. Haidine, and R. Lehnert, "Broadband powerline communications networks-network design," *John Wiley & Sons*, Jun. 2004.

[7] M. Schwartz, "Carrier-wave telephony over power lines: Early history [history of communications]," *IEEE Communications Magazine*, vol. 47, pp. 14 –18, Jan. 2009.

[8] H. C. Ferreira, L. Lampe, J. Newbury, and T. G. Swart, "Power line communications: Theory and applications for narrowband and broadband communications over power lines," *John Wiley & Sons*, 2010.

[9] M. Hosono, "Broadband powerline communications networks-network design," in *4th International Conference on Metering, Apparatus and Tariffs for Electricity Supply*, pp. 26–28, Oct. 1982.

[10] J. T. Tengdin, "Distribution line carrier communications - an historical perspective," *IEEE Transactions on Power Delivery*, vol. 2, pp. 321 –329, Apr. 1987.

[11] M. Jackson, "Liverpool uk to trial 200mbps powerline communications broadband technology," in *ISP review*, Dec. 2010.

[12] S. T. Mak and D. L. Reed, "Twacs, a new viable two-way automatic communication system for distribution networks part i: Outbound communication," *IEEE Power Engineering Review*, vol. PER-2, p. 65, Aug. 1982.

[13] S. T. Mak and T. G. Moore, "Twacs, a new viable two-way automatic communication system for distribution networks. part ii: Inbound communication," *IEEE Power Engineering Review*, vol. PER-4, p. 51, Aug. 1984.

[14] D. Clark, "Powerline communications: finally ready for prime time?," *IEEE Internet Computing*, vol. 2, pp. 10 –11, Jan./Feb. 1998.

[15] H. Philipps, "Performance measurements of power line channels at high frequencies," in *IEEE International Symposium on Power Line Communications and Its Applications*, pp. 229 –237, Mar. 1998.

[16] O. Hooijen, "A channel model for the residential power circuit used as a digital communications medium," *IEEE Transactions on Electromagnetic Compatibility*, vol. 40, pp. 331–336, Nov. 1998.

[17] D. Liu, E. Flint, B. Gaucher, and Y. Kwark, "Wideband ac power line characterization," *IEEE Transactions on Consumer Electronics*, vol. 45, pp. 1087–1097, Nov. 1999.

[18] M. Zimmermann and K. Dostert, "A multipath model for the powerline channel," *IEEE Transactions on Communications*, vol. 50, pp. 553 –559, Apr. 2002.

[19] T. Sartenaer and P. Delogne, "Deterministic modeling of the (shielded) outdoor power line channel based on the multiconductor transmission line equations," *IEEE Journal on Selected Areas in Communications*, vol. 24, pp. 1277 – 1291, Jul. 2006.

[20] S. Galli and T. Banwell, "A deterministic frequency-domain model for the indoor power line transfer function," *IEEE Journal on Selected Areas in Communications*, vol. 24, pp. 1304 – 1316, Jul. 2006.

[21] S. Galli, "A simplified model for the indoor power line channel," in *IEEE International Symposium on Power Line Communications and Its Applications*, pp. 13 –19, Apr. 2009.

[22] A. Tonello and F. Versolatto, "Bottom-up statistical plc channel modeling;part ii: Inferring the statistics," *IEEE Transactions on Power Delivery*, vol. 25, pp. 2356 –2363, Oct. 2010.

[23] Wikipedia, "List of broadband over power line deployments." `http://en.wikipedia.org/wiki/List_of_broadband_over_power_line_deployments`, 2013. [Online; accessed 13-February-2013].

[24] K. Afkhamie, S. Katar, L. Yonge, and R. Newman, "An overview of the upcoming homeplug av standard," in *2005 International Symposium on Power Line Communications and Its Applications*, pp. 400 – 404, Apr. 2005.

[25] D. Cooper and T. Jeans, "Narrowband, low data rate communications on the low-voltage mains in the cenelec frequencies. ii. multiplicative signal fading and efficient modulation schemes," *IEEE Transactions on Power Delivery*, vol. 17, pp. 724 – 729, Jul. 2002.

[26] A. M. Tonello, "Wideband impulse modulation and receiver algorithms for multiuser power line communication," *EURASIP Journal on Advances in Signal Processing*, Jun. 2007.

[27] L. Lampe and J. B. Huber, "Bandwidth efficient power line communications based on ofdm," *International Journal of Electronics and Communications*, vol. 54, pp. 200–0, 2000.

[28] M. Crussiere, J.-Y. Baudais, and J.-F. Helard, "Adaptive spread-spectrum multicarrier multiple-access over wirelines," *IEEE Journal on Selected Areas in Communications*, vol. 24, pp. 1377 – 1388, Jul. 2006.

[29] S. Alessandro, A. M. Tonello, and L. Lampe, "Adaptive pulse-shaped ofdm with application to in-home power line communications," *Telecommunication Systems*, vol. 51, pp. 3–13, Sept. 2012.

[30] A. Tonello and F. Pecile, "Efficient architectures for multiuser fmt systems and application to power line communications," *IEEE Transactions on Communications*, vol. 57, pp. 1275 –1279, May. 2009.

[31] H. Koga, N. Kodama, and T. Konishi, "High-speed power line communication system based on wavelet ofdm," in *Internation Symposium on Power Line Communications and Its Applications*, Mar. 2003.

[32] R. Pighi, M. Franceschini, G. Ferrari, and R. Raheli, "Fundamental performance limits of communications systems impaired by impulse noise," *IEEE Transactions on Communications*, vol. 57, pp. 171 –182, Jan. 2009.

[33] J. Y. Kim, "Turbo coded ofdm/qam scheme for a high-speed power line," in *Internation Symposium on Power Line Communications and Its Applications*, Mar. 2004.

[34] D. Fertonani and G. Colavolpe, "On reliable communications over channels impaired by bursty impulse noise," *IEEE Transactions on Communications*, vol. 57, pp. 2024 –2030, Jul. 2009.

[35] C. Liu, S. Weiss, S. Redif, T. Cooper, L. Lampe, and J. McWhirter, "Channel coding for power line communication based on oversampled filter banks," in *2005 International Symposium on Power Line Communications and Its Applications*, pp. 246–249, 2005.

[36] S. Galli, A. Scaglione, and Z. Wang, "For the grid and through the grid: The role of power line communications in the smart grid," *Proceedings of the IEEE*, vol. 99, pp. 998 –1027, Jun. 2011.

[37] E. Bassi, F. Benzi, L. Almeida, and T. Nolte, "Powerline communication in electric vehicles," in *IEEE International Electric Machines and Drives Conference*, pp. 1749 –1753, May. 2009.

[38] S. Barmada, M. Raugi, M. Tucci, Y. Maryanka, and O. Amrani, "Plc systems for electric vehicles and smart grid applications," in *2013 17th IEEE International Symposium on Power Line Communications and Its Applications*, pp. 23–28, 2013.

[39] S. Galli, T. Banwell, and D. Waring, "Power line based lan on board the nasa space shuttle," in *2004 IEEE 59th Vehicular Technology Conference*, vol. 2, pp. 970 – 974 Vol.2, May. 2004.

[40] P. Crolla, A. Tonello, S. Weiss, and G. Burt, "Evaluation of narrowband power line communications on a smart grid testbed," in *2011 2nd IEEE PES International Conference and Exhibition on Innovative Smart Grid Technologies (ISGT Europe)*, pp. 1–5, 2011.

[41] A. Aruzuaga, I. Berganza, A. Sendin, M. Sharma, and B. Varadarajan, "Prime interoperability tests and results from field," in *2010 First IEEE International Conference on Smart Grid Communications (SmartGridComm)*, pp. 126 –130, Oct. 2010.

[42] K. Razazian, M. Umari, A. Kamalizad, V. Loginov, and M. Navid, "G3-plc specification for powerline communication: Overview, system simulation and field trial results," in *2010 IEEE International Symposium on Power Line Communications and Its Applications*, pp. 313 –318, Mar. 2010.

[43] V. Oksman and J. Zhang, "G.hnem: the new itu-t standard on narrowband plc technology," *IEEE Communications Magazine*, vol. 49, no. 12, pp. 36–44, 2011.

[44] M. Tlich, A. Zeddam, F. Moulin, and F. Gauthier, "Indoor power-line communications channel characterization up to 100 mhz;part ii: Time-frequency analysis," *IEEE Transactions on Power Delivery*, vol. 23, pp. 1402 –1409, Jul. 2008.

[45] M. Tlich, A. Zeddam, F. Moulin, and F. Gauthier, "Indoor power-line communications channel characterization up to 100 mhz;part i: One-parameter deterministic model," *IEEE Transactions on Power Delivery*, vol. 23, pp. 1392 –1401, Jul. 2008.

[46] M. Y. Chung, M. H. Jung, T. J. Lee, and Y. Lee, "Performance analysis of homeplug 1.0 mac with csma/ca," *IEEE Journal on Selected Areas in Communications*, vol. 24, pp. 1411 – 1420, Jul. 2006.

[47] K. Afkhamie, S. Katar, L. Yonge, and R. Newman, "An overview of the upcoming homeplug av standard," in *2005 International Symposium on Power Line Communications and Its Applications*, pp. 400 – 404, Apr. 2005.

[48] B. Mashburn, H. Latchman, T. VanderMey, L. Yonge, and K. Tripathi, "Signal processing challenges in the design of the homeplug av powerline standard to ensure coexistence with homeplug 1.0.1," in *2005 IEEE 6th Workshop on Signal Processing Advances in Wireless Communications*, pp. 1001 – 1005, Jun. 2005.

[49] S. Galli, H. Koga, and N. Kodama, "Advanced signal processing for plcs: Wavelet-ofdm," in *IEEE International Symposium on Power Line Communications and Its Applications*, pp. 187 –192, Apr. 2008.

[50] S. Galli and O. Logvinov, "Recent developments in the standardization of power line communications within the ieee," *IEEE Communications Magazine*, vol. 46, pp. 64 –71, Jul. 2008.

[51] S. Goldfisher and S. Tanabe, "Ieee 1901 access system: An overview of its uniqueness and motivation," *IEEE Communications Magazine*, vol. 48, pp. 150 –157, Oct. 2010.

[52] V. Oksman and S. Galli, "G.hn: The new itu-t home networking standard," *IEEE Communications Magazine*, vol. 47, pp. 138 –145, Oct. 2009.

[53] P. Janse Van Rensburg and H. Ferreira, "Coupling circuitry: understanding the functions of different components," in *International Symposium on Power Line Communications and Its Applications*, pp. 204–209, Mar. 2003.

[54] P. Van Rensburg and H. Ferreira, "Design of a bidirectional impedance-adapting transformer coupling circuit for low-voltage power-line communications," *IEEE Transactions on Power Delivery*, vol. 20, no. 1, pp. 64–70, 2005.

[55] P. Van Rensburg, H. Ferreira, and A. Snyders, "Coupler winding ratio selection for effective power transfer to a power-line communications receiver," in *2006 IEEE International Symposium on Power Line Communications and Its Applications*, pp. 290–295, 2006.

[56] A. Kosonen and J. Ahola, "Comparison of signal coupling methods for power line communication between a motor and an inverter," *IET Electric Power Applications*, vol. 4, no. 6, pp. 431–440, 2010.

[57] S. Galli, A. Kurobe, and M. Ohura, "The inter-phy protocol (ipp): A simple coexistence protocol for shared media," in *IEEE International Symposium on Power Line Communications and Its Applications*, Apr. 2009.

[58] M. Zimmermann and K. Dostert, "Analysis and modeling of impulsive noise in broadband powerline communications," *IEEE Transactions on Electromagnetic Compatibility*, vol. 44, pp. 249 –258, Feb. 2002.

[59] V. Degardin, M. Lienard, A. Zeddam, F. Gauthier, and P. Degauquel, "Classification and characterization of impulsive noise on indoor power lines used for data communications," *IEEE Transactions on Consumer Electronics*, vol. 48, pp. 913–918, Nov. 2002.

[60] M. Katayama, T. Yamazato, and H. Okada, "A mathematical model of noise in narrowband power line communication systems," *IEEE Journal on Selected Areas in Communications*, vol. 24, no. 7, pp. 1267–1276, 2006.

[61] J. A. Corts, L. Dłez, F. J. Caete, and S.-M. J. J., "Analysis of the indoor broadband power line noise scenario," *IEEE Transactions on Electromagnetic Compatibility*, vol. 52, pp. 849–858, Nov. 2010.

[62] A. Kawaguchi, H. Okada, T. Yamazato, and M. Katayama, "Correlations of noise waveforms at different outlets in a power-line network," in *IEEE International Symposium on Power Line Communications and Its Applications*, pp. 92–97, Mar. 2006.

[63] S. Miyamoto, M. Katayama, and N. Morinaga, "Performance analysis of qam systems under class a impulsive noise environment," *IEEE Transactions on Electromagnetic Compatibility*, vol. 37, pp. 260 –267, May. 1995.

[64] J. Haring and A. J. H. Vinck, "Ofdm transmission corrupted by impulsive noise," in *Internation Symposium on Power Line Communications and Its Applications*, 2000.

[65] S. Zhidkov, "Analysis and comparison of several simple impulsive noise mitigation schemes for ofdm receivers," *IEEE Transactions on Communications*, vol. 56, pp. 5 –9, Jan. 2008.

[66] R. Pighi, M. Franceschini, G. Ferrari, and R. Raheli, "Fundamental performance limits of communications systems impaired by impulse noise," *IEEE Transactions on Communications*, vol. 57, pp. 171 –182, Jan. 2009.

[67] S. Galli, "Power line communications," in *IEEE Communication Theory Workshop*, May. 2010.

[68] S. Galli and T. Banwell, "A novel approach to the modeling of the indoor power line channel-part ii: transfer function and its properties," *IEEE Transactions on Power Delivery*, vol. 20, pp. 1869 – 1878, Jul. 2005.

[69] H. Meng, S. Chen, Y. Guan, C. Law, P. So, E. Gunawan, and T. Lie, "Modeling of transfer characteristics for the broadband power line communication channel," *IEEE Transactions on Power Delivery*, vol. 19, pp. 1057 – 1064, Jul. 2004.

[70] S. Guzelgoz, H. Celebi, and H. Arslan, "Statistical characterization of the paths in multipath plc channels," *IEEE Transactions on Power Delivery*, vol. 26, pp. 181 –187, Jan. 2011.

[71] S. Galli, "A simple two-tap statistical model for the power line channel," in *IEEE International Symposium on Power Line Communications and Its Applications*, pp. 242 –248, Mar. 2010.

[72] A. A. Tahat and N. P. Galatsanos, "Channel estimation in a dmt based power-line communication system using sparse bayesian regression," in *11th WSEAS international conference on Multimedia systems and signal processing*, pp. 104–109, 2011.

[73] D. Schneider, A. Schwager, W. Baschlin, and P. Pagani, "European mimo plc field measurements: Channel analysis," in *2012 16th IEEE International Symposium on Power Line Communications and Its Applications*, pp. 304–309, Mar.

[74] S. Weiss, N. Moret, A. Millar, A. Tonello, and R. Stewart, "Initial results on an mmse precoding and equalisation approach to mimo plc channels," in *2011 IEEE International Symposium on Power Line Communications and Its Applications*, pp. 146–152, 2011.

[75] F. Versolatto and A. Tonello, "A mimo plc random channel generator and capacity analysis," in *2011 IEEE International Symposium on Power Line Communications and Its Applications*, pp. 66–71, 2011.

[76] A. Tomasoni, R. Riva, and S. Bellini, "Spatial correlation analysis and model for in-home mimo power line channels," in *2012 16th IEEE International Symposium on Power Line Communications and Its Applications*, pp. 286–291, 2012.

[77] M. Zimmermann and K. Dostert, "A multi-path signal propagation model for the power line channel in the high frequency range," in *IEEE International Symposium on Power Line Communications and Its Applications*, Mar. 1999.

[78] H. Zou, A. Chowdhery, S. Jagannathan, J. Cioffi, and J. Le Masson, "Multi-user joint subchannel and power resource-allocation for powerline relay networks," in *IEEE International Conference on Communications*, pp. 1 –5, Jun. 2009.

[79] C. Shannon, "Communication in the presence of noise," *Proceedings of the IEEE*, vol. 86, pp. 447 –457, Feb. 1998.

[80] J. G. Proakis, "Digital communications, 4th edition," *McGraw Hill Higher Education*, 2000.

[81] J. Anatory, N. Theethayi, R. Thottappillil, M. Kissaka, and N. Mvungi, "The effects of load impedance, line length, and branches in typical low-voltage channels of the bplc systems of developing countries: Transmission-line analyses," *IEEE Transactions on Power Delivery*, vol. 24, pp. 621 –629, Apr. 2009.

[82] F. Corripio, J. Arrabal, L. del Rio, and J. Munoz, "Analysis of the cyclic short-term variation of indoor power line channels," *IEEE Journal on Selected Areas in Communications*, vol. 24, pp. 1327 – 1338, Jul. 2006.

[83] K. H. Kim, H. B. Lee, Y. H. Kim, and S. C. Kim, "Channel adaptation for time-varying powerline channel and noise synchronized with ac cycle," in *IEEE International Symposium on Power Line Communications and Its Applications*, pp. 250 –254, Apr. 2009.

[84] F. Canete, J. Cortes, L. Diez, and J. Entrambasaguas, "A channel model proposal for indoor power line communications," *IEEE Communications Magazine*, vol. 49, no. 12, pp. 166–174, 2011.

[85] X. Ding and J. Meng, "Channel estimation and simulation of an indoor power-line network via a recursive time-domain solution," *IEEE Transactions on Power Delivery*, vol. 24, pp. 144 –152, Jan. 2009.

[86] S. Galli and T. Banwell, "A deterministic frequency-domain model for the indoor power line transfer function," *IEEE Journal on Selected Areas in Communications*, vol. 24, pp. 1304 – 1316, Jul. 2006.

[87] T. Banwell and S. Galli, "A novel approach to the modeling of the indoor power line channel part i: circuit analysis and companion model," *IEEE Transactions on Power Delivery*, vol. 20, pp. 655 – 663, Apr. 2005.

[88] T. Banwell, "Accurate indoor residential plc model suitable for channel and emc estimation," in *IEEE 6th Workshop on Signal Processing Advances in Wireless Communications*, pp. 985 – 990, Jun. 2005.

[89] M. Babic, M. Hagenau, K. Dostert, and J. Bausch, "Theoretical postulation of plc channel model," 2005. Released by OPERA in 2005, but not accessible currrently.

[90] A. Tonello and F. Versolatto, "Bottom-up statistical plc channel modeling;part i: Random topology model and efficient transfer function computation," *IEEE Transactions on Power Delivery*, vol. 26, pp. 891 –898, Apr. 2011.

[91] H. Philipps, "Development of a statistical model for powerline communication channels," in *International Symposium on Power Line Communications and Its Applications*, Apr. 2000.

[92] H. Philipps, "Performance measurements of powerline channels at high frequencies," in *International Symposium on Power Line Communications and Its Applications*, pp. 229 – 237, Mar. 1998.

[93] H. Meng, Y. Guan, and S. Chen, "Modeling and analysis of noise effects on broadband power-line communications," *IEEE Transactions on Power Delivery*, vol. 20, pp. 630 – 637, Apr. 2005.

[94] D. Benyoucef, "A new statistical model of the noise power density spectrum for power-line communications," in *International Symposium on Power Line Communications and Its Applications*, pp. 136 – 141, Mar. 2003.

[95] W. Bo, Q. Yinghao, H. Peiwei, and C. Wenhao, "Indoor powerline channel simulation and capacity analysis," in *IET Conference on Wireless, Mobile and Sensor Networks*, pp. 154 –157, Dec. 2007.

[96] V. Degardin, M. Lienard, P. Degauque, A. Zeddam, and F. Gauthier, "Impulsive noise on indoor power lines: characterization and mitigation of its effect on plc systems," in *IEEE International Symposium on Electromagnetic Compatibility*, vol. 1, pp. 166–169 Vol.1, 2003.

[97] V. Balakirsky and A. J. Vinck, "Potential limits on powerline communication over impulsive noise channels," in *International Symposium on Power Line Communications and Its Applications*, Mar. 2003.

[98] M. Tlich, H. Chaouche, A. Zeddam, and P. Pagani, "Novel approach for plc impulsive noise modelling," in *IEEE International Symposium on Power Line Communications and Its Applications*, pp. 20 –25, Apr. 2009.

[99] M. Zimmermann and K. Dostert, "An analysis of the broadband noise scenario in powerline networks," in *IEEE International Symposium on Power Line Communications and Its Applications*, Apr. 2000.

[100] M. Tlich, A. Zeddam, F. Moulin, and F. Gauthier, "Indoor power-line communications channel characterization up to 100 mhz ;part i: One-parameter deterministic model," *IEEE Transactions on Power Delivery*, vol. 23, pp. 1392 –1401, Jul. 2008.

[101] F. Versolatto and A. Tonello, "On the relation between geometrical distance and channel statistics in in-home plc networks," in *2012 16th IEEE International Symposium on Power Line Communications and Its Applications*, pp. 280–285, 2012.

[102] C. Delestre, G. Ndo, and F. Labeau, "A binary tree network topology for statistical and physical plc channel modeling," in *2013 17th IEEE International Symposium on Power Line Communications and Its Applications*, pp. 327–332, 2013.

[103] L. Liu, T. Cheng, and L. Yanan, "Analysis and modeling of multipath for indoor power line channel," in *10th International Conference on Advanced Communication Technology*, vol. 3, pp. 1966 –1969, Feb. 2008.

[104] F. Harris, "Performance and design considerations of the farrow filter when used for arbitrary resampling of sampled time series," in *Conference Record of the Thirty-First*

Asilomar Conference on Signals, Systems Computers, vol. 2, pp. 1745 –1749 vol.2, Nov. 1997.

[105] B. Tan and J. Thompson, "Relay transmission protocols for in-door powerline communications networks," in *2011 IEEE International Conference on Communications Workshops*, pp. 1 –5, Jun. 2011.

[106] L. Lampe, R. Schober, and S. Yiu, "Distributed space-time coding for multihop transmission in power line communication networks," *IEEE Journal on Selected Areas in Communications*, vol. 24, no. 7, pp. 1389–1400, 2006.

[107] J. Hao Zou; Jagannathan, S.; Cioffi, "Multiuser ofdma resource allocation algorithms for in-home power-line communications," in *IEEE Global Telecommunications Conference*, pp. 1 –5, Nov. 2008.

[108] K. Kim, H. Lee, Y. Kim, J. Lee, and S. Kim, "Cooperative multihop af relay protocol for medium-voltage power-line-access network," *IEEE Transactions on Power Delivery*, vol. pp, no. 99, pp. 1–1, 2011.

[109] A. Tonello, F. Versolatto, and S. D'Alessandro, "Opportunistic relaying in in-home plc networks," in *IEEE Global Telecommunications Conference*, pp. 1 –5, Dec. 2010.

[110] S. D'Alessandro, A. Tonello, and F. Versolatto, "Power savings with opportunistic decode and forward over in-home plc networks," in *IEEE International Symposium on Power Line Communications and Its Applications*, pp. 176 –181, Apr. 2011.

[111] X. Cheng, R. Cao, and L. Yang, "On the system capacity of relay-aided powerline communications," in *2011 IEEE International Symposium on Power Line Communications and Its Applications*, pp. 170 –175, Apr. 2011.

[112] X. Cheng, R. Cao, and L. Yang, "Relay-aided amplify-and-forward powerline communications," *IEEE Transactions on Smart Grid*, vol. 4, no. 1, pp. 265–272, 2013.

[113] G. Bumiller, L. Lampe, and H. Hrasnica, "Power line communication networks for large-scale control and automation systems," *IEEE Communications Magazine*, vol. 48, pp. 106 – 113, Apr. 2010.

[114] L. Lampe and A. Vinck, "On cooperative coding for narrowband plc networks," *International Journal of Electronics and Communications*, vol. 65, pp. 681–687, Aug. 2011.

[115] L. Lampe and A. J. H. Vinck, "Cooperative multihop power line communications," in *2012 16th IEEE International Symposium on Power Line Communications and Its Applications*, pp. 1–6, 2012.

[116] B. Xia, Y. Fan, J. Thompson, and H. Poor, "Buffering in a three-node relay network," *IEEE Transactions on Wireless Communications*, vol. 7, pp. 4492 –4496, Nov. 2008.

[117] Y. Jing and H. Jafarkhani, "Network beamforming using relays with perfect channel information," *IEEE Transactions on Information Theory*, vol. 55, no. 6, pp. 2499–2517, 2009.

[118] J. Zhang and M. Gursoy, "Relay beamforming strategies for physical-layer security," in *2010 44th Annual Conference on Information Sciences and Systems*, pp. 1–6, 2010.

[119] Q. Zhou, Y. Li, F. Lau, and B. Vucetic, "Decode-and-forward two-way relaying with network coding and opportunistic relay selection," *IEEE Transactions on Communications*, vol. 58, pp. 3070 –3076, Nov. 2010.

[120] E. Larsson and B. Vojcic, "Cooperative transmit diversity based on superposition modulation," *IEEE Communications Letters*, vol. 9, pp. 778 – 780, Sept. 2005.

[121] D. Altolini, N. Benvenuto, S. Pupolin, and R. Riva, "Preamble-based channel estimation in homeplug av systems," in *2012 16th IEEE International Symposium on Power Line Communications and Its Applications*, pp. 176–181, 2012.

[122] O. Edfors, M. Sandell, J.-J. van de Beek, S. Wilson, and P. Borjesson, "Ofdm channel estimation by singular value decomposition," *IEEE Transactions on Communications*, vol. 46, pp. 931 –939, Jul. 1998.